Penetration in concrete for projectiles with L/D≈9

Håkan Hansson

FOI-R-- 1659 --SE
ISSN 1650-1942

Weapons and Protection
Technical report

June 2005

Penetration in concrete for projectiles with L/D≈9

FOI-R--1659--SE
ISSN 1650-1942

Weapons and Protection
Technical report

June 2005

Issuing organization FOI – Swedish Defence Research Agency Weapons and Protection SE-147 25 Tumba	**Report number, ISRN** FOI-R--1659--SE	**Report type** Technical report
	Research area code 5. Strike and protection	
	Month year June 2005	**Project no.** E2011
	Sub area code 53 Protection and Fortification	
	Sub area code 2	
Author/s (editor/s) Håkan Hansson	**Project manager** Peter Skoglund	
	Approved by	
	Sponsoring agency Swedish Armed Forces	
	Scientifically and technically responsible	

Report title

Penetration in concrete for projectiles with L/D≈9

Abstract (not more than 200 words)

The performance of penetrating warheads has increased the last few years by introducing penetrators with a length to diameter ratio of almost 10. This type of weapon is primarily intended for use against hardened structures e.g. bunkers. Model scale tests with ogive nosed projectiles with a L/D ratio of approximately nine against concrete targets is reported here, using projectile designs developed at FOI. Three types of concretes were used for the tests, incl. two types of High Performance Concrete (HPC). Further, penetration of heavy reinforced concrete targets was also studied during the tests. The study considered both perforation of targets with measurement of exit velocities, and penetration into targets with measurement of the penetration depths. The tests were performed at two nominal impact velocities, i.e. 420 and 460 m/s, and two impact angles for the projectiles, i.e. 90° och 60°.

The tests were performed to obtain data for comparison with equations for concrete penetration and numerical simulations of concrete penetration. The tests for the projectiles with normal impact angles are compared with an empirical equation for estimations of penetration depths into concrete targets.

Keywords

Concrete, HPC, reinforcement, penetration, non-normal impacts, experiments

Further bibliographic information	**Language** English
ISSN 1650-1942	**Pages** 124 p.
	Price acc. to pricelist

Utgivare FOI - Totalförsvarets Forskningsinstitut - Vapen och skydd 147 25 Tumba	**Rapportnummer, ISRN** FOI-R--1659--SE	**Klassificering** Teknisk rapport
	Forskningsområde 5. Bekämpning och skydd	
	Månad, år Juni 2005	**Projektnummer** E2011
	Delområde 53 Skydd och anläggningsteknik	
	Delområde 2	

Författare/redaktör Håkan Hansson	**Projektledare** Peter Skoglund
	Godkänd av
	Uppdragsgivare/kundbeteckning Försvarsmakten
	Tekniskt och/eller vetenskapligt ansvarig

Rapportens titel (i översättning)

Penetration i betong för projektiler med L/D≈9

Sammanfattning (högst 200 ord)

Penetrationsdjupet för penetrerande bomber har ökat de senaste åren i och med introduktionen av penetratorer med ett förhållande mellan längd och diameter (L/D) på upp till 10. Den här typen av vapen är främst avsedda för att slå ut fortifikatoriska skydd, t ex undermarksanläggningar. Modellförsök med projektiler mot betongmål redovisas i rapporten, dessa modellprojektiler med L/D förhållande på ca nio är framtagna vid FOI. Vid försöken användes tre typer av betong, dels standardbetong men även två typer av högpresterande betong (HPC). Kraftigt armerade mål av standardbetong studerades också vid försöken. Vid försöken studerades både genomslag av mål med registrering av utgångshastighet och penetrationsdjup i betongmål utan genomslag. Försöken genomfördes vid de nominella anslagshastigheterna 420 och 460 m/s, samt för anslagsvinklarna 90° och 60°.

Försöken genomfördes för att erhålla data för jämförelse med empiriska formler och numeriska modeller. Försöken med vinkelrätt anslag i målet är jämförda med en empirisk modell för uppskattning av penetrationsdjupet i betongmål.

Nyckelord

Betong, HPC, armering, penetration, experiments

Övriga bibliografiska uppgifter	**Språk** Engelska
ISSN 1650-1942	**Antal sidor:** 124 s.
Distribution enligt missiv	**Pris: Enligt prislista**

This page intentionally blank.

Contents

This page intentionally blank.

Utökad sammanfattning

Introduktion: Prestandan för penetrerande stridsdelar har ökat de senaste åren med introduktionen av penetratorer med ett förhållande mellan längd och diameter (L/D) på nästan 10. Denna vapentyp är främst avsedd att användas mot fortifikatoriska skydd och därmed krävs förbättrade typer av skyddskonstruktioner för att förhindra penetration. Denna del av studien är huvudsakligen inriktad på att erhålla ett experimentellt underlag för fortsatta studier, men ska även ge möjlighet till att uppskatta penetration i betongkonstruktioner med hjälp av en enkel empirisk modell. Resultat av studien kan även användas för att bedöma verkan mot civila byggnadskonstruktioner, t ex vid strid i bebyggelse och för att bedöma behov av förstärkningsåtgärder.

Försöksgenomförande: En första försöksserie med penetratorer utformade vid FOI genomfördes 2002 (Hansson, 2003b), med kompletterade försök genomförda under 2004. De först nämnda försöken är kort redovisade i denna rapport, men tyngdpunkten ligger på redovisning av de senare genomförda försöken. De modellpenetratorer som användes vid försöken har en diameter på 50 mm och ett L/D mellan 9 och 9,4. Vid försöken som genomfördes 2002 var massan för projektilerna 3,65 kg och för försöken som genomfördes 2004 med en förbättrad projektilkonstruktion var massan 4,50 kg för projektilerna. Egenskaperna för projektilerna finns redovisade i tabell 2.2 och foton av penetratorer visas i figur 2.1.

Försöken har genomförts mot tre olika typer av betong: standardbetong (K45), samt två typer av högpresterande betong (HPC). Dessa var dels en HPC med tryckhållfasthet på ca 100 MPa och dels en speciellt framtagen HPC med bra skydd mot penetration. Den senare har en tryckhållfasthet på ca 135 MPa. Försök genomfördes även mot kraftigt armerade standardbetongmål, dessa innehöll ca 5 vol-% armering. Armeringen för dessa mål visas i figurerna 2.4 och 2.5. Försöken genomfördes vid två nominella anslagshastigheter, 420 och 460 m/s, samt även för två anslagsvinklar. Dessa var vinkelrätt anslag och 30° snedställning av målet, måluppställningen för dessa två fall visas i figur 2.7. Vid försöken registrerades anslagshastighet med s k ”short circuit screens”, dessa registreringar jämfördes även med anslagshastigheter bestämda från höghastighetsfilmer. Bilderna från höghastighetsfilmerna användes även för att bestämma horisontell och vertikal snedställning av projektilerna (”yaw” och ”pitch”).

Försöksgenomförande och försöksresultat finns redovisade i kapitel 2 respektive kapitel 3 i denna rapport. Försöksresultaten från 2002 är sammanställda i tabell 3.1 och försöksresultaten från 2004 i tabellerna 3.2 till 3.8.

Empirisk modell: De genomförda försöken vid FOI och tillgängliga försöksresultat från litteraturen användes för att modifiera en tidigare publicerad metod för att bestämma penetration i betongkonstruktioner (Hansson, 2003c). Den empiriska modellen är baserad på ekvationen för penetration i betong enligt programmet ConWep (1992). Den föreslagna modellen, samt jämförelser med de experimentella resultaten, redovisas i kapitel 4. I figur 4.8 visas jämförelser mellan den föreslagna empiriska modellen och försöken med vinkelrätt anslag genomförda vid FOI under 2002 och 2004, varvid maximal avvikelse är under 20%. Detta gäller även försöken mot den kraftigt armerade betongen och HPC:n. Den föreslagna modellen kan användas för att ge en uppskattning av penetrationen i betong, både avseende stridsdelars prestanda och skyddsförmågan för skyddskonstruktioner, se figur 4.8. Begränsningarna är att endast vinkelrätt anslag utan snedställning av projektilen kan beaktas, samt att utstötning och kraterbildning på baksidan av målet ej heller beaktas. Det senare gör att formeln endast kan användas för mål som kan betraktas som långa, d v s risk för perforation föreligger inte. Detta fall måste beaktas separat.

Numerisk simulering: Inom ett annat projekt sker utvärdering av numerisk simulering för bedömning av penetrationsförlopp och av förbättrade skyddskonstruktioner. Ett antal av försöken har studerats inom det projektet och några preliminära resultat redovisas kort i kapitel 5. Simuleringarna ger en bra överensstämmelse med försöksresultaten, se tabell 5.1 och 5.2.

Fördelen med numerisk simulering är att flera parametrar kan studeras, exempel på detta är snedställning av mål och projektil, inverkan av armering, samt projektilens deformation. Även kombinationer av olika verkanssätt kan studeras, t ex RSV och penetrerande stridsdelar. Detta ökar möjligheten att bedöma verkan från nuvarande och framtida stridsdelar mot skyddskonstruktioner.

Diskussion: Beroende på utformning av målet och anslagshastigheten så bedöms penetrationsdjupet för denna typ av stridsdelar vara 1 till 1,6 gånger stridsdelens längd, dock måste även risken för utstötning och därmed genomslag av målet beaktas.

Försöken visar att både kraftigt armerad standardbetong och HPC har ett ökat penetrationsmotstånd jämfört med standardbetong. Kombinationen av HPC och kraftig armering har ej studerats, men anses ha ytterligare förbättrat penetrationsmotstånd. För fallet med 60° anslagsvinkel, d v s 30° snedställning av målet, visade det sig att HPC-målen var överlägsna målen av standardbetong. Den högre tryckhållfastheten för HPC resulterade i att projektilen endast åstadkom en avlång ingångskrater, varvid projektilerna återfanns framför målet respektive parallellt med målets frontyta i kratern.

Den modifierade empiriska modellen anses ge en uppskattning inom ±20% av penetrationen i betong för projektiler med en diameter >20 mm, L/D mellan 3 och 10 och anslagshastigheter <1000 m/s. Projektiler av denna typ kan t ex vara granater från artilleri, granatkastare och handburna raketgevär, samt flygbomber och stridsdelar i kryssningsmissiler. Verkan från RSV-stridsdelar beaktas för närvarande ej inom projektet. Studier av verkan avseende RSV sker inom andra projekt (Elfving m fl, 2005 och Helte m fl, 2005).

För utförligare diskussioner och förslag på framtida studier hänvisas till kapitel 6 och 7 i rapporten.

1. Introduction

The performance of penetrating warheads has increased the last few years by introducing penetrators with a length to diameter ratio of almost 10. This type of weapon is primarily intended for use against hardened structures e.g. bunkers. This requires new designs to prevent penetration of future protective structures. The main objective of this study is to investigate the protective performance of concrete structures. Another aim with this work is to further increase the capability to predict weapon effects on normal building structures, e.g. for combat situations in urban environments and important application areas are also strengthening methods for building structures.

A series of tests with ogive nosed projectiles were performed earlier in 2002 (Hansson, 2003b), and further tests were performed in 2004 with modified projectile designs. Similar projectile designs developed at FOI with a length to diameter (L/D) ratio of approximately 9 were used for both test series. Three types of concretes were used for the earlier tests, incl. two types of High Performance Concrete (HPC). A short summary of these tests is given in this report. The experimental study performed in 2004 considers penetration into two types of concrete with different strengths using ogive nosed model projectiles. The two concrete types are normal strength concrete with an uniaxial compressive strength of approximately 45 MPa and HPC with approximately 135 MPa compressive strength. These two types were also used for the earlier test series. Further, penetration of heavy reinforced concrete targets was also studied for this test series. The experimental study considered both perforation of targets with measurement of the impact and exit velocities, and penetration into targets with measurement of the penetration depths. The tests were performed at two nominal impact velocities, i.e. 420 and 460 m/s, and two impact angles for the projectiles. The experimental set up and material properties for the tests are described in chapter 2, with the test results given in chapter 3 of the report.

The tests were performed to obtain data for comparison with equations for concrete penetration and numerical simulations of concrete penetration. The tests with normal impact angles for the projectiles are compared with an empirical equation for estimations of penetration depths in chapter 4 in the report. The test results are used to further modify an earlier published empirical method for normal impact of concrete targets (Hansson, 2003c) to penetrators with increased L/D ratios. The new empirical model and recommendations replaces the earlier publication. The empirical method is now considered to give a fair prediction of penetration depths for projectiles with L/D ratios between 3 and 10, and impact velocities below 1000 m/s. However, the structural behaviour of the projectile is not considered. The method can be used to predict penetration depths for different types of penetrating warheads or projectiles with a diameter greater than 20 mm, e.g. rocket propelled grenades, artillery shells and penetrating bombs. The use of shaped charges, explosively formed penetrators and other types of eroding projectiles are not considered with this method.

Further, a study to evaluate the use of numerical simulations to study penetration in concrete is also performed within another project and will be published in the autumn of 2005 (Hansson, 2005). Some preliminary results from this study are presented and discussed in chapter 5 in this report, together with comparison with the experimental results. The use of numerical methods extend the cases that can be studied, with the opportunity to consider e.g. heavy reinforced concrete targets, penetrator and target interactions, penetrator deformations and failure, combinations of different target materials, and also combinations of different weapons effects.

The performance of penetrators with a length to diameter ratio of approximately 9 is discussed, and also recommendations for future research regarding the possibility to evaluate weapons effects against protective and hardened structures are given.

The high-speed films from the tests are compiled in appendix 1.

2. Experimental set up

The designs of penetrators and targets are described in this chapter, together with the material properties for the used materials and the used measurement techniques.

2.1. Penetrators

A penetrator design developed at FOI was used for the tests. The diameter of the used model penetrator was 50 mm. The properties for the used projectiles are given in table 2.1 below. The FOI designed projectiles are shown in figure 2.1. The projectiles are fabricated from 34CrNiMo6 steel (Swedish standard SS 14 2541) with HV 500-620. The hardness was determined on a cross section of a projectile after the test series for the tests performed in 2002, and on an unused projectile for the tests in 2004. Measured stress vs. strain for the used steel type at a nominal strain rate of approximately 400/s is shown in figure 2.2. The stress-strain relationships for the SS 14 2541 steel are given for HV values of 300, 450 and 600.

Ballast consisting of cement based mortar was used to obtain the desired mass of the projectiles for the earlier tests performed in 2002. An empty space of approximately 90 mm length was left between the mortar and the 10 mm base plate, i.e. the mortar was poured in the projectile to a distance of 350 mm measured from the projectile nose. A dentist mould plaster, i.e. dental stone casting material, with a lower density than the mortar was used as ballast for the projectiles used for the tests performed in 2004. This, together with the increase of the casing thickness, results in a penetrator with increased performance compared with the earlier test series. Further, three nose designs with different ogive radius were used for the tests in 2004, see table 2.1 below.

Table 2.1. Properties of the used projectiles for the test series performed in 2002 and 2004.

	Test series in 2002	**Test series in 2004**	
Body diameter	50 mm	50 mm	
Length	450 mm	450 mm	470 mm
Total mass	≈3.65 kg	4.50 ±0.02 kg	
Solid nose length	≈ 83 mm	≈ 85 mm	≈ 105 mm
Case thickness for cylindrical section	5.0 mm	10.0 mm	
Ogive radius	400 mm	150 and 400 mm	600 mm
Casing material	34CrNiMo6 (SS 14 2541)	34CrNiMo6 (SS 14 2541)	
Hardness of casing material	HRC 50.2-50.6 [1] HV 560-620 [1]	HV ≈500 [2]	
Filling material	Cement based mortar with $\rho \approx 2.4 \times 10^3$ kg/m^3	Dental stone casting material with $\rho \approx 1.8 \times 10^3$ kg/m^3	

Note: [1]: HRC and HV values were measured on a cross section of a projectile after the test series.
[2]: HV values were measured on a cross section of an unused projectile.

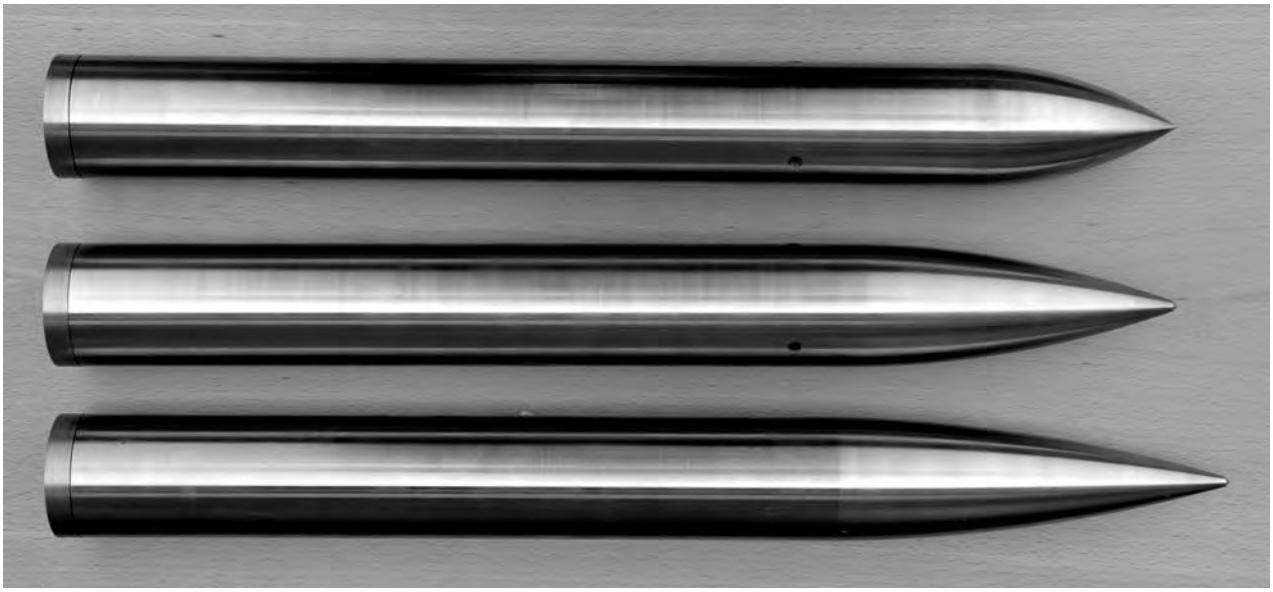

a)

b)

Figure 2.1. The used types of projectiles for the test, (a) the three different nose shapes of the projectiles used in 2004, and (b) the 50 mm diameter projectile shown with guidance ring and aluminium pusher plate. The masses of the guidance ring and pusher plate are approximate 130 and 350 g, respectively.

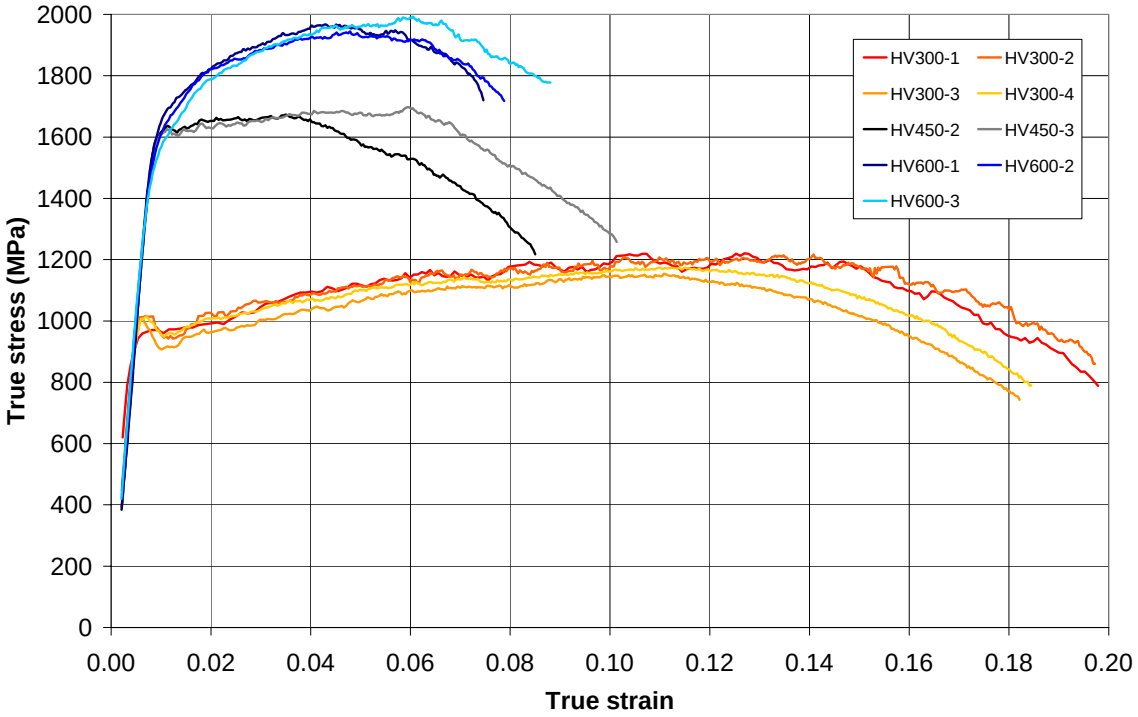

Figure 2.2. Measured stress-strain relationship at a nominal strain rate of approximately 400/s for SS 14 2541 steel with HV300, HV450 and HV600. The data in the figure are not valid for strains referring to necking of the samples, and is only shown to give an estimation of the ductility of the used material.

2.2. Concrete types and targets

The experiments performed in 2002 were performed with three types of concrete, a normal strength concrete (NSC) and two grades of High Performance Concrete (HPC), see table 2.2. Mix proportions for the NSC is given in table 2.3 below, and the properties for the two HPC grades are described by Magnusson et al. (2001). The concrete grades are designated by the approximate uniaxial cube ("Kub") strength in MPa, i.e. K45, K100 and K140.

Table 2.2. Approximate values for material properties of the used concrete types, based on earlier material test and literature data.

Parameter	**NSC K45**	**HPC K100**	**HPC K140**
Density	≈2300 kg/m^3	≈2400 kg/m^3	≈2500 kg/m^3
Compressive cube strength at 28 days for 150 mm cubes	45-50 MPa	85-100 MPa	135-145 MPa
Compressive cylinder strength after several months [1]	45-50 MPa	95±10 MPa	140±10 MPa
Splitting strength [2] (Brazilian test)	3-4 MPa	6.0-6.5 MPa	≈7 MPa
E_0 and E_c modulus	≈30-35 GPa	≈40 GPa	≈45 GPa

Note [1]: Determined on ∅100×200 mm cylinders
[2]: The tensile strength is approximately 80 to 90 % of the tensile splitting strength.

Table 2.3. Mix proportions of the normal strength concrete.

Materials	**Amount**
Cement, *c*	330 kg/m^3
Aggregate 0 – 4 mm	990 kg/m^3
Aggregate 4 – 8 mm	825 kg/m^3
Water, *w*	215 kg/m^3
w/c = 0.65	
Total:	2360 kg/m^3

Standard strength tests were performed on the concrete batches used in 2002, these tests are compiled in tables 2.4 to 2.6.

Table 2.4. Tested compressive strength for the used concrete targets in 2002, NSC K45.

Sample geometry	**Age**	**Compressive strength (MPa)**		
		Average	**Standard deviation**	**No. of samples**
150 mm cubes [1]	28 days	49.2	±1.9	4
∅100×200 mm cylinders [1]		45.5	±0.9	4
150 mm cubes [2]	42 days	41.8	------	2
150 mm cubes [2]	91 days	47.0	±3.0	3
∅100×200 mm cylinders [2]		48.2	±1.7	5
∅100×200 mm cylinders [3]	131 days	42.5	±0.3	4
		Density (kg/m^3)		
		Average	**Standard deviation**	**No. of samples**
150 mm cubes [1]	28 days	2.31×10³	±0.03×10³	4
∅100×200 mm cylinders [1]		2.33×10³	±0.01×10³	4
150 mm cubes [2]	42 days	2.24×10³	------	2
150 mm cubes [2]	91 days	2.28×10³	±0.02×10³	3
∅100×200 mm cylinders [2]		2.33×10³	±0.01×10³	5
∅100×200 mm cylinders [3]	131 days	2.28×10³	±0.01×10³	4

Note [1]: Cured in water the first four days and then stored dry at 20°C.
[2]: Cured with the targets at approximately 20°C.
[3]: Cored cylinders.

Table 2.5. Tested compressive strength for the used concrete targets in 2002, HPC K100.

Sample geometry	**Age**	**Compressive strength (MPa)**			
		Sample 1	**Sample 2**	**Sample 3**	**Average**
150 mm cubes	28 days	83.6	83.6	87.9	85
150 mm cubes	47 days	101.5	101.6	103.1	102
∅100×200 mm cylinders	46 days	81.4	82.8	85.4	83
150 mm cubes	9 months	105.4	88.9 [1]	104.6	105 [1]
∅100×200 mm cylinders	9 months	96.8	99.1	95.2	97
		Density (kg/m^3)			
		Sample 1	**Sample 2**	**Sample 3**	**Average**
∅100×200 mm cylinders	46 days	2410	2420	2416	2.42×10^3
150 mm cubes	9 months	2400	2400	2400	2.40×10^3
∅100×200 mm cylinders	9 months	2430	2420	2420	2.42×10^3

Note [1]: Sample no. 2 not used for the calculation of average value.

Table 2.6. Tested compressive and tensile strength for the used concrete targets in 2002, HPC K140.

Sample geometry	**Age**	**Compressive strength (MPa)**			
		Sample C1	**Sample C2**	**Sample C3**	**Average**
∅100×200 mm cylinders	28 days	129.0	127.0	130.7	129
∅100×200 mm cylinders	7 months	146.4	144.6	146.0	146
		Tensile splitting strength (MPa)			
		Sample 1	**Sample 2**	**Sample 3**	**Average**
∅100×200 mm cylinders	28 days	5.7	6.7	6.3	6.2
∅100×200 mm cylinders	7 months	7.1	8.1	6.6	7.2
		Density (kg/m^3)			
		Sample C1	**Sample C2**	**Sample C3**	**Average**
∅100×200 mm cylinders	28 days	2510	2500	2500	2.50×10^3
∅100×200 mm cylinders	7 months	2500	2480	2490	2.49×10^3

The NSC target used in 2002 was cast in a steel pipe with 1.25 m diameter and 8 mm thickness of the steel. The concrete was approximately eight months old when the test was performed. The HPC targets of both K100 and K140 concrete were confined by 1.2 m diameter welded steel pipes with 5 mm thickness of material, which also served as mould for the casting. A few steel rebars were welded inside the steel cylinders to obtain an axial join between concrete and steel pipe for all targets. The locations of these bars were chosen to minimize the influence on the projectile penetration path, see figure 2.3.

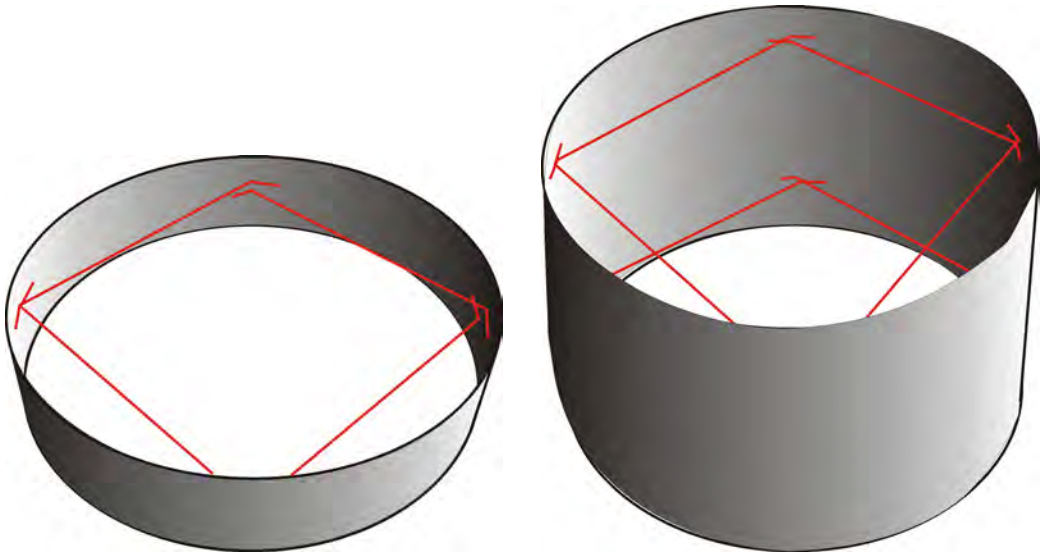

Figure 2.3. Location of steel bars in the un-reinforced concrete targets.

The two types of concrete that were used for the tests in 2004 were of the same types as the NSC and HPC K140 used in 2002. The normal strength concrete targets were manufactured around the 3rd of December 2003, and the HPC targets were manufactured around the 17th of November 2003. Standard tests were performed for these concrete batches at the end of the test series by the Royal institute of technology (KTH) to obtain uni-axial compressive strength. Further, the samples were fitted with strain gauges for the uni-axial strength tests to obtain the initial Young's modulus and stress-strain relationship for the concretes. The fracture energy was also determined for the HPC K140 concrete. The results from these material tests are compiled in tables 2.7 to 2.9. The increase of the compressive strength during the test series is estimated to less than 10% for the normal strength concrete, and the increase of the compressive strength of the HPC is assumed to be neglectable during the same time period. The thickness for the steel confinement was 8 mm for the un-reinforced cylindrical targets for the test performed in 2004.

Table 2.7. Tested compressive strength for the used concrete targets in 2004, NSC K45.

Sample geometry	Age Date	Compressive strength (MPa)				
		Sample 1	**Sample 2**	**Sample 3**	**Sample 4**	**Average**
150 mm cubes [1]	291 days 2004-09-20	59.7	60.0	61.4	---	60.4
∅100×200 mm cylinders [1]	291 days 2004-09-20	53.7	56.5	54.2	54.9	54.8
		Density (kg/m^3)				
		Sample 1	**Sample 2**	**Sample 3**	**Sample 4**	**Average**
150 mm cubes [1]	291 days 2004-09-20	2303	2305	2296	---	2.30×10^3
∅100×200 mm cylinders [1]	291 days 2004-09-20	2311	2304	2310	2324	2.31×10^3
		Young's modulus (GPa)				
		Sample 1	**Sample 2**	**Sample 3**	**Sample 4**	**Average**
∅100×200 mm cylinders [1]	291 days 2004-09-20	30.5	30.5	32.5	31.5	31.5

Note [1]: Cured in water the first four days and then stored with the targets.

Table 2.8. Tested compressive strength for the used concrete targets in 2004, HPC K140.

Sample geometry	Age Date	Compressive strength (MPa)				
		Sample 1	**Sample 2**	**Sample 3**	**Sample 4**	**Average**
∅100×200 mm cylinders [1]	307 days 2004-09-20	133.7	134.0	131.9	132.0	132.9
		Density (kg/m^3)				
		Sample 1	**Sample 2**	**Sample 3**	**Sample 4**	**Average**
∅100×200 mm cylinders [1]	307 days 2004-09-20	2517	2499	2525	2509	2.51×10^3
		Young's modulus (GPa)				
		Sample 1	**Sample 2**	**Sample 3**	**Sample 4**	**Average**
∅100×200 mm cylinders [1]	307 days 2004-09-20	45.0	44.0	45.5	45.5	45.0

Note [1]: Cured in water the first four days and then stored with the targets.

Table 2.9. Tested fracture energy for the used concrete targets in 2004, HPC K140.

Sample geometry	Age Date	Fracture energy, G_f (N/m)				
		Sample 1	**Sample 2**	**Sample 3**	**Sample 4**	**Average**
840×100×100 mm beams [1]	307 days 2004-09-20	163	148	160	161	158
		Density (kg/m^3)				
		Sample 1	**Sample 2**	**Sample 3**	**Sample 4**	**Average**
840×100×100 mm beams [1]	307 days 2004-09-20	2536	2531	2503	2530	2.53×10^3

Note [1]: Cured in water until testing.

The high performance concrete type with a nominal compressive strength of 140 MPa was partly characterized by EMI earlier. The equation of state was derived by plate tests and meso-mechanical simulations (Wicklein and Riedel, 2002), and the pressure dependent yield strength was established by the use of tri-axial tests (Riedel and Machens, 2004).

The reinforcement cage for a reinforced concrete target is shown in figure 2.4, with a drawing of the same reinforcement cage shown in figure 2.5. The reinforcement is of B500BT type 1 grade, and has a nominal diameter of 14 mm. The reinforcement layers consist of 19 bars in each direction with a centre to centre distance of 60 mm for the 1.2×1.2×0.6 m target. The cover of concrete for the first and last reinforcement layers are approximately 30 mm, and layer two to four are then distributed equally along the length of the target. The individual reinforcement layers are welded to the longitudinal reinforcement bars, which has a centre to centre distance of 180 mm. As can be seen in figure 2.5, the layer numbers 2 and 4 of the reinforcement are shifted 28 mm sideways. This applies to the bars in both directions for these layers. This avoids a clear path for a projectile through the target at impact angles close to normal impact.

Table 2.10. Specifications for reinforced concrete targets.

Target type		**0.60 m targets**	**0.54 m targets**
Target no.		2004-19, 2004-20	2004-23, 2004-24
Dimensions:	Thickness	0.60 m	0.54 m
	Width	1.20 m	1.20 m
	Heigth	1.20 m	1.50 m
Reinforcement:	Type	B500 BT	B500 BT
	Diameter	14 mm	14 mm
	No. of layers	5	5
	c/c distance	60 mm	60 mm
	c/c distance for connecting bars between the layers	180 mm	180 mm
	Amount of reinforcement steel	4.71 vol-% 291 kg/m^3	5.19 vol-% 325 kg/m^3
Notes:		All reinforcement connections are welded.	

Figure 2.4. Example of welded reinforcement cages for targets used in tests performed in 2004.

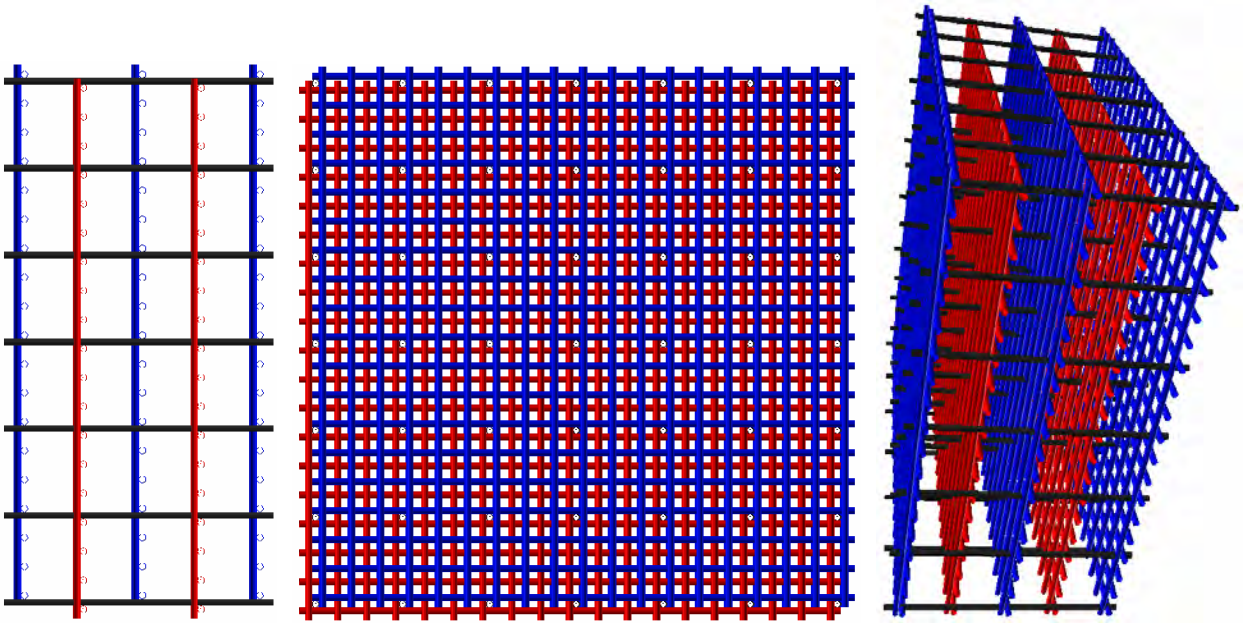

Figure 2.5. Location of reinforcement for a 1.2×1.2×0.6 m target, from left is side view, front view and a perspective view shown.

2.3. Shooting and measurement techniques

A 61 mm smooth bore gun was used for the tests, and is shown in figure 2.6. Both horizontal and vertical view of the projectile before impact and at exit were filmed with two 70 mm high speed cameras at approximately 900 to 950 frames/s, to estimate the yaw and pitch of the projectile. Both cameras covered front and back face of the target for redundancy if a camera failed to record the event. The films from the 1st camera, i.e. the camera with the best view of the impact conditions, were used to determine the yaw and pitch, i.e. angle of attack, of the projectile for the major part of the tests. Further, the films from camera no. 2 with the best view of the projectile after perforation were used to determine exit velocities. The firing of the gun was synchronized with the high-speed camera to allow the film transport mechanism to accelerate the film before the firing of the projectile. The impact velocities for the projectiles were determined with short circuit screens mounted in front of and on the target, see figure 2.7. The velocity error for the velocity determined from the high-speed film is estimated to be within ±10 m/s. Therefore, the velocity determined in this way is only used for a verification of the short circuit screen velocity measurement. A digital high-speed video was also used for some of the tests to get additional frames of some of the tests. This high-speed video used a frame rate of 8000/s, and a resolution of 1024×256 pixels. This high-speed video was also used to study the interaction of the short circuit screens with the projectile, see figures 2.8 and 2.9.

The distance between the lines of the reference grid on the reflective background is approximately 264 mm for the tests performed 2004. This results in a reference grid measured on the film, along the path of the projectile, of 250.3±1.0 mm.

The targets were placed so the sight line through the gun barrel determined by a laser beam would pass through the centre of gravity. However, due to a small variation of thickness for the inclined targets the line of sight is only approximately through the centre of these. The placement of targets for normal impact, and also for impacts with inclined targets, are shown in figure 2.7.

Figure 2.6. 61 mm smooth bore gun.

Figure 2.7. Target placement for the tests with approximately 90° and 60° impact angles. The positions of the short circuit screens for velocity measurement are also shown in the upper figure, with a third short circuit screen mounted on the surface of the target.

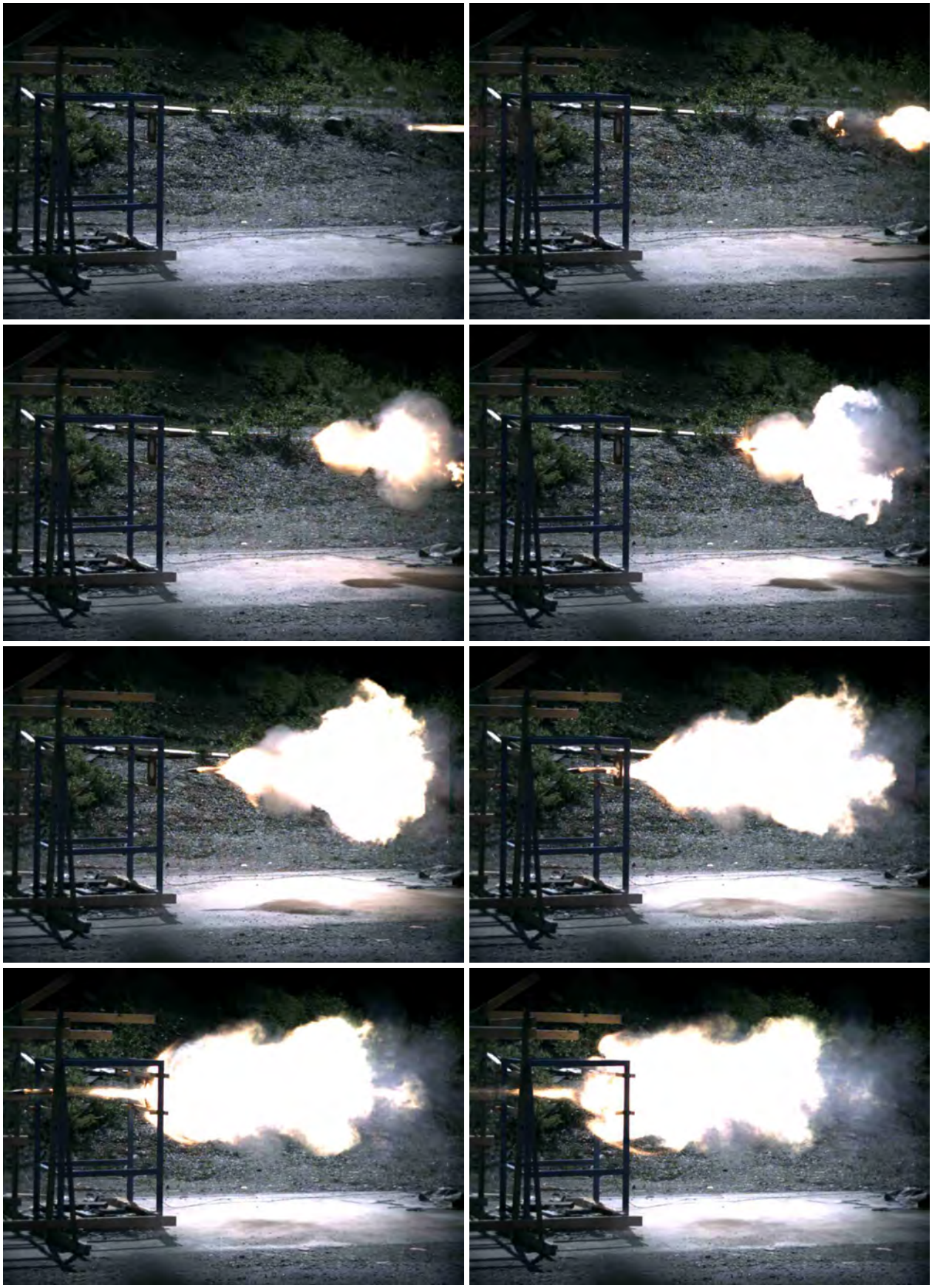

Figure 2.8. Frames from high-speed video showing the projectile interaction with short circuit screens. The time between each showed frame is 2.0 ms.

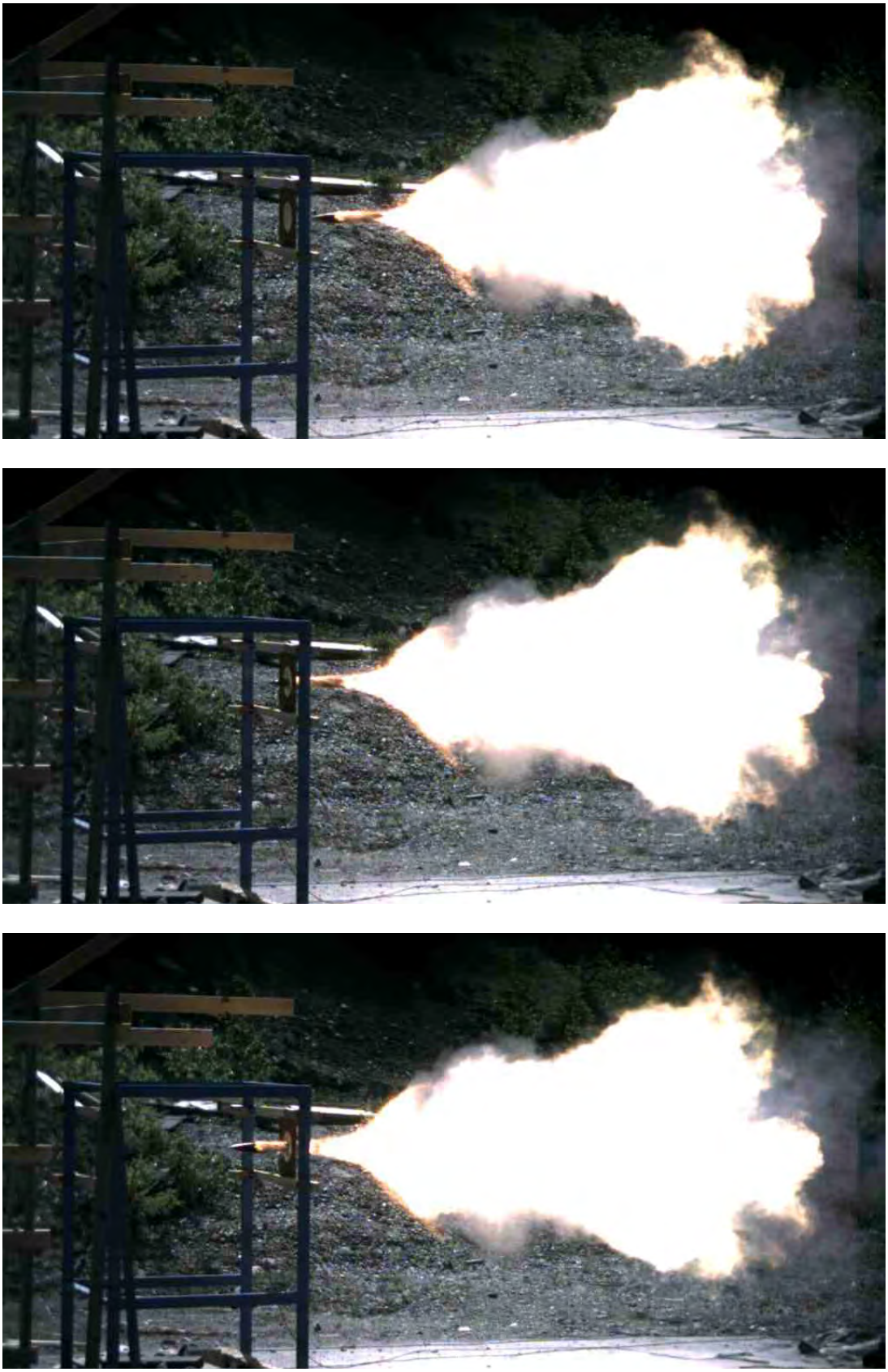

Figure 2.9. Frames from high-speed video showing the projectile interaction with short circuit screens. The time between each showed frame is 0.5 ms.

This page intentionally blank.

3. Penetration experiments

Tests were performed both in 2002 and 2004 using normal strength concrete (NSC) and high performance concrete (HPC). The impact velocities and impact angles were varied. As discussed earlier, three nose shapes and two different masses were used for the projectiles. A short summary of the test results from 2002 are given in chapter 3.1 (Hansson, 2003b), and then the results from the tests performed in 2004 are given in chapter 3.2. Figure 3.1 below show a typical concrete target after perforation of a projectile.

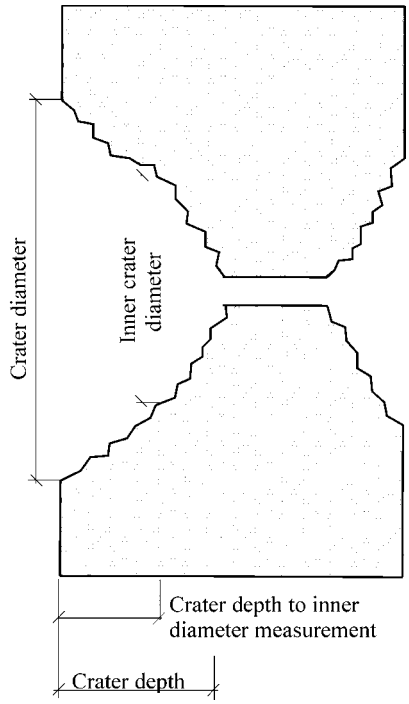

Figure 3.1. Figure of a concrete target, with definitions of crater measurements. The entrance crater is to the left in the figure. The entrance crater normally consist of two parts with different slope angles, this is the reason to define two crater diameters.

3.1. Test results from 2002

A short overview of the results from the test series in 2002 is presented in table 3.1 and figure 3.2 below. Only one test was performed with a normal strength concrete, using a concrete with a compressive strength of approximately 48 MPa. Three tests were performed with the K100 HPC, and four tests with the K140 HPC. The results obtained during the tests and post conditions of the targets are given in this chapter. Core drilling was used to obtain the projectiles after the penetration tests for a post-test analysis for this test series. More detailed information of the tests is given by Hansson (2003b).

Table 3.1. Overview of the concrete penetration test results.

Test no.	**f_{cc}** (MPa)	**Target dimensions (diameter × length)** (m)	**Impact velocity** [1] (m/s)	**Pitch**	**Yaw**	**Exit velocity** [2] **or Penetration depth**
2002-10	48	1.25 × 1.50	420	≈0.8°	≈1.0°	0.49 m
2002-1	97	1.20 × 1.50	411	≈0.6°	<0.2°	0.50 m
2002-2 [3]	97		417	≈1.3°	≈0.7°	0.47 m
2002-3	97		462	≈0.5°	≈2.2°	0.46 m [4]
2002-4	146	1.20 × 1.20	407	≈1.0°	≈1.0°	0.38 m
2002-7	146		410	≈1.5°	≈1.0°	0.41 m
2002-11	146	1.20 × 0.45	424	≈0.6°	≈0.2°	≈129 m/s
2002-12	146		417	≈1.1°	≈0.2°	≈64 m/s

Note: [1]: Determined from short circuit screens.
[2]: Determined from high-speed film, with an estimated error of ±10 m/s.
[3]: Back face of target used.
[4]: The projectile fractured.

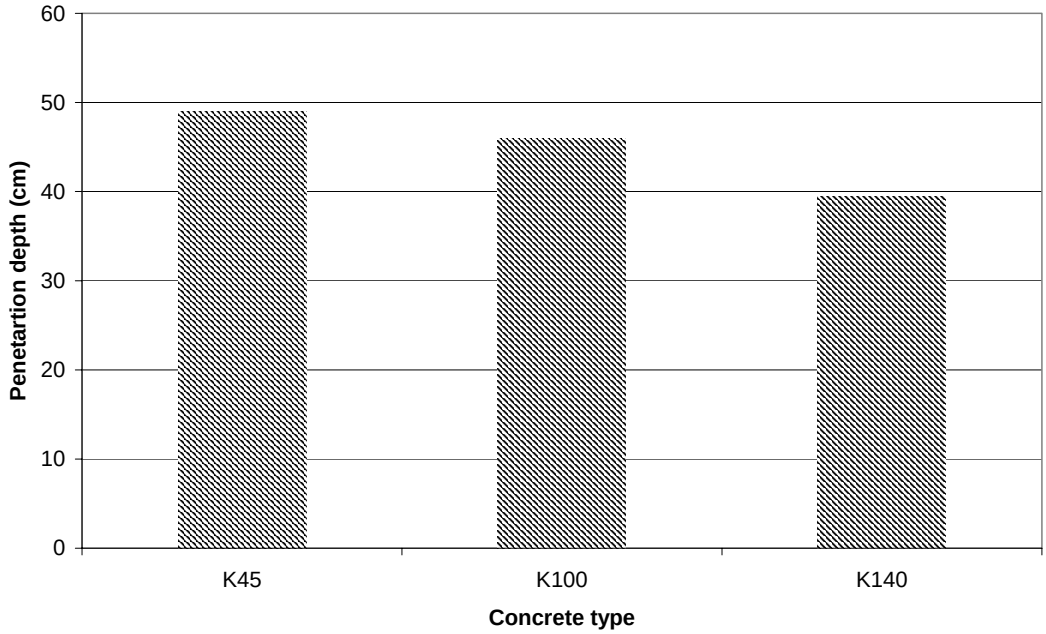

Figure 3.2. Penetration depths in K45, K100 and K140 grade concrete at an impact velocity of approximately 420 m/s and for the projectiles with a mass of 3.65 kg.

A normal strength concrete (NSC) target was used for comparison with the HPC targets. The post-test condition of this target is shown in figure 3.3, and the high-speed film from the test is shown in figure 3.4.

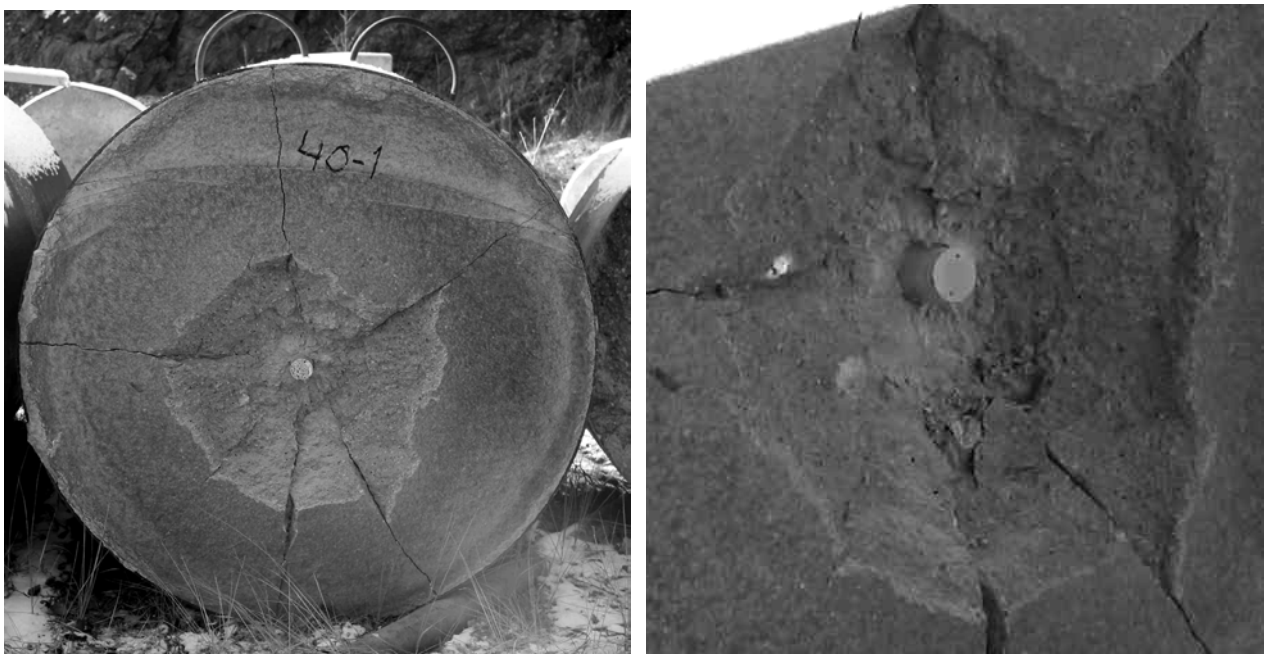

Figure 3.3. Normal strength concrete target after test number 2002-10, with a close up of the projectile shown to the right.

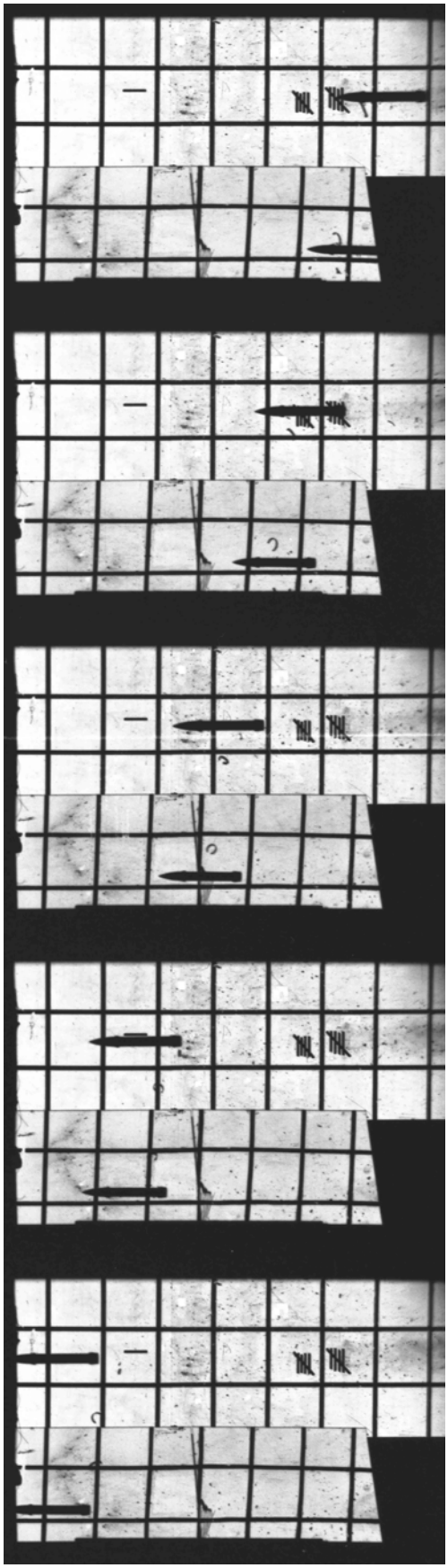

Figure 3.4. High-speed film from test number 2002-10 showing vertical and horizontal projections, see also figure 2.7.

Two tests with concrete grade K100 and approximate 415 m/s impact velocity were performed in 2002. The post-test conditions of these targets are shown in figure 3.5, and the projectiles are compared with an unfired one in figure 3.6. The projectile from test no. 2002-2 was slightly bent with a radius of approximately 11.3 m. This curvature is equal to 1.0 mm concaveness for 300 mm measurement length. The surface erosion was considered to be negligible for both projectiles.

A test with increased impact velocity to 462 m/s was also performed. This projectile fractured during the test due to the increased force caused by the higher impact velocity. The target and a close up of the projectile are shown in figure 3.7.

a) 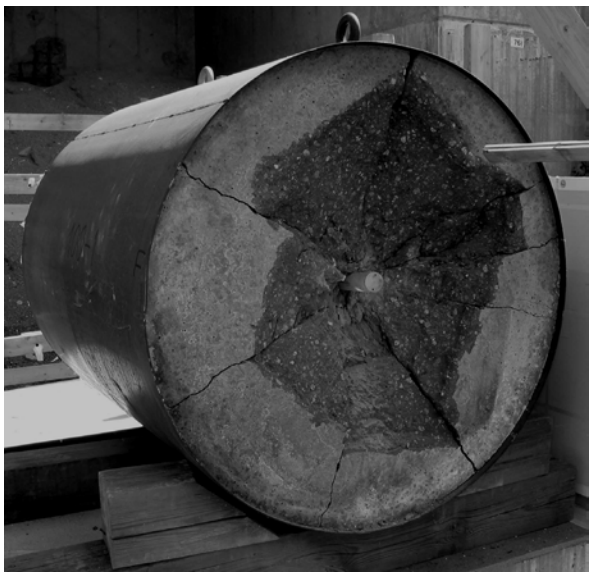 b) 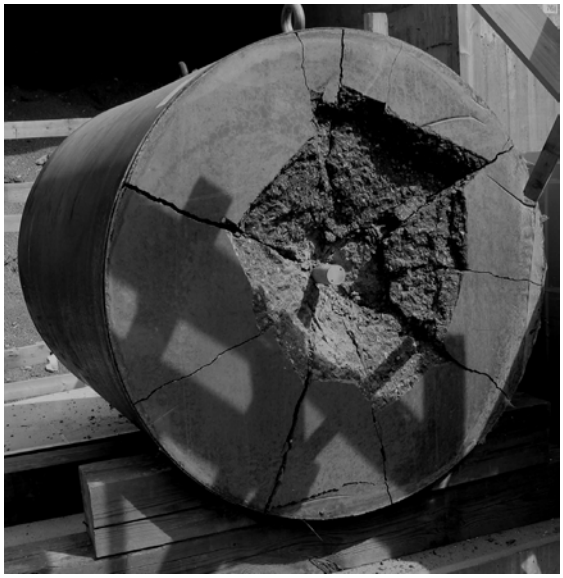

Figure 3.5. Targets from test numbers 2002-1 (a) and 2002-2 (b) with HPC K100 concrete.

Figure 3.6. Projectiles after tests compared with an unfired projectile, from top unfired projectile, test projectiles 2002-1 and 2002-2.

a)  b) 

Figure 3.7. The HPC K100 grade concrete target from test number 2002-3 with an increased impact velocity of approximately 460 m/s (a), and close up of the fractured projectile from this test.

The main objective of the test series in 2002 was to study the penetration resistance in HPC with 140 MPa nominal compressive cube strength, for this reason both short targets that were perforated and longer targets that stopped the projectile were used. The post-test conditions of the later targets are shown in figure 3.8, and the projectile from test 2002-7 is shown in figure 3.9

a)  b) 

Figure 3.8. Targets from test numbers 2002-4 (a) and 2002-7 (b) with HPC K140 concrete.

Figure 3.9. Projectile from test number 2002-7.

The test numbers 2002-11 and 2002-12 with 0.45 m targets resulted in perforation of the targets as shown earlier in table 3.1. The high-speed films from the front and rear side of the targets for these perforation tests are shown in figures 3.10 and 3.11, with post test conditions for the targets shown in figures 3.12 and 3.13. The projectiles from these tests are shown in figures 3.14 and 3.15, with approximately 90° rotation between the photos. The projectile from test 2002-11 is heavily bent.

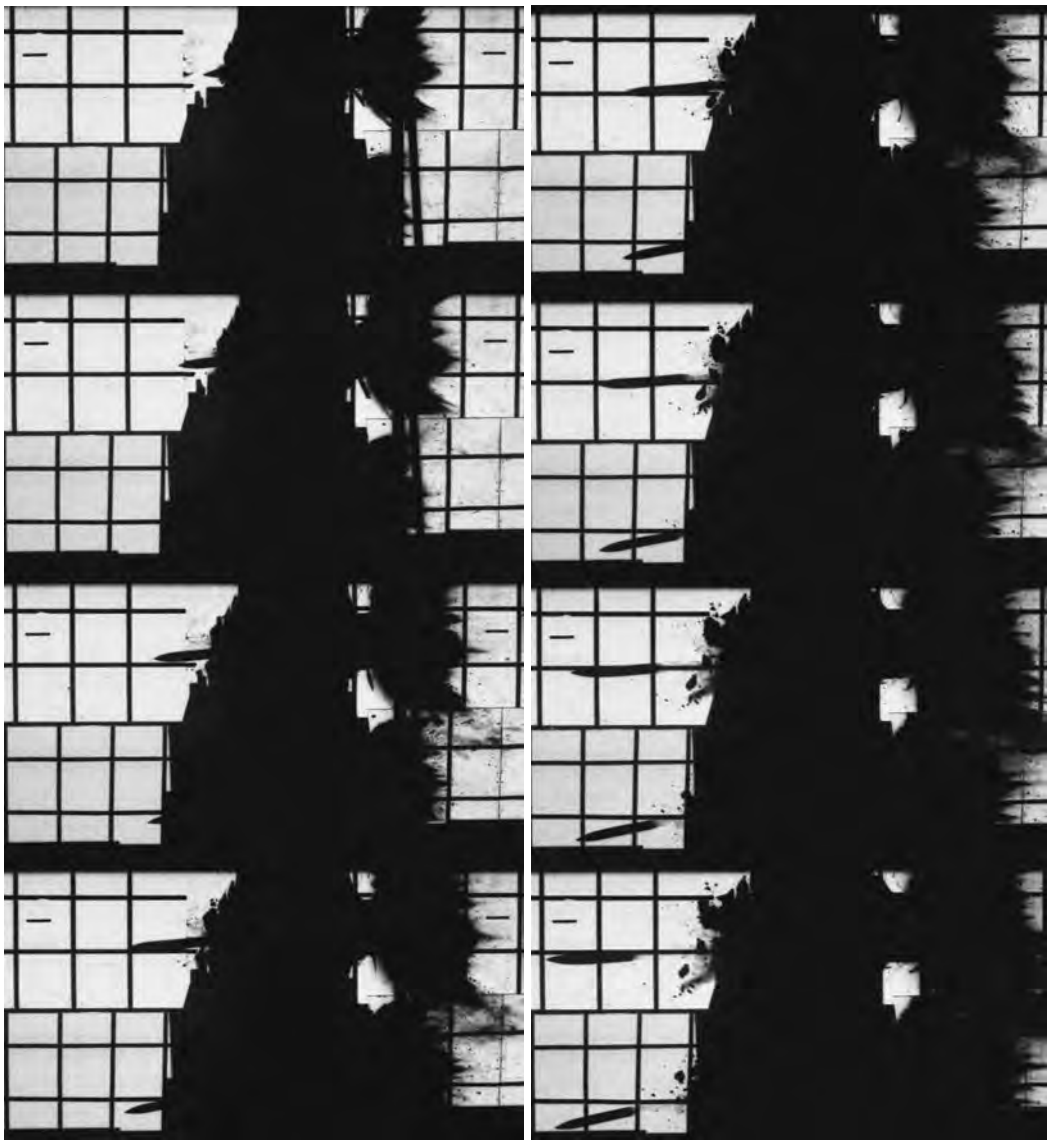

Figure 3.10. High-speed film from back face camera for test number 2002-11.

Figure 3.11. High-speed film from back face camera for test number 2002-12.

Figure 3.12. Target from test number 2002-11 with HPC K140 concrete, front face to the left and back face to the right.

Figure 3.13. Target from test number 2002-12 with HPC K140 concrete, front face to the left and back face to the right.

Figure 3.14. Projectile from test number 2002-11.

Figure 3.15. Projectile from test number 2002-12.

3.1.1. Summary of test series in 2002

The quality of the high speed photos for the first part of the test series was good, and both yaw and pitch could be determined with good resolution. However, the quality of the high speed photos for the second part of the test series was not that good. The mounting of the mirror to obtain the horizontal views needs to be improved for future test series. This is necessary to obtain a good quality of the photos in the future. The mirror should therefore be mounted on a flat panel, e.g. a steel plate, to prevent bending of the mirror. It is also important that the mirror is adjusted to give a horizontal view without parallax errors of the projectile. Due to the placement of the mirror it was not possible to obtain good data for the yaw of the projectiles before impact for several tests.

3.2. Test results from 2004

During 2004 tests of penetration in normal strength concrete, and also in HPC with approximately 135 MPa unconfined compressive strength, were performed. These concrete types were the same as for the earlier tests performed in 2002 (Hansson, 2003b). Further, tests with heavy reinforced normal strength concrete targets were also performed. Two impact angles were used during the tests, these were normal impact, i.e. 90°, and 59.5°. Two nominal impact velocities were also used for the tests, these were 420 m/s and 460 m/s. The projectile velocities were determined by three short circuit screens, and then checked against the high speed film. The yaw and pitch angles, and exit velocities, were also determined from the high speed films. Three types of projectile designs were used with different ogive radius, these were 150 mm, 400 mm and 600 mm. This corresponds to CRH (Calibre Radius Head) values of 3, 8 and 12. A digital high-speed video was also used for a few tests, these were tests numbers 2004-10, -18, -19, -23, -24, -26, -27 and -28. The frame rate for the high-speed video was 8000 frames/s with a resolution of 1024×256 pixels.

All the tests are compiled in tables 3.2 to 3.8, with further data given later in the report.

Table 3.2. Impact velocities and test results for concrete targets.

Test no.		**2004-1**	**2004-2**	**2004-3**	**2004-4**
Date	(yyyy-mm-dd)	2004-04-16	2004-04-27	2004-04-28	2004-05-04
Target	Concrete type	NSC	NSC	NSC	NSC
	Diameter	1.20 m	1.20 m	1.20 m	1.20 m
	Length	0.90 m	0.90 m	0.90 m	1.20 m
	Age in months	4.4	4.8	4.8	5.0
Projectile	CRH	3	3	8	8
	Impact velocity [1]	415 m/s	419 m/s	409 m/s	463 m/s
	Impact velocity [2]	415 m/s	415 m/s	404 m/s	455 m/s
	Impact angle	90°	90°	90°	90°
	Pitch [3]	0.56°	0.72°	1.25°	0.21°
	Yaw [3]	1.00°	0.84°	0.49°	0.42°
Exit velocity		---	---	---	---
Penetration depth [4]		54.5 cm	57.0 cm	62.0 cm	69.0 cm
Front crater	Diameter	≈55 cm	≈80 cm	≈60 cm	≈80 cm
	Depth [4]	≈10.0 cm	≈10.0 cm	≈12.5 cm	≈15.0 cm
Frame rates	1st camera	918/s	909/s	913/s	911/s
	2nd camera	Not used	Not used	Not used	Not used
Note					

Note: [1] Measured by short circuit screens.
[2] Measured from high speed film.
[3] Estimated measurement error: ≤0.20°
[4] Estimated within ±2.5 mm

Table 3.3. Impact velocities and test results for concrete targets.

Test no.		**2004-5**	**2004-6**	**2004-8**	**2004-10**
Date	(yyyy-mm-dd)	2004-05-05	2004-05-06	2004-05-10	2004-05-13
Target	Concrete type	NSC	NSC	HPC	HPC
	Diameter	1.20 m	1.20 m	1.20 m	1.20 m
	Length	0.90 m	0.60 m	0.51 m	0.75 m
	Age in months	5.0	5.1	5.7	5.8
Projectile	CRH	12	8	8	8
	Impact velocity [1]	422 m/s	425 m/s	421 m/s	422 m/s
	Impact velocity [2]	424 m/s	425 m/s	419 m/s	423 m/s
	Impact angle	90°	90°	90°	90°
	Pitch [3]	0.60°	1.10°	1.59°	1.01°
	Yaw [3]	0.41°	0.21°	0.30°	0.41°
Exit velocity		---	139 m/s	136 m/s	---
Penetration depth [4]		64.0 cm	---	---	48.0 cm
Front crater	Diameter	≈ 90 cm	60-65 cm	≈70 cm	≈70 cm
	Depth [4]	≈ 15.5 cm	≈11.0 cm	≈15.0 cm	≈21.0 cm
Back crater	Diameter	---	50-90 cm	25-27cm	---
	Depth [4]	---	≈ 15.5 cm	≈21.0 cm	---
Frame rates	1st camera	922/s	929/s	923/s	Out of order
	2nd camera	Not used	916/s	918/s	922/s
Note					

Note: [1] Measured by short circuit screens.
[2] Measured from high speed film.
[3] Estimated measurement error: ≤0.20°
[4] Estimated within ±2.5 mm

Table 3.4. Impact velocities and test results for concrete targets.

Test no.		**2004-12**	**2004-13**	**2004-14**	**2004-15**
Date	(yyyy-mm-dd)	2004-05-24	2004-05-25	2004-05-26	2004-05-27
Target	Concrete type	HPC	HPC	HPC	HPC
	Diameter	1.20 m	1.20 m	1.20 m	1.20 m
	Length	0.65 m	0.90 m	0.90 m	0.90 m
	Age in months	6.2	6.2	6.2	6.3
Projectile	CRH	8	3	12	8
	Impact velocity [1]	426 m/s	422 m/s	417 m/s	457 m/s
	Impact velocity [2]	423 m/s	422 m/s	414 m/s	452 m/s
	Impact angle	90°	90°	90°	90°
	Pitch [3]	1.54°	1.26°	0.14°	0.56°
	Yaw [3]	0.14°	0.14°	0.98°	0.61°
Exit velocity		---	---	---	---
Penetration depth [4]		50.0 cm	41.0 cm	49.5 cm	53.5 cm
Front crater	Diameter	≈105 cm	≈65 cm	≈60 cm	≈85 cm
	Depth [4]	≈25.0 cm	≈21.0 cm	≈16.5 cm	≈16.0 cm
Back crater	Diameter	25-60 cm	---	---	---
	Depth [4]	≈22.5 cm	---	---	---
Frame rates	1st camera	921/s	923/s	924/s	923/s
	2nd camera	Not used	Not used	Not used	Not used
Note		Back face spalling ≈67 m/s	Small fracture at back face of target	Small fracture at back face of target	L shaped fracture at back face of target

Note: [1] Measured by short circuit screens.
[2] Measured from high speed film.
[3] Estimated measurement error: ≤0.20°
[4] Estimated within ±2.5 mm

Table 3.5. Impact velocities and test results for concrete targets.

Test no.		**2004-16**	**2004-36**	**2004-17**	**2004-18**
Date	(yyyy-mm-dd)	2004-05-28	2004-06-01	2004-06-02	2004-06-23
Target	Concrete type	HPC	HPC	HPC	HPC
	Diameter	1.20 m	1.20 m	1.20 m	1.20 m
	Length	0.90 m	0.90 m	0.66 m	0.66 m
	Target angle	90°	90°	90°	90°
	Age in months	6.3	6.4	6.5	7.2
Projectile	CRH	12	3	8	12
	Impact velocity [1]	460 m/s	460 m/s	456 m/s	455 m/s
	Impact velocity [2]	455 m/s	456 m/s	448 m/s	448 m/s
	Impact angle	90°	90°	90°	90°
	Pitch [3]	1.23°	0.10°	0.14°	1.58°
	Yaw [3]	0.14°	0.26°	0.14°	1.51°
Exit velocity		---	---	---	---
Penetration depth [4]		56.0 cm	47.5 cm	54.0 cm	55.0 cm
Front crater	Diameter	≈80 cm	≈80 cm	≈95 cm	100-120 cm
	Depth [4]	≈19.0 cm	≈15.5 cm	≈16.5 cm	≈25.0 cm
Back crater	Diameter	---	---	---	---
	Depth [4]	---	---	---	---
Frame rates	1st camera	913/s	929/s	929/s	932/s
	2nd camera	Not used	Not used	Not used	Not used
Note		Fracture across back face of target	L shaped fracture at back face of target	The centre part of the target dislocated 2 cm	Damage of crater when target was moved

Note: [1] Measured by short circuit screens.
[2] Measured from high speed film.
[3] Estimated measurement error: ≤0.20°
[4] Estimated within ±2.5 mm

Table 3.6. Impact velocities and test results for concrete targets.

Test no.		**2004-19**	**2004-20**	**2004-21***
Date	(yyyy-mm-dd)	2004-06-08	2004-06-09	2004-06-07
Target	Concrete type	Reinforced NSC	Reinforced NSC	NSC
	Width	1.20 m	1.20 m	1.20 m
	Height	1.20 m	1.20 m	1.20 m
	Length	0.60 m	0.60 m	1.20 m
	Age in months	6.1	6.2	6.1
Projectile	CRH	3	8	8
	Impact velocity [1]	422 m/s	424 m/s	424 m/s
	Impact velocity [2]	416 m/s	416 m/s	421 m/s
	Impact angle	90°	90°	90°
	Pitch [3]	0.55°	0.55°	2.44°
	Yaw [3]	0.41°	0.69°	1.12°
Exit velocity		---	---	---
Penetration depth [4]		48.5 cm	53.0 cm	>120 cm
Front crater	Diameter	55-60 cm	50-60 cm	Totally destroyed target ---
	Depth [4]	≈4.5 cm	≈4.5 cm	
Back crater	Diameter	≈70 cm	70-80 cm	
	Depth [4]	≈5.0 cm	≈5.0 cm	
Frame rates	1st camera	918/s	926/s	927/s
	2nd camera	Not used	Not used	Not used
Note		Spalling recovered directly behind target	Spalling recovered directly behind target	Perforation of target with negligible exit velocity

Note: [1] Measured by short circuit screens.
[2] Measured from high speed film.
[3] Estimated measurement error: ≤0.20°
[4] Estimated within ±2.5 mm
* Target for test no. 2004-21 was without steel confinement and reinforcement.

Table 3.7. Impact velocities and test results for concrete targets.

Test no.		**2004-23-1**	**2004-23-2**	**2004-24-1**	**2004-24-2**
Date	(yyyy-mm-dd)	2004-06-15	2004-06-14	2004-06-16	2004-06-16
Target	Concrete type	Reinforced Normal Strenght Concrete			
	Width	1.20 m	1.20 m	1.20 m	1.20 m
	Height	1.50 m	1.50 m	1.50 m	1.50 m
	Length	0.54 m	0.54 m	0.54 m	0.54 m
	Age in months	6.4	6.3	6.4	6.4
Projectile	CRH	3	3	8	8
	Impact velocity [1]	424 m/s	423 m/s	421 m/s	420 m/s
	Impact velocity [2]	422 m/s	425 m/s	420 m/s	417 m/s
	Impact angle	59.5° ±¼°	59.5° ±¼°	59.5° ±¼°	59.5°±¼°
	Pitch [3]	2.19°	1.47°	1.59°	1.06°
	Yaw [3]	0.39°	0.59°	0.38°	0.14°
Exit velocity		---	---	---	---
Penetration depth [4]		35.0 cm	34.0 cm	39.0 cm	34.5 cm
Estimated penetration path		56.0 cm	50.0 cm	56.5 cm	71.0 cm
Angle between projectile and front face of target		≈39°	≈43°	≈45.5°	≈29°
Front crater	Diameter	85-90 cm	55-60 cm	≈60 cm	85-100 cm
	Depth [4]	10.5 cm	3.0 cm	8.0 cm	8.5 cm
Back crater	Diameter	---	---	---	Minor spalling
	Depth [4]	---	---	---	---
Frame rates	1st camera	937/s	942/s	910/s	923/s
	2nd camera	Not used	Not used	Not used	Not used
Note		Test no. 2 in target 2004-23 Fractures on target back face	Test no. 1 in target 2004-23 Small fractures on target back face	Test no. 1 in target 2004-24 Fractures on target back face	Test no. 2 in target 2004-24

Note: [1] Measured by short circuit screens.
[2] Measured from high speed film.
[3] Estimated measurement error: ≤0.20°
[4] Estimated within ±2.5 mm

Table 3.8. Impact velocities and test results for concrete targets.

Test no.		**2004-25**	**2004-26**	**2004-27**	**2004-28**
Date	(yyyy-mm-dd)	2004-08-08	2004-08-09	2004-09-13	2004-09-14
Target	Concrete type	NSC	NSC	HPC	HPC
	Diameter	1.50 m	1.50 m	1.50 m	1.50 m
	Length	0.54 m	0.54 m	0.45 m	0.45 m
	Age in months	8.1	8.2	9.8	9.9
Projectile	CRH	8	8	8	8
	Impact velocity [1]	424 m/s	422 m/s	421 m/s	456 m/s
	Impact velocity [2]	419 m/s	422 m/s	418 m/s	459 m/s
	Impact angle	59.5° ±¼°	59.5° ±¼°	59.5° ±¼°	59.5°±¼°
	Pitch [3]	1.07°	1.19°	1.01°	0.39°
	Yaw [3]	0.00°	0.23°	0.81°	0.77°
Exit velocity		16 m/s	---	---	---
Penetration depth [4]		---	≈50 cm	≈25 cm	≈25 cm
Estimated penetration path		---	---	≈70 cm	≈80 cm
Angle between projectile and front face of target		---	≈40°	---	---
Front crater	Diameter	80-90 cm	≈65 cm	---	85-100 cm
	Depth	≈24 cm	≈23 cm	≈25 cm	≈25 cm
Back crater	Diameter	90-105 cm	75-105 cm	---	---
	Depth	≈22 cm	≈18 cm	---	---
Frame rates	1st camera	916/s	921/s	927/s	935/s
	2nd camera	913/s	Not used	Not used	Not used
Note			Angle between projectile and front face of target: 40°	Projectile recovered in front of target after deflection	Fracture on the back face of target

Note: [1] Measured by short circuit screens.
[2] Measured from high speed film.
[3] Estimated measurement error: ≤0.20°
[4] Penetration depth measured perpendicular to front face of target.

The measured impact conditions for the tests are compiled in figures 3.16 and 3.17. The impact velocities for the projectiles measured with short circuit screens is in good agreement with velocities obtained from the high-speed films. The pitch and yaw for the projectiles determined from high-speed films, with an average value of 1.00° for the pitch and an average value of 0.50° for the yaw.

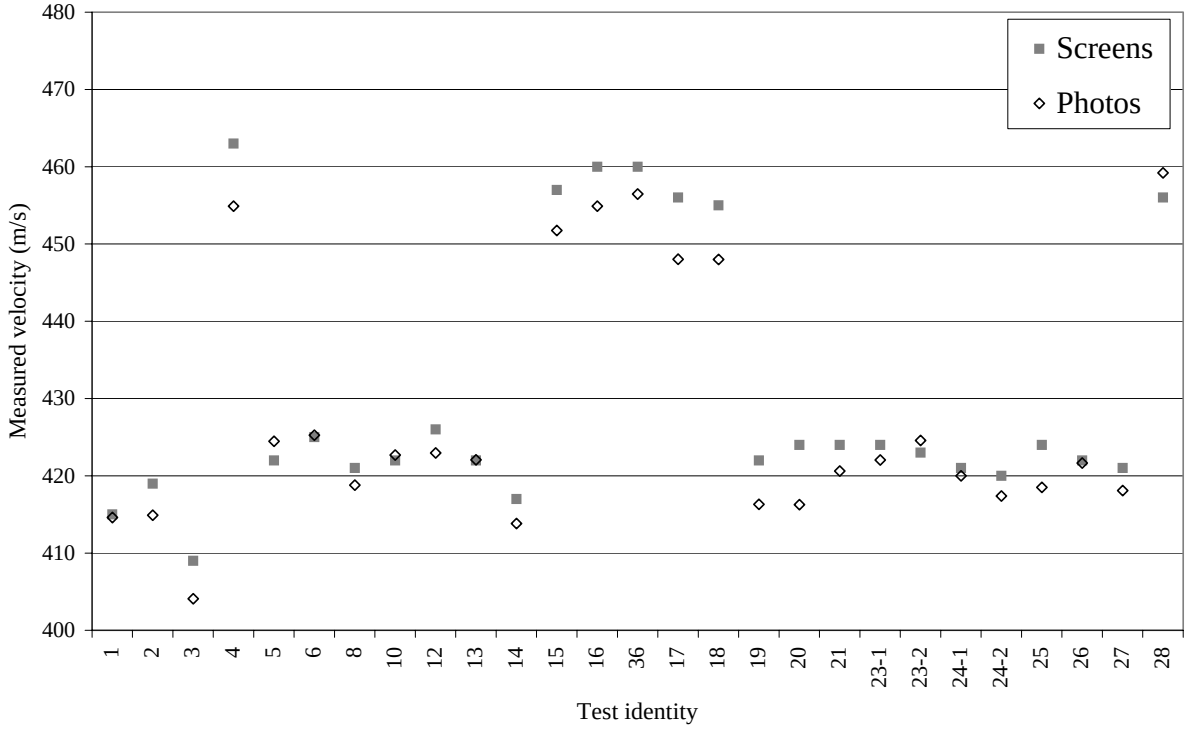

Figure 3.16. Comparison between impact velocities for the test series measured with short circuit screens and determined from high-speed film.

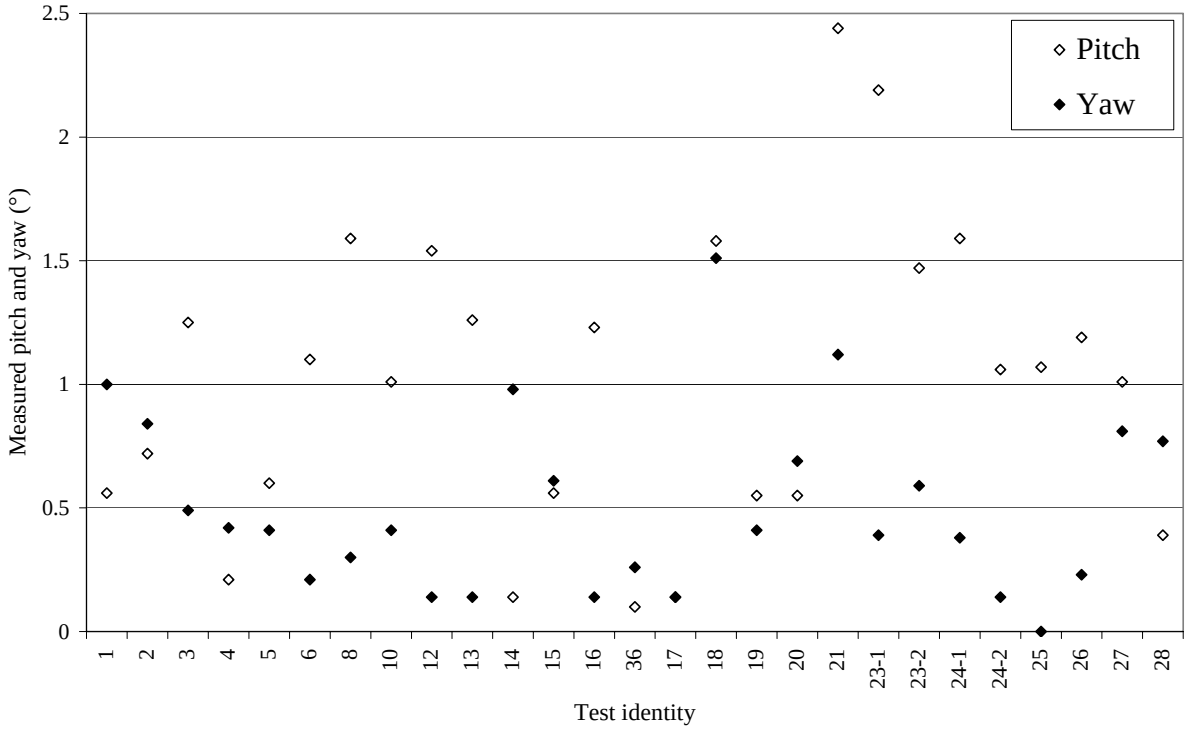

Figure 3.17. Measured pitch and yaw of the projectiles from high-speed film frames before impact of targets. The average values for the pitch and yaw are 1.00° and 0.50°, respectively.

3.2.1. Tests with normal impact angle of the projectile

Tests with an impact angle of the projectile close to 90° were performed with confined concrete targets of NSC and HPC, reinforced NSC targets, and also an unreinforced and unconfined NSC target. The location of the cylindrical concrete targets is shown in figure 3.18 below, with a similar arrangement also used for the other targets with normal impact angle.

Figure 3.18. Target location for tests with normal impact angle.

Unreinforced concrete targets

The first two tests in the unreinforced NSC used the projectile design with a CRH value of 3, and the impact velocities were 415 m/s and 419 m/s, respectively. This resulted in the penetration depths of approximately 54.5 cm for test 2004-1 and 57.0 cm for test 2004-2. Post test photos of these targets are shown in figures 3.19 and 3.20. Test no. 2004-3 used the projectile design with a CRH value of 8. This projectile impacted the target at 409 m/s with a resulting penetration depth of approximately 62.0 cm. Post test photos of this target are shown in figure 3.21.

Figure 3.19. Normal strength concrete target after test number 2004-1, front and back views.

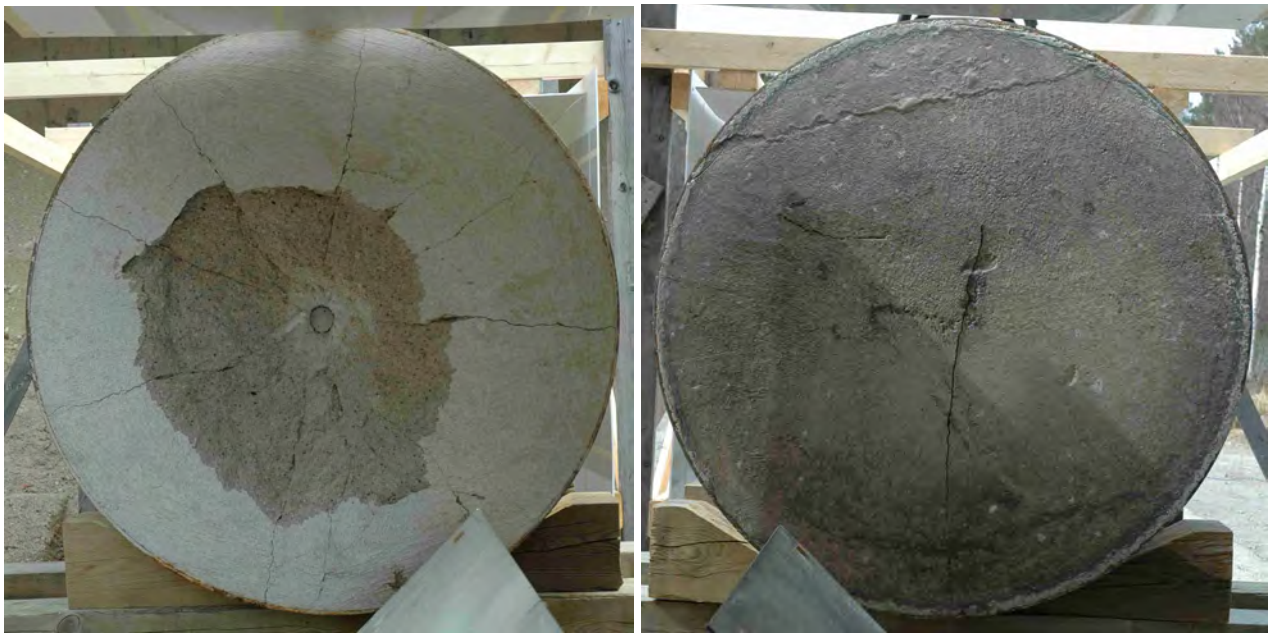

Figure 3.20. Normal strength concrete target after test number 2004-2, front and back views.

Figure 3.21. Normal strength concrete target after test number 2004-3, front and back views.

The impact velocity for test 2004-4 in the NSC was increased to 463 m/s, resulting in an increased penetration depth to approximately 69.0 cm for the projectile with CRH value of 8. The post test condition of this target is shown in figure 3.22. The projectile with a CRH value of 12 was also used for penetration test no. 2004-5 against a NSC target. The penetration depth was approximately 64.0 cm for an impact velocity of 422 m/s for this test. This is approximately the same impact velocity and penetration depth as for test no. 2004-3 earlier discussed. The post test condition of this target is shown in figure 3.23.

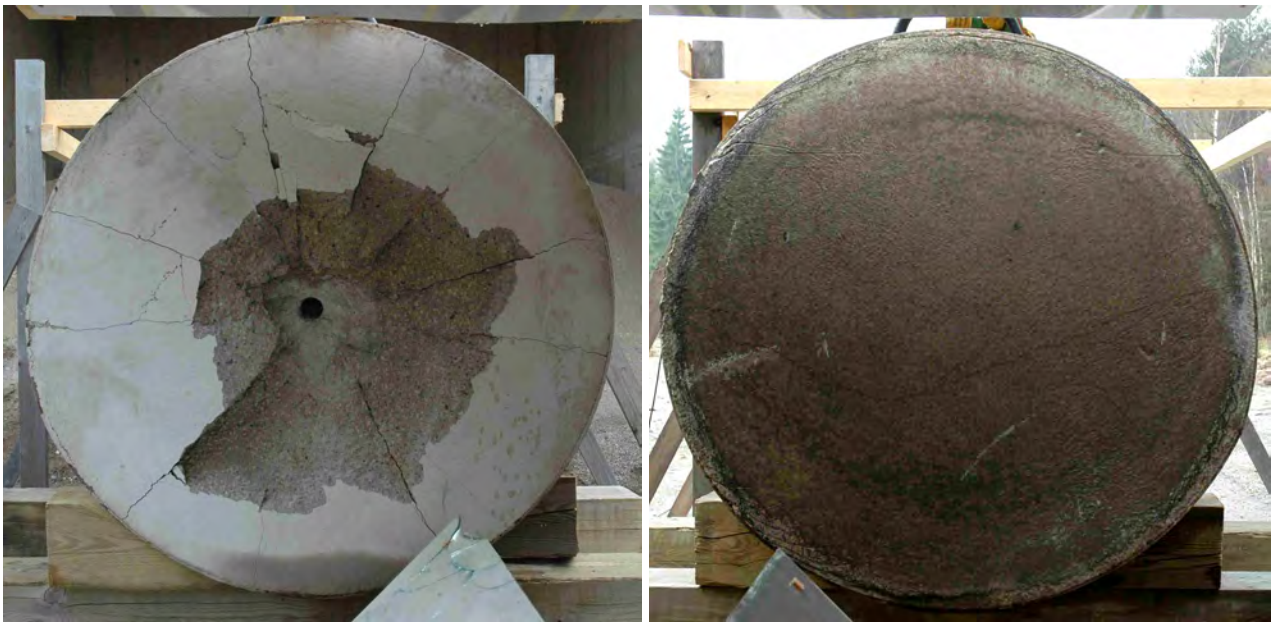

Figure 3.22. Normal strength concrete target after test number 2004-4, front and back views.

Figure 3.23. Normal strength concrete target after test number 2004-5, front and back views.

The last test of a confined NSC was performed against a 60 cm thick target, resulting in perforation of the target with an exit velocity of approximately 139 m/s for an impact velocity of 425 m/s. The target from this test, i.e. 2004-6, is shown in figure 3.24. The same test set up was used for a confined HPC with a thickness of 51 cm, resulting in an exit velocity of 136 m/s for an impact velocity of 421 m/s. The target from this test, i.e. 2004-8, is shown in figure 3.25. The high speed films from these two tests are shown in figure 3.26. Both these tests were performed with the projectile design using a CRH value of 8.

Figure 3.24. Normal strength concrete target after test number 2004-6, front and back views.

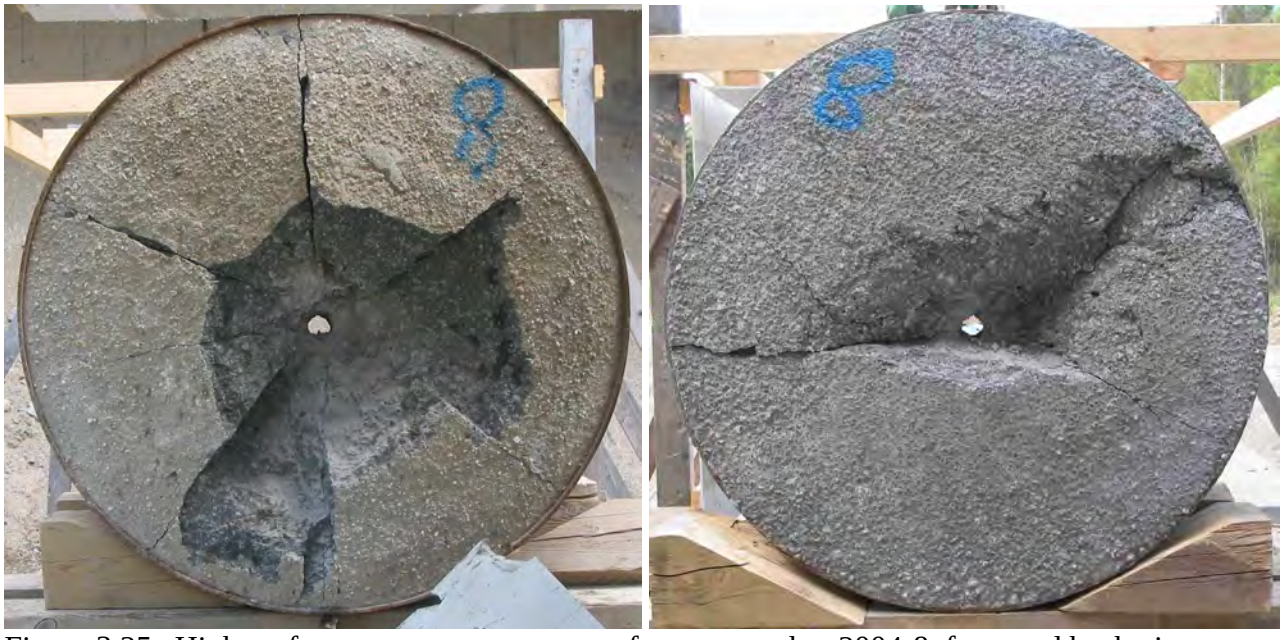

Figure 3.25. High performance concrete target after test number 2004-8, front and back views.

a) b)

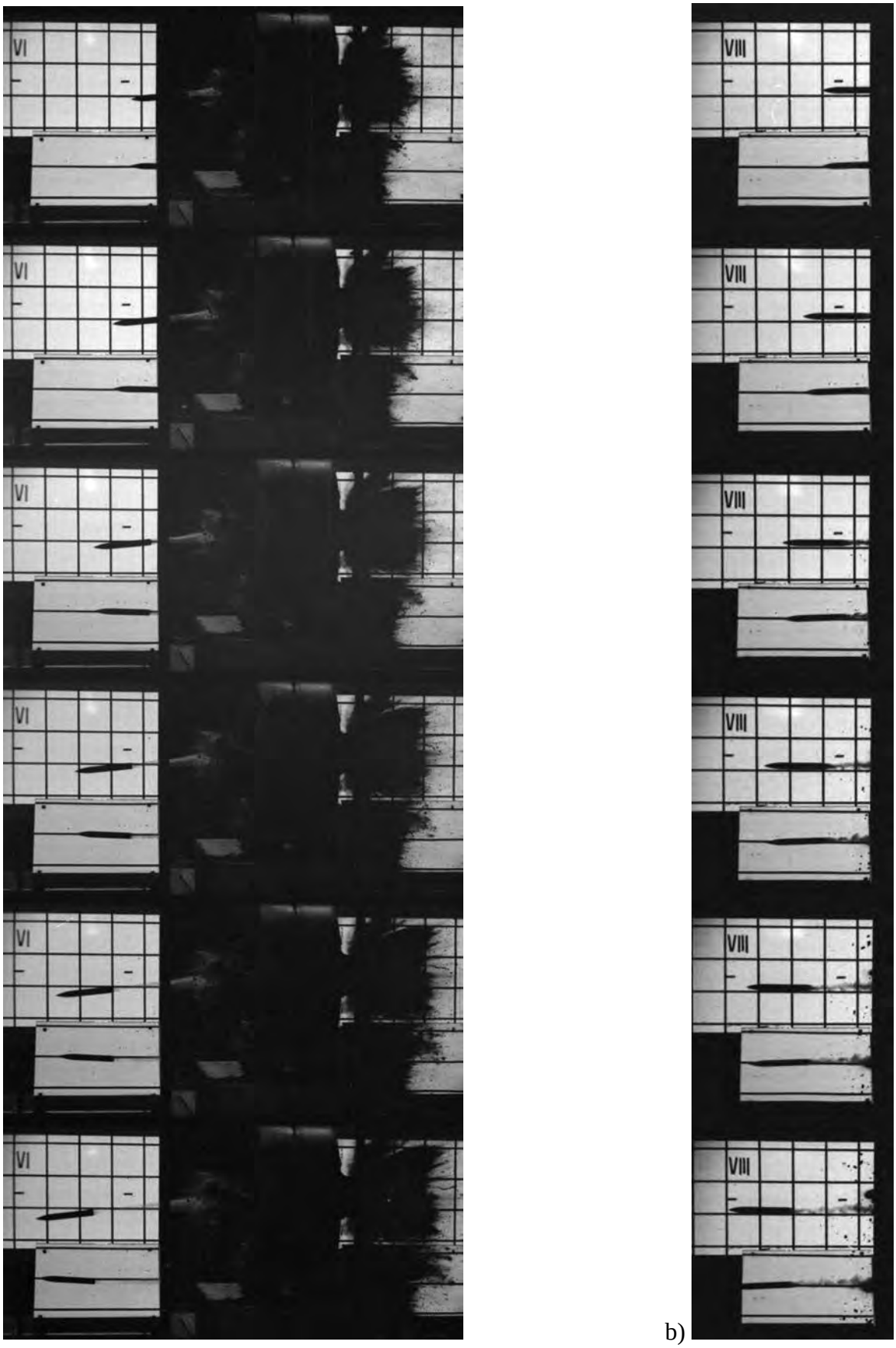

Figure 3.26. High-speed films of back face from test numbers 2004-6 (a) and 2004-8 (b).

The target thickness was then varied to obtain a ballistic thickness for the HPC, using the projectile with a CRH value of 8. The tests 2004-10 and 2004-12 used 75 cm and 65 cm targets, respectively. The impact velocity for test no. 2004-10 was 422 m/s, resulting in a penetration depth of approximately 48.0 cm. For test no. 2004-12 the penetration depth was approximately 50.0 cm for an impact velocity of 426 m/s. The penetration depths and impact velocities are approximately the same for both tests. However, the projectile is visible in the back face crater for the target with 65 cm thickness. These targets are shown in figures 3.27 and 3.28.

Figure 3.27. High performance concrete target after test number 2004-10, front and back views.

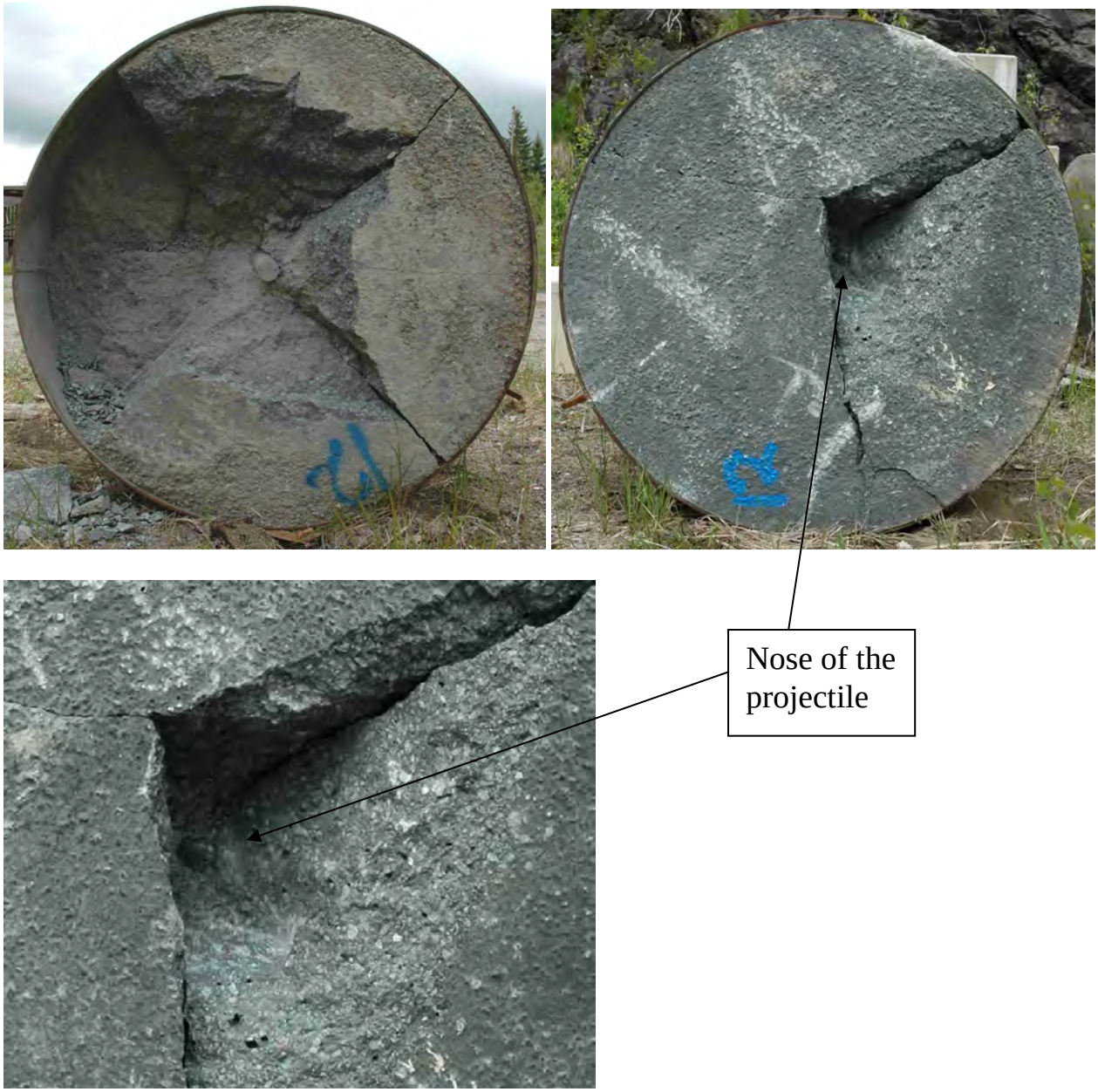

Figure 3.28. High performance concrete target after test number 2004-12, incl. detail of back face crater with projectile.

The influence of the ogive radius of the projectile on the penetration in HPC was studied by performing two tests using the projectile designs with CRH values of 3 and 12. Test no. 2004-13 used a projectile with an ogive radius of 150 mm and impacted the target at 422 m/s, resulting in a penetration depth of approximately 41.0 cm. Test no. 2004-14 used a projectile with an ogive radius of 600 mm and impacted the target at 417 m/s, resulting in a penetration depth of approximately 49.5 cm. Comparing this with the earlier discussed test 2004-10 it is seen that the penetration increases for an increase of the CRH value from 3 to 8. However, for a further increase of the CRH value to 12 there is only minor increase of the penetration depth. The same phenomenon was seen for the NSC targets earlier. The post test conditions of targets numbers 2004-13 and 2004-14 are shown in figures 3.29 and 3.30, respectively.

Figure 3.29. High performance concrete target after test number 2004-13, front and back views.

Figure 3.30. High performance concrete target after test number 2004-14, front and back views.

An increase of the impact velocity from 422 m/s to 457 m/s, for the projectile design with a CRH value of 8, increased the penetration depth from approximately 48.0 cm for test no. 2004-10 to approximately 53.5 cm for test no. 2004-15. Further, an increase of the impact velocity from 417 m/s to 460 m/s, for the projectile design with a CRH value of 12, increased the penetration depth from approximately 49.5 cm for test no. 2004-14 to approximately 56.0 cm for test no. 2004-16. Comparing the different projectile designs, i.e. with CRH values of 8 and 12, at the nominal impact velocity of 460 m/s shows only minor difference for the penetration depth. The targets from tests numbers 2004-15 and 2004-16 are shown in figures 3.31 and 3.32, respectively.

Figure 3.31. High performance concrete target after test number 2004-15, front and back views.

Figure 3.32. High performance concrete target after test number 2004-16, front and back views.

An additional test was performed at 460 m/s with the use of a projectile with an ogive radius of 150 mm, resulting in a penetration depth of approximately 47.5 cm for test no. 2004-36. For this projectile type the penetration depth was 41.0 cm at an impact velocity of 422 m/s, i.e. test no. 2004-13. The target 2004-36 is shown in figure 3.33.

Figure 3.33. High performance concrete target after test number 2004-36, front and back views.

Tests were conducted to obtain a ballistic thickness of the HPC at the higher nominal impact velocity. Two tests were therefore performed with a target thickness of 66 cm. Test no. 2004-17 used the projectile design with CRH value of 8 and an impact velocity of 456 m/s, resulting in a penetration depth of approximately 54.0 cm. Test no. 2004-18 used the projectile design with CRH value of 12 and an impact velocity of 455 m/s, resulting in a penetration depth of approximately 55.0 cm. For this test both yaw and pitch for the projectile were approximately 1.5°. However, the influence on the penetration depths are almost neglectable for tests with 66 cm targets when comparing with the earlier tests, i.e. numbers 2004-15 and 2004-16. The post test conditions of targets 2004-17 and 2004-18 are shown in figures 3.34 and 3.35, respectively.

Figure 3.34. High performance concrete target after test number 2004-17, front and back views.

Figure 3.35. High performance concrete target after test number 2004-18, front and back views.

Reinforced concrete targets

Two tests were performed in reinforced concrete with approximately normal impact of the projectiles. The targets are 1.20 m by 1.20 m, with a thickness of 0.60 m. The projectiles for test numbers 2004-19 and 2004-20 were with CRH values 3 and 8, respectively. The projectile with CRH value of 3 impacted the target at a velocity of 422 m/s and penetrated to a depth of approximately 48.5 cm. The projectile with CRH value of 8 impacted the target at a velocity of 424 m/s and penetrated to a depth of approximately 53.0 cm. Back face spalling occurred for both tests. However, the visual damage at the back face was limited to the concrete cover behind the reinforcement. Post test photos of the reinforced targets are shown in figures 3.36 and 3.37. The impact event for test no. 2004-19, with a CRH value of the projectile of 3, was recorded by the high speed video and is shown in figures 3.38 and 3.39.

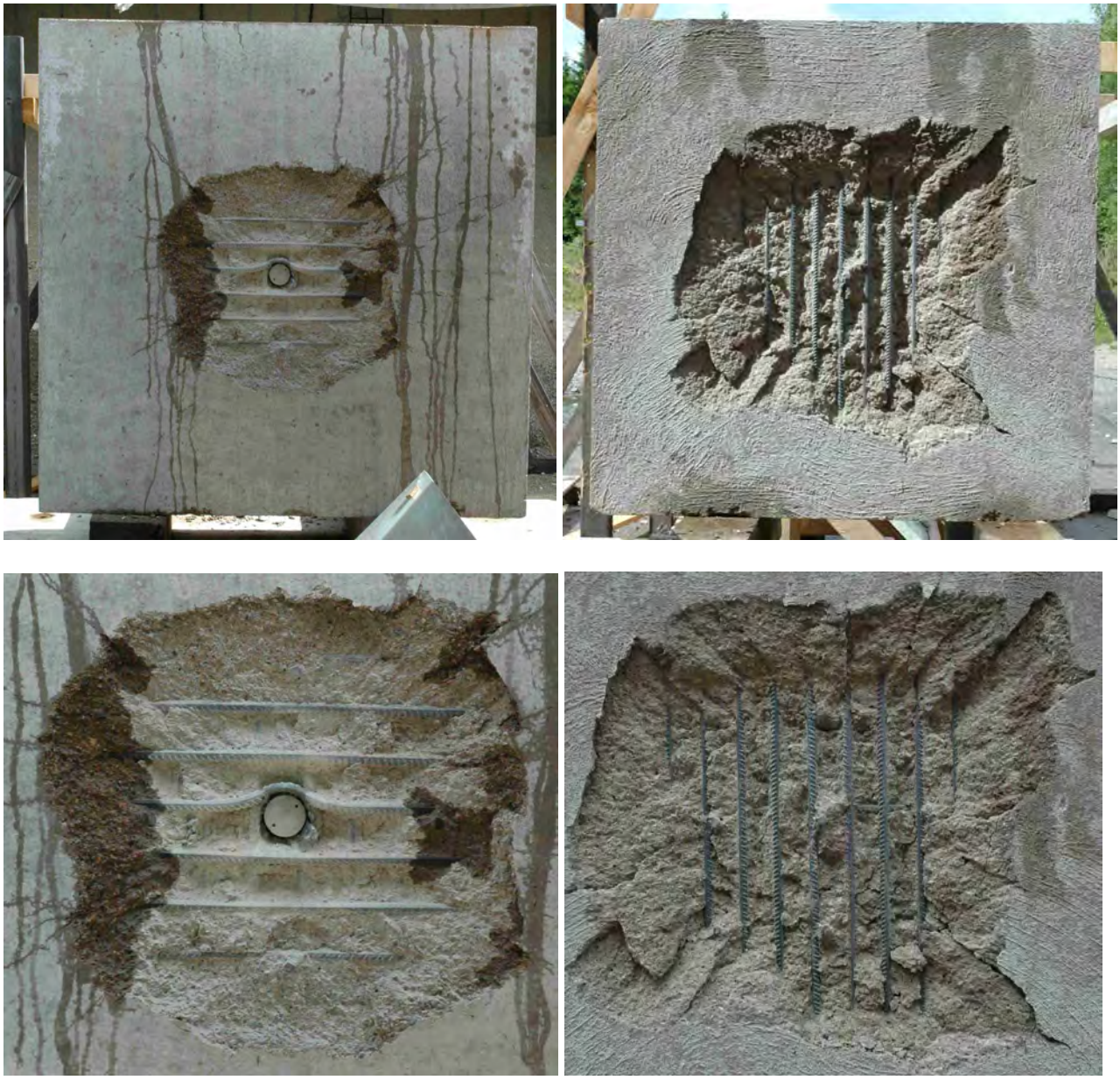

Figure 3.36. Reinforced normal strength concrete target after test number 2004-19, incl. details of craters. Front views to the left, and back face shown to the right.

Figure 3.37. Reinforced normal strength concrete target after test number 2004-20, incl. details of craters. Front views to the left, and back face shown to the right.

Figure 3.38. Frames from high-speed video of test no. 2004-19, before impact.

Figure 3.39. Frames from high-speed video of test no. 2004-19, after impact.

Unreinforced and unconfined concrete target

The influence from the boundary effect was studied by comparing the earlier shown targets with steel confinement or reinforcement, with an unreinforced target without confinement. This target was 1.2 m thick, and as expected it was completely destroyed and the projectile with a CRH value of 8 was recovered behind the target. The impact velocity for this test, i.e. 2004-21, was 424 m/s. Photos of the target before and after impact are shown in figure 3.40, and the recovered projectile is shown in figure 3.41.

Figure 3.40. Normal strength concrete target without confinement and reinforcement before and after test number 2004-21.

Figure 3.41. Recovered projectile after test no. 2004-21.

Summary of tests with normal impact angle

The penetration depths from the tests with approximately normal impact conditions are compiled in figures 3.42 to 3.43. The increase of the ogive radius from 150 mm to 400 mm, i.e. from CRH value 3 to 8, results in a considerable increase of the penetration depths, However, a further increase of the CRH value to higher than 8 is only considered to result in a minor increase of the penetration depth for projectiles with a normal impact angle. This is shown in figure 3.43 were the projectiles with a CRH value of twelve has only a small increase of the penetration depth compared to the projectiles with a CRH value of 8. The introducing of reinforcement for a NSC target, or the use of HPC, reduces the penetration depths.

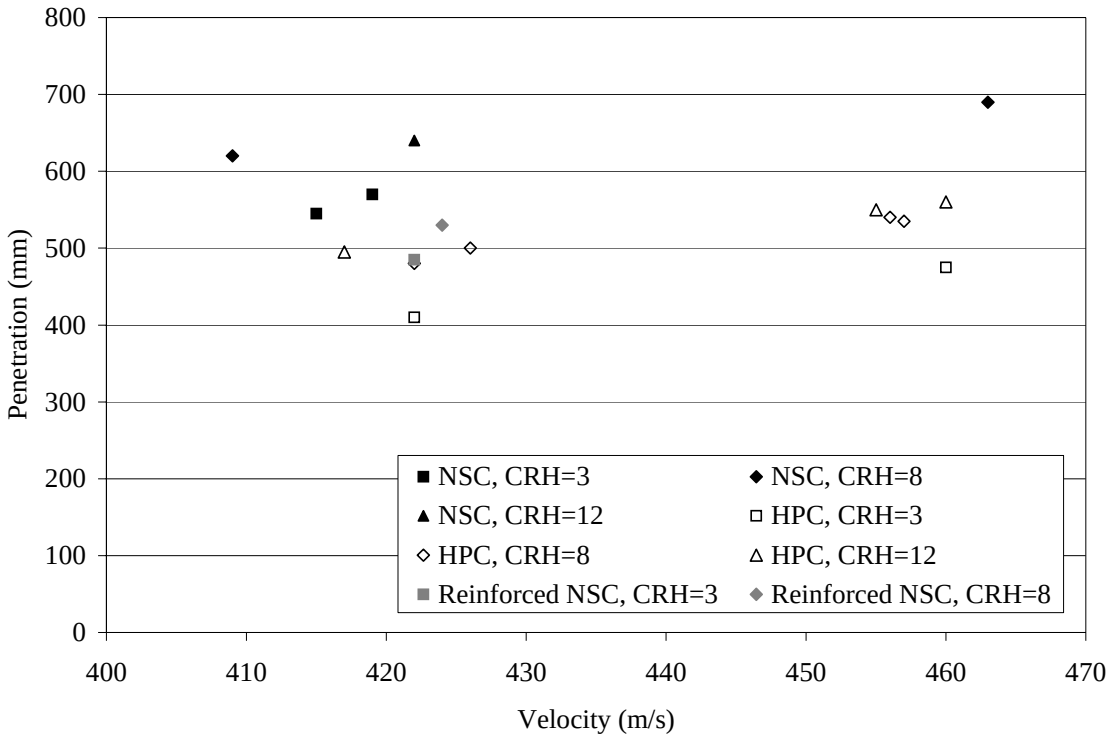

Figure 3.42. Penetration depths vs. impact velocity for tests with normal impact angle, and for the projectiles with approximately 4.50 kg mass.

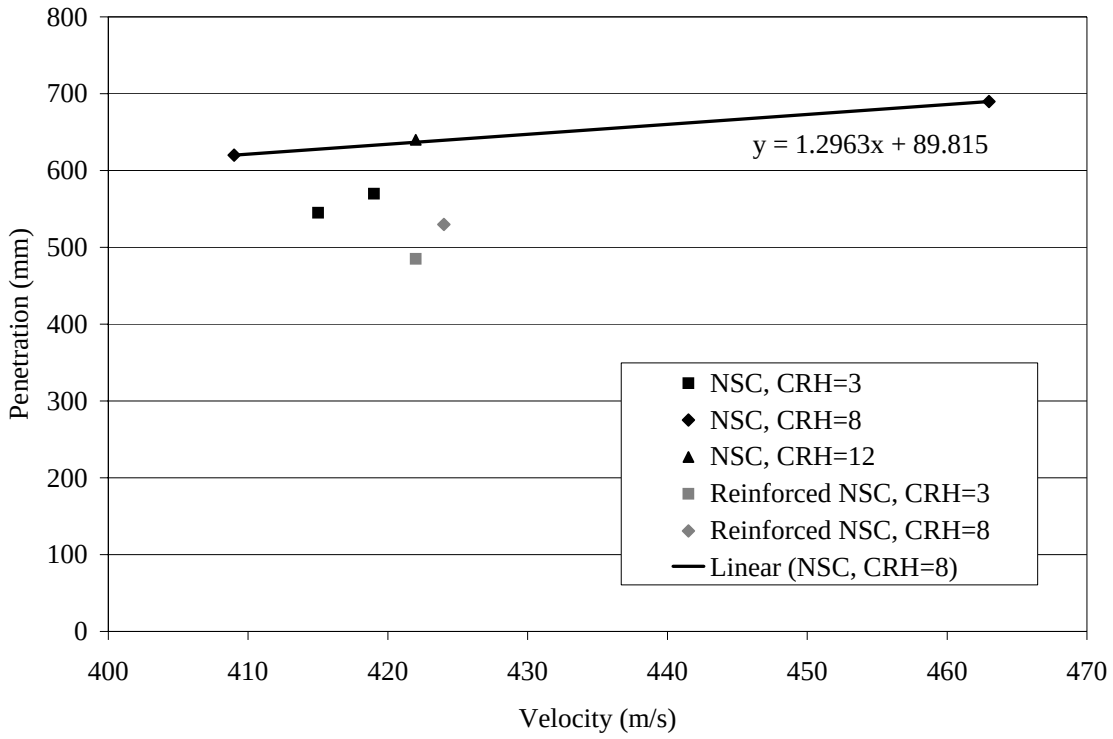

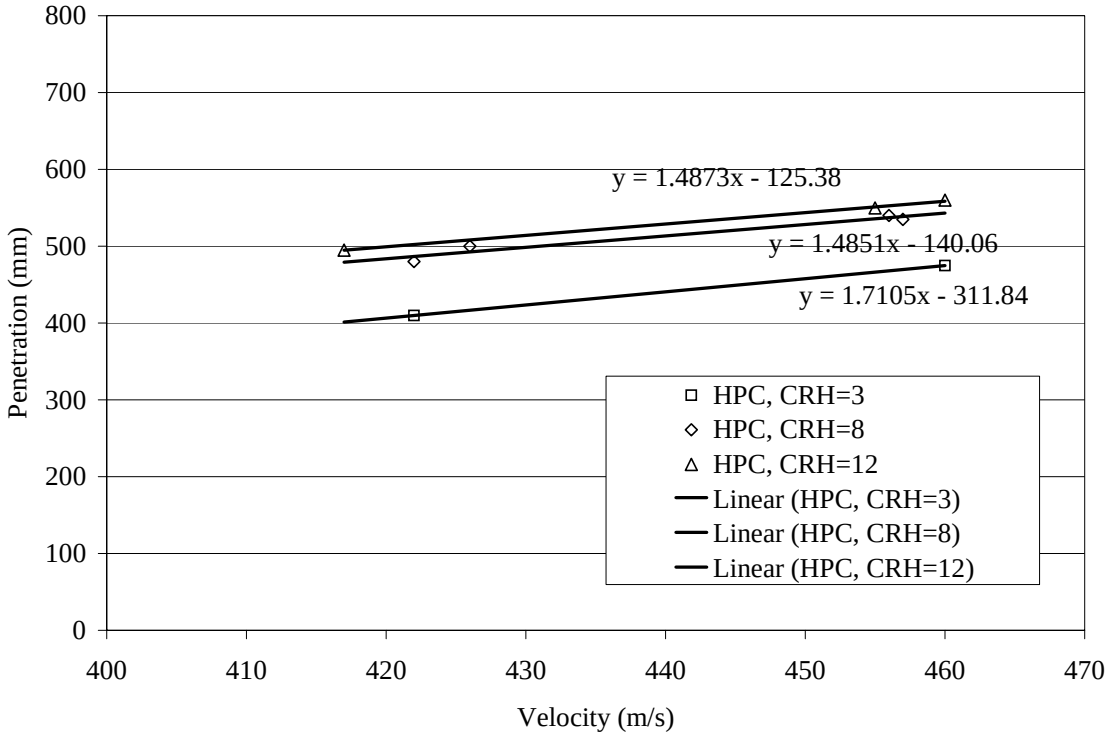

Figure 3.43. Penetration depths vs. impact velocity for tests with normal impact angle for NSC and HPC, respectively. The masses of the projectiles are approximately 4.50 kg. Linear approximations for the data sets are also given.

3.2.2. Tests with approximately 60° impact angle of the projectile

Test with an impact angle of the projectile close to 59.5° were performed with confined concrete targets of NSC and HPC, and reinforced NSC targets.

Unreinforced concrete targets

Tests with inclined unreinforced targets were performed using both NSC and HPC targets. The targets were placed in a rig to obtain the same angle for each test, and the line of sight through the gun barrel was determined by a laser and adjusted approximately through the centre of the target. The height of the projectile impact is marked with a white tape strip in figure 3.44 below.
The targets for these tests have a diameter of 1.50 m. The thickness for the NSC and HPC targets are 0.54 m and 0.45 m, respectively.

Figure 3.44. Target location for test no. 2004-25 to 2004-28.

The targets for test numbers 2004-25 and 2004-26 were 54 cm unreinforced NSC, and for targets 2004-27 and 2004-28 the 45 cm thick targets were of unreinforced HPC. All these tests used the projectile design with a CRH value of 8. The impact velocity for test no. 2004-25 was 424 m/s, resulting in a perforation of the target and an exit velocity for the projectile of 16 m/s. For test no. 2004-26 the impact velocity was 422 m/s, and the projectile was stopped close to the back face of the target. These targets are shown in figures 3.45 and 3.46, with the recovered projectile from test no. 2004-25 shown in figure 3.47. Figure 3.48 show the high-speed films of the front and back face of target 2004-25, with figure 3.49 showing frames from the high-speed video of test no. 2004-26.

The two tests of inclined HPC targets were performed at impact velocities 421 and 456 m/s. Both these tests resulted in a similar behaviour, with the projectile recovered in front of the target for the first test at the lower velocity, and the projectile recovered in the front face crater for the second test with increased impact velocity. Post test photos of the HPC targets from tests 2004-27 and 2004-28 are shown in figures 3.50 and 3.51, with the recovered projectiles shown in figure 3.52.

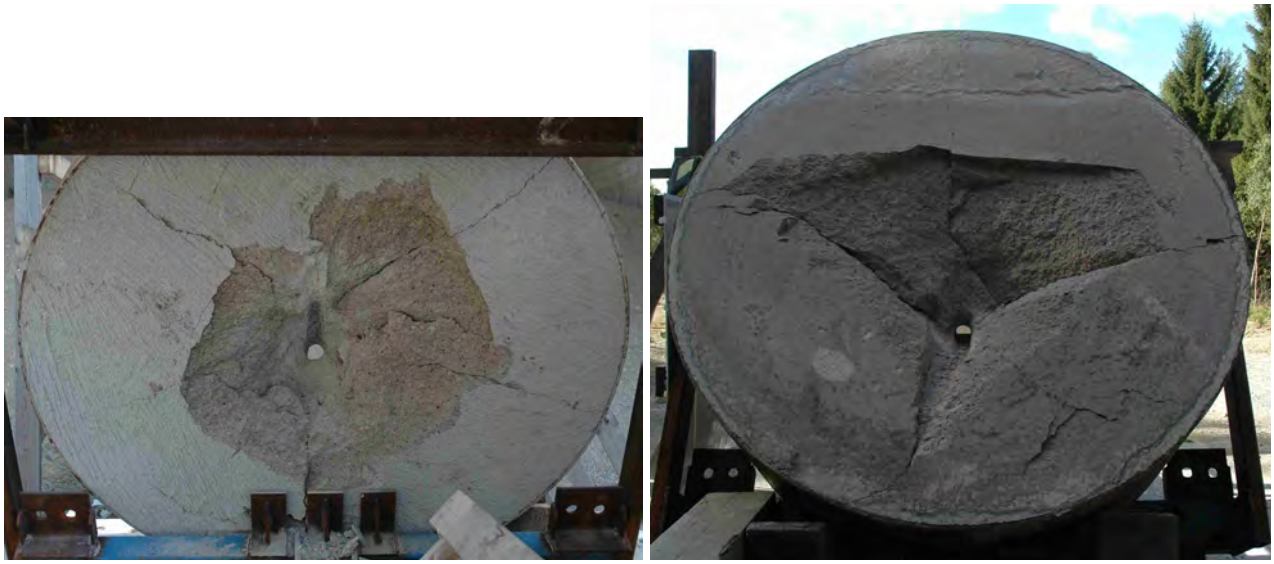

Figure 3.45. Normal strength concrete targets after test number 2004-25.

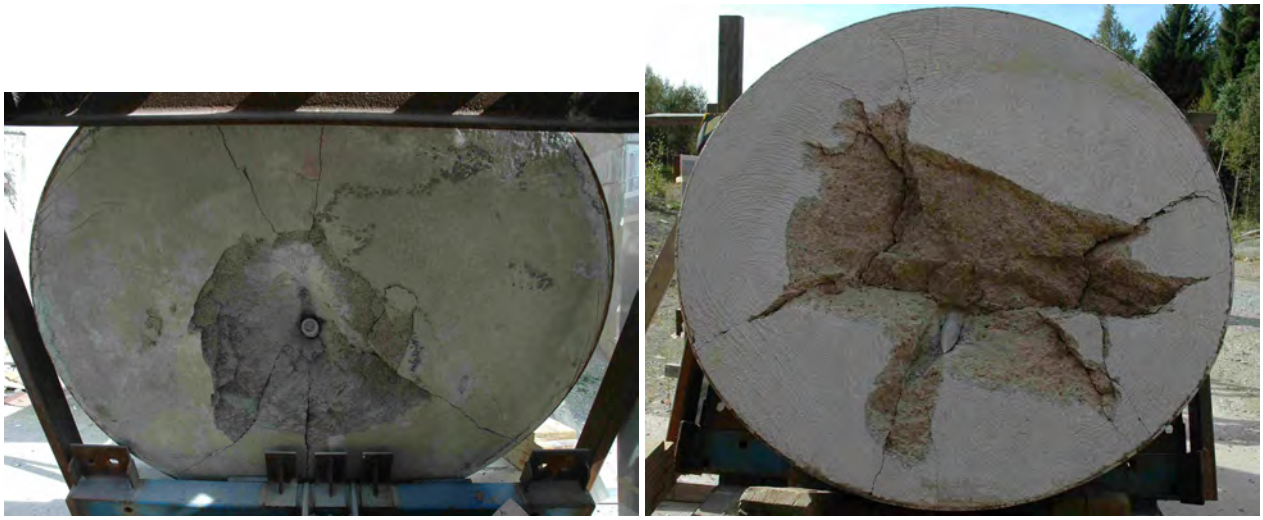

Figure 3.46. Normal strength concrete targets after test number 2004-26.

Figure 3.47. Recovered projectile from test number 2004-25.

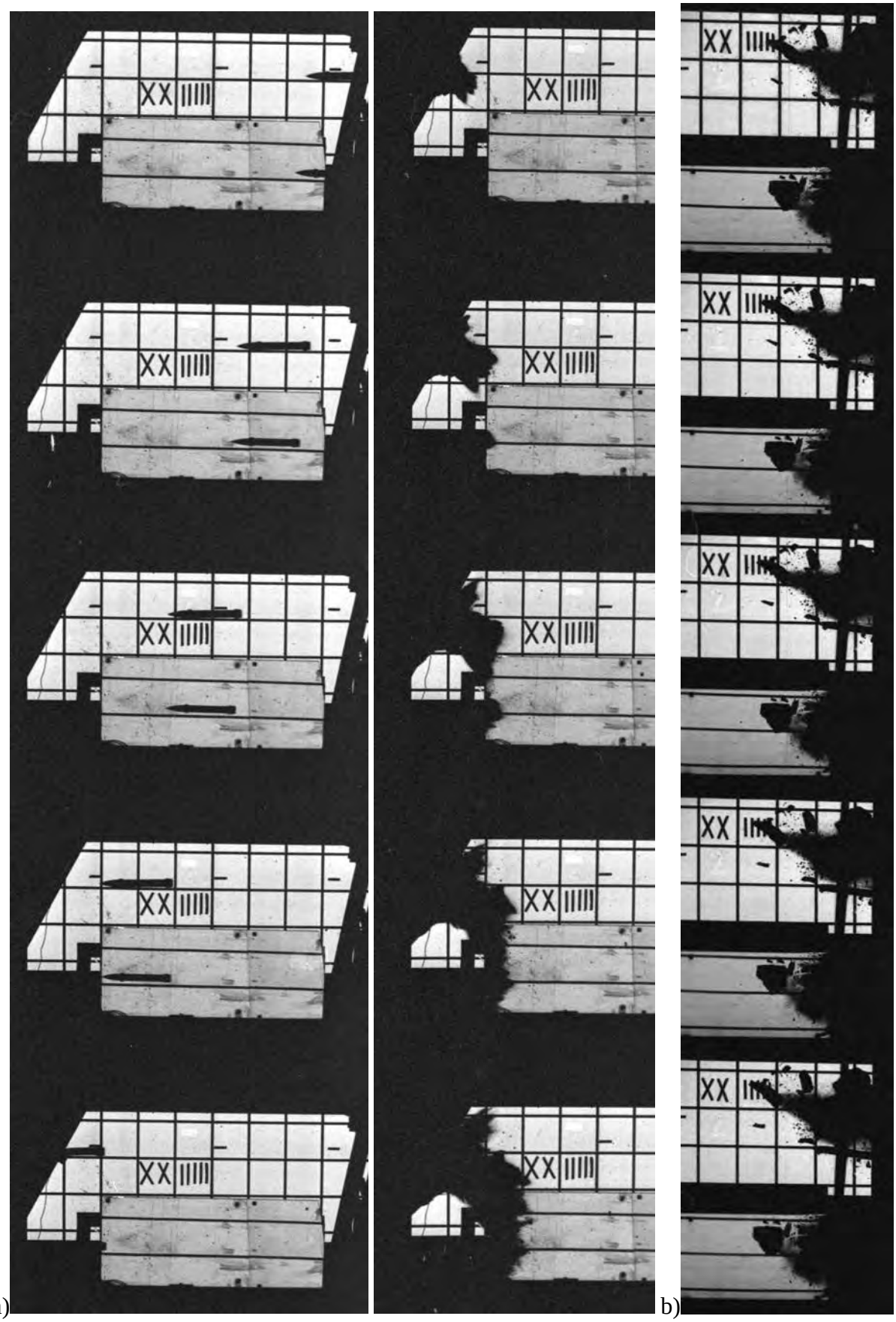

a) b)

Figure 3.48. High-speed film of test number 2004-25, with front face (a) and back face (b) of target viewed.

Figure 3.49. Frames from high-speed video of test no. 2004-26.

Figure 3.50. High performance concrete target after test number 2004-27.

Figure 3.51. High performance concrete target after test number 2004-28.

Figure 3.52. Recovered projectiles from test numbers 2004-27 and 2004-28.

Reinforced concrete targets

Reinforced NSC targets were also used to study the effect of non-normal impacts. The heights of these targets are 1.50 m, with a width of 1.20 m. The thicknesses of the reinforced targets are the same as for the unreinforced NSC, i.e. 0.54 m. Two tests were performed in each of the two targets, to study the influence of multiple impacts of a target. The placement of the targets in the test rig is shown in figure 3.53. The targets were then moved sideways before the second test in the target.

Figure 3.53. Target location for first test in targets no. 2004-23 and 2004-24. The targets were then moved to the right before the second test in the target.

The projectile design with a CRH value of 3 was used for the tests in target 2004-23. Unfortunately the first test in this target is designated as test no. 2004-23-2, this was due to the markings of the used projectile. The second test in this target is then marked 2004-23-1. The impact velocity for the first test was 423 m/s, resulting in a penetration depth of approximately 34.0 cm measured perpendicular to the front face. The impact velocity for the second test in the target was 424 m/s, resulting in a penetration depth of approximately 35.0 cm measured perpendicular to the front face of the target.

A major fracture developed in the projectile during the first test, and the projectile used for the second test was completely broken into two pieces. Post test photos of the target are shown in figures 3.54 to 3.56, with the recovered projectiles shown in figure 3.57.

Figure 3.54. Reinforced normal strength concrete target after test number 2004-23-2. This is the first test in target 2004-23.

Figure 3.55. Reinforced normal strength concrete target after test number 2004-23-1. This is the second test in target 2004-23.

Figure 3.56. Reinforced normal strength concrete target 2004-23 shown during removal of the projectiles. The projectile from test no. 2004-23-2 is shown to the right. Projectile 2004-23-1 shown to the left is broken into two pieces, this was the second test in the target.

Figure 3.57. Recovered projectiles from target 2004-23. A major fracture occurred in the projectile from test no. 2004-23-2, and the projectile from test 2004-23-1 was broken into two pieces at approximately 17 cm from the back face.

Target 2004-24 was used for tests with two projectiles with CRH value of 8. The impact velocity for the first test was 421 m/s, resulting in a penetration depth of approximately 39.0 cm measured perpendicular to the front face. The impact velocity for the second test in the target was 420 m/s, resulting in a penetration depth of approximately 34.5 cm measured perpendicular to the front face of the target.

Both projectiles that penetrated target 2004-24 were broken into two pieces. Post test photos of the target are shown in figures 3.58 to 3.60, with the recovered projectiles shown in figure 3.61. High-speed video frames from test no. 2004-24-1 are shown in figure 3.62 and 3.63.

Figure 3.58. Reinforced normal strength concrete target after test number 2004-24-1. This is the first test in target 2004-24.

Figure 3.59. Reinforced normal strength concrete target after test number 2004-24-2. This is the second test in target 2004-24.

Figure 3.60. Reinforced normal strength concrete target 2004-24 shown during removal of the projectiles. The projectile from test no. 2004-24-1 is shown to the right.

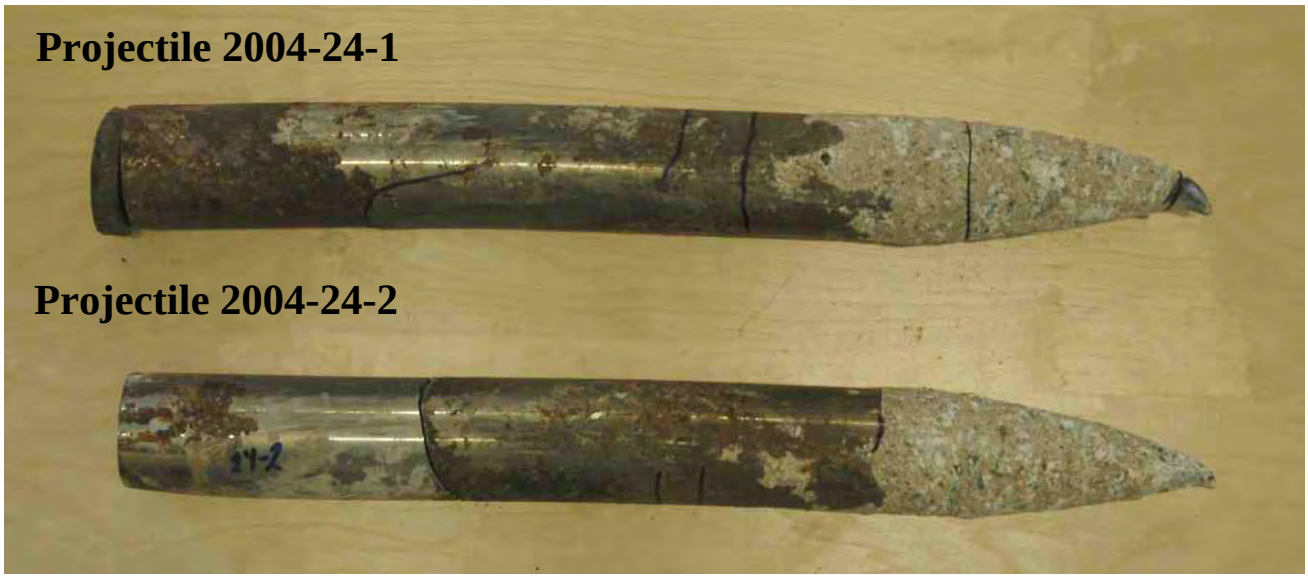

Figure 3.61. Recovered projectiles from target number 3004-24. Both of the projectiles were broken into two pieces, with the projectile from test 2004-24-2 fractured approximately 10 cm from the nose and the projectile from test 2004-24-2 fractured approximately 13 cm from the back face.

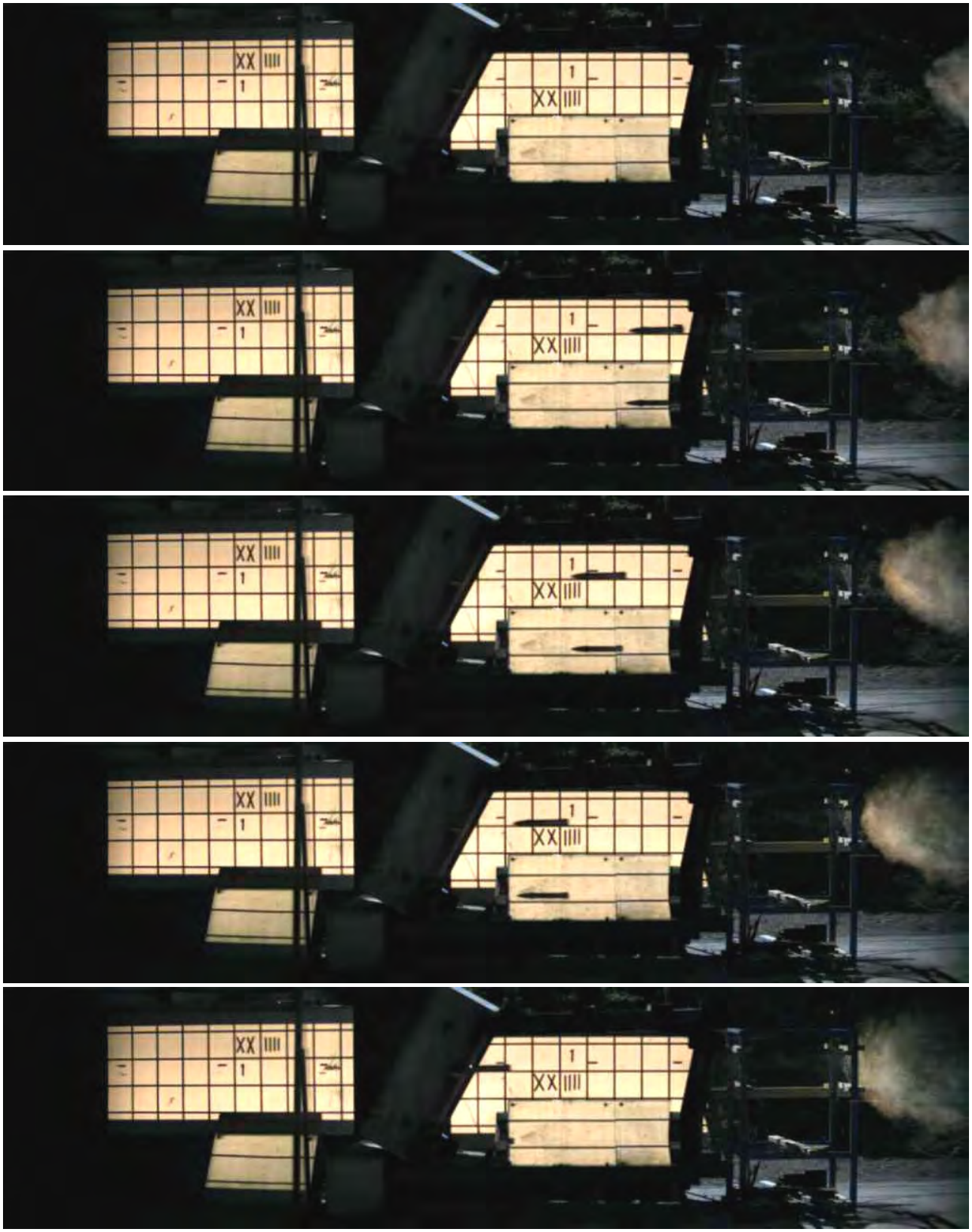

Figure 3.62. Frames from high-speed video of test no. 2004-24-1, before impact.

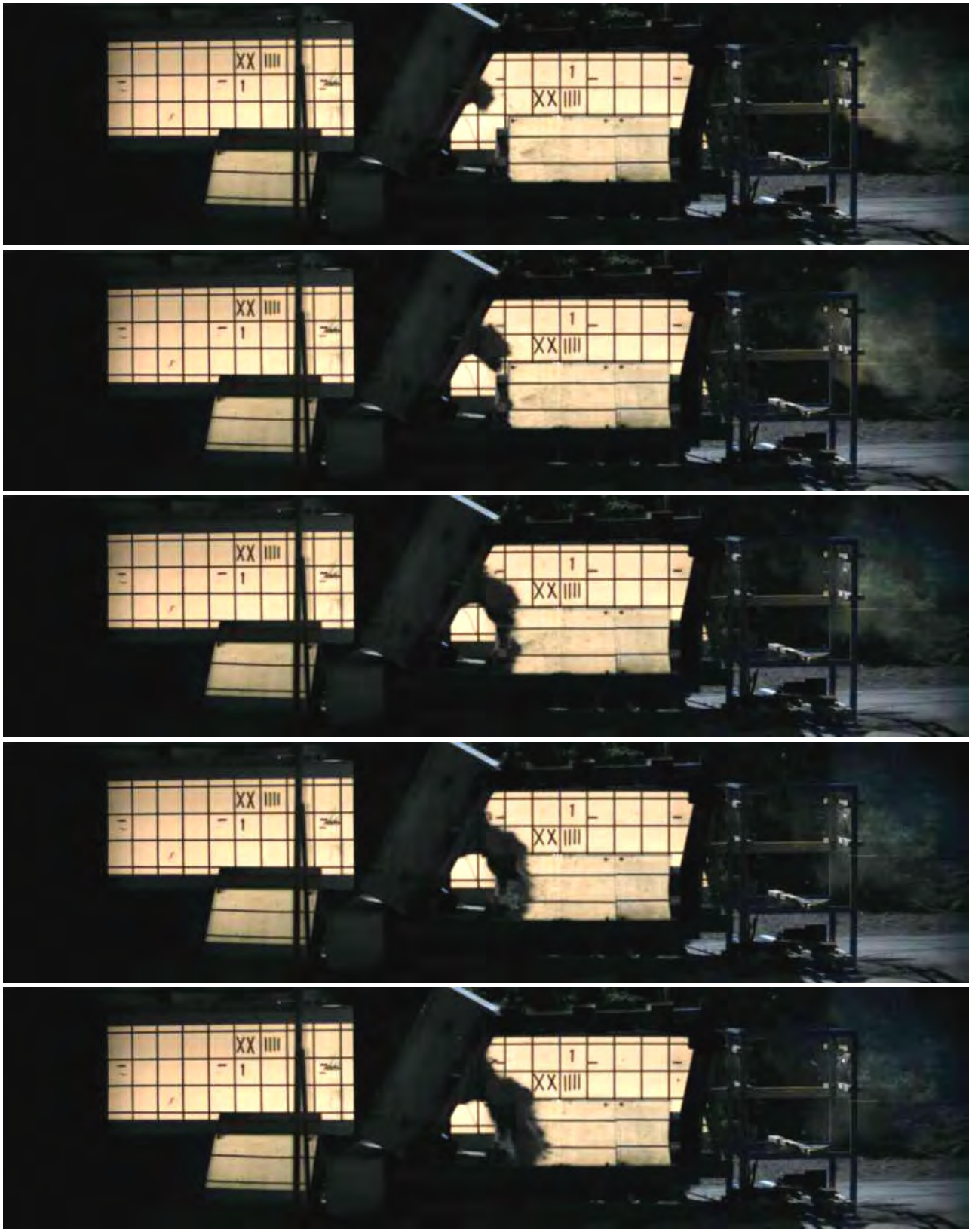

Figure 3.63. Frames from high-speed video of test no. 2004-24-1, after impact.

Summary of tests with approximately 60° impact angle

The penetration resistance for the inclined normal strength targets with a thickness of 0.54 m were slightly improved compared to the 0.60 m targets impacted by projectiles at approximately normal impact conditions. Therefore, a first approximation of the penetration resistance of an un-reinforced normal strength target may be obtained by using the projected thickness of the target with correction for the impact angle of the projectile. According to this the 0.54 m inclined target should be equal to a target of approximately 0.54/sin 60°= 0.62 m impacted at 90°.

However, the use of HPC for the 45 cm targets with non-normal impact conditions, i.e. 59.5° impact angle for the projectiles, prohibited perforation of the targets. The projectile was recovered in front of the target for the test with impact velocity 421 m/s, and in the crater at the front face of target for the test with an impact velocity of 459 m/s.

All projectiles that penetrated the inclined reinforced concrete targets were subjected to large bending forces, resulting in fracturing of the projectiles with three out of four projectiles completely broken into two pieces. Further, the impact of a second projectile in a reinforced target resulted in similar results regarding the penetration depths as was obtained for the first projectile. This indicate that the damaged zone around a penetrator might be relatively small for heavily reinforced concrete targets.

3.3. Summary of penetration tests

The maximum penetration depths for this type of projectiles, with L/D approximately 9, in a semi-infinite normal strength concrete target without heavy reinforcement are likely to be 1.6 times the projectile length, and perforation is likely to occur for targets with a thickness that are even greater due to back face spalling and cratering.

The penetration depth are considerable increased when the CRH (Calibre Radius Head) value for projectiles are increased from 3 to 8. A further increase of the CRH value to 12 only results in a minor increase of the penetration depth. However, other types of nose designs for projectiles may be more effective than the ogive nose design, e.g. conical nose shapes.

The increase of the mass for the projectile with approximately 24%, i.e. from 3.64 kg in 2002 to 4.50 kg for the tests performed in 2004, resulted in an increased penetration depth for the projectile of approximately 20-25%. Further conclusions are not possible to draw due to the limited data that are available. However, it seems that the case thickness of approximately 20% of the diameter for the penetrator used in 2004 is necessary to avoid fracturing and large deformations of the penetrator for impacts of unreinforced concrete. This will result in penetrator designs that are similar to the design used for the latest test series. The use of heavy reinforced targets increases the forces on the penetrator even more, resulting in breakage of this type of penetrators in the targets. Further, the mass of the pusher plate for the projectile might have influenced the penetration depth. The mass of the pusher plate is approximately 8% of the mass of the projectile (4.50 kg), because of this the penetration depth is likely to be increased if the kinetic energy from the pusher plate is transferred to the projectile. This causes an uncertainty for the measured penetration depths. However, in most cases the transferred kinetic energy from the pusher plate probably is neglectable. The use of a discarding sabot instead of the pusher plate may improve the shooting technique. However, this type of design is more complicated to use for the test.

An average increase of the penetration depth by 12% was obtained for an increase of the impact velocity by 10% for both NSC and HPC, this is a mean value for tests using the same projectile design and concrete type at the two nominal impact velocities. This 10% increase of the velocity increases the kinetic energy by 21%, so it seems that increasing the impact velocity may not be the most effective way to enhance the penetration performance into unreinforced concrete targets. The inefficient use of the increased kinetic energy due to the increased velocity may be caused by the pressure and strain rate dependent material properties of concrete, i.e. the increased deformation rate is likely to increase the penetration resistance of the concrete.

The high performance concrete reduces the penetration for normal impacts of projectiles compared with the NSC. However, the decrease in penetration depth is only approximately 23%. If the crater depths are subtracted from the penetration depth it is shown that the penetration channels in the concrete actually are approximately 40% shorter for the HPC compared with values for the normal strength concrete. This is probably due to the fact that the HPC is relatively more brittle in comparison to a normal strength concrete. For non-normal impact with an impact angle of 60° it seems that the high compressive strength of a HPC causes the projectile to be deflected by the target, with a great increase of the penetration resistance compared with the unreinforced NSC targets.

The introducing of 5 vol-% reinforcement with welded connections for the normal strength concrete targets limits the craters at both front and back face of the targets. This reduces the penetration depths for normal impact angles with approximately 15% in the target, and also reduces the risk for perforation of the target. The major part of the increased penetration resistance is probably due to the prohibited crater formation at the front of the target. If the crater depths are subtracted from the penetration depths, and the length of the penetration channel is obtained, these values are only approximately 4% lower for the reinforced targets. Further, the reduced penetration depth is also a result of the confinement created by the reinforcement steel and the pressure dependency of the concrete strength, i.e. the increased confinement results in an increased penetration resistance for the concrete. The energy required for the tensile fracturing during crater formation of front and back face craters is only a small fraction of the energy required to crush the material during penetration. This is also indicated by the test with the unconfined and unreinforced target, which was totally destroyed due to radial cracking and the crater formation process.

The bending forces on the projectile increases for a non-normal impact of the reinforced concrete target, with an increased risk for fracturing the projectile. Further, the use of heavily reinforced HPC structures may further increase the protection levels for hardened structures. This will be discussed later in the report.

This page intentionally blank.

4. Comparison with empirical equation

The tests in normal strength concrete and HPC show that the penetration depths of this type of projectile are approximately 1 to 1.6 times the length of the penetrator, depending on the concrete type and impact velocity. As shown earlier, a rough estimate of the penetration depth for normal impact of this type of penetrators can be obtained by using empirical equations (Hansson, 2003c). This present work extends the use of the proposed method to penetrators with a maximum length to diameter ratio of approximately 10, and a maximum CRH (Calibre Radius Head) value of 12. The modified empirical model suggested here replaces the earlier proposed model (Hansson, 2003b-c). The empirical method can also be used to predict weapon effects on normal building structures, e.g. for combat situations in urban environments and for assessing strengthening methods for building structures.

In general penetration formulas consider concrete strength, impact energy, CRH value and projectile cross section. Minor influences from other factors are also considered for some formulas, e.g. amount of reinforcement, aggregate type and ratio between projectile length and diameter. Structural failure, e.g. tensile failure caused by radial expansion of the target, is normally not considered in empirical formulas. Therefore, these types of predictions are only valid if the influence from boundaries of the structure can be neglected. This is normally the case for a reinforced concrete structure, where the rebars prohibit tensile cracking of the target, and the dominating modes of failure are the formation of impact crater and crushing of concrete.

Further, failure and deformation of the penetrators are not considered for these type of empirical equations, and therefore they can only predict the performance of penetrators subjected to small deformations.

4.1. Penetration formula

The formula used in ConWep (1992) is shown below in equation 1, which is an updated version from the one used in the technical manual TM 5-855-1. This formula is used in this study for comparison with penetration data from available literature. The unconfined compressive strength of the concrete should be determined on cylinder samples with a length to diameter ratio of two. Diameters of the concrete samples or cores are normally between 75 to 100 mm. If cube strength is used as a quality measurement of the concrete it is necessary to reduce this value with approximately 10% to obtain an unconfined compressive strength. However, the ratio between concrete strength measured on cubes and cylinders varies depending on the used concrete type. The unconfined compressive strength for cored cylinders is reduced in comparison with the strength of poured cylinders, and the strength also varies due to sample size. Both these phenomena need to be accounted for when a representative unconfined compressive strength is determined.

$$X = \frac{222 \times N \times W \times V^{1.8}}{D^{1.8} \times f'_c{}^{0.5}} + D \quad \text{for } X > 2D \text{ (inch)} \qquad \text{(eq. 1.)}$$

where

X = Penetration depth, inch
f'_c = Compressive strength of concrete, psi
N = Nose shape factor or nose performance coefficient (see eq. 2)
W = Projectile weight, lb
D = Projectile diameter, inch
$V = \frac{\text{Impact velocity in fps}}{1000}$

with

1 inch	≈ 25.4 mm
1 psi	≈ 6.89 kPa
1 lb	≈ 0.454 kg
1 fps	≈ 0.304 m/s

The nose performance coefficient N is given by:

$$N = 0.72 + 0.25(CRH - 0.25)^{0.5} \qquad \text{(eq. 2.)}$$

where

CRH = Calibre Radius Head, i.e. ratio between the tangent ogive radius and the projectile diameter.

A conversion of the units gives the formula

$$X = \frac{11.76 \times N \times M \times V^{1.8}}{D^{1.8} \times f'_c{}^{0.5}} + D \quad \textit{for } X > 2D \text{ (mm)} \qquad \text{(eq. 3.)}$$

where

X = Penetration depth, mm
f'_c = Compressive strength of concrete, MPa
N = Nose shape factor or nose performance coefficient (see eq. 2. above)
M = Projectile mass, kg
D = Projectile diameter, mm
V = Impact velocity, m/s

Equation 3 results almost in a lower limit of the penetration performance of penetrators with L/D ratios below 10 when compared with the data from the literature compiled in appendix 2, see also figures 4.1 and 4.2. A better estimation of the penetration performance of warheads with L/D between 3 and 10 is obtained with the introducing of the factor *k* in the equation (eq. 4). With the introducing of this factor *k*, an average value for the penetration depth is obtained for the penetration depth. The higher value for the constant *k* is recommended for all types of projectiles impacting a concrete target constructed with limestone aggregate. The modified equation (eq. 4) also use an effective concrete strength ($f'_{c\,eff}$) that is limited to a maximum value of 65 MPa. This upper limit for the effective unconfined compressive strength is used due to the uncertainty of the properties of different types of high performance concrete. The reason for this is that the original model was developed for normal strength concrete.

$$X = k\left(\frac{11.76 \times N \times M \times V^{1.8}}{D^{1.8} \times f'^{\,0.5}_{c\,eff}} + D\right) \quad \text{for } X > 2D \text{ (mm) and } L/D \le 10 \qquad \text{(eq. 4.)}$$

with

$$k = \begin{cases} 1.25 & \text{for } 3 \le L/D \le 7, \text{ granite/gneiss aggregate} \\ 1.07 & \text{for } 7 < L/D \le 10, \text{ granite/gneiss aggregate} \\ 1.25 & \text{for } 3 \le L/D \le 10, \text{ limestone aggregate} \end{cases}$$

$$f'_{c\,eff} = \begin{cases} f'_c & \text{for } 30 \le f'_c \le 65\,\text{MPa} \\ 65 & \text{for } f'_c > 65\,\text{MPa} \end{cases} \qquad \text{(Effective concrete strength)}$$

L= Projectile length, mm
X = Penetration depth, mm
f'_c = Compressive strength of concrete, MPa
N = Nose shape factor or nose performance coefficient (see eq. 2. above)
M = Projectile mass, kg
D = Projectile diameter, mm
V = Impact velocity, m/s

4.2. Comparison between empirical equation and experimental data

A comparison between the predictions and experimental data from the literature was performed, with the used data range given in tables 4.1 and 4.2. The predictions according to eq. 3 are compared with experimental data in figures 4.1 and 4.2, and estimated penetrations according to eq. 4 are compared with the same data in figures 4.3 and 4.4. The predicted penetration depths according to eq. 4 are approximately within ±20% of the experimentally determined penetration depth. These limits are also shown in the figure.

Table 4.1. Used data ranges from the literature for comparison between experimental results and the empirical equation for projectiles with 3≤ L/D<7, all the data are compiled in appendix 2. Concrete with granite or gneiss aggregates is used for the tests.

Parameter	**Minimum value**	**Maximum value**
Projectile diameter (mm)	25	363
Projectile length (mm)	151	1200
Projectile length to diameter ratio, L/D	3.0	7.0
Projectile ogive radius to diameter ratio, CRH	1.7	3.0
Projectile mass (kg)	0.50	485
Impact velocity (m/s)	132	653
Uni-axial compressive strength, f´c (MPa)	34.5	140
Penetration depth (mm)	55	1350
Penetration depth/projectile length, X/L	0.36	4.4

Table 4.2. Used data ranges from the literature for comparison between experimental results and the empirical equation for projectiles with 7<L/D≤10, all the data are compiled in appendix 2. Concrete with granite or gneiss aggregates is used for the tests.

Parameter	**Minimum value**	**Maximum value**
Projectile diameter (mm)	20.3	50.8
Projectile length (mm)	203	387
Projectile length to diameter ratio, L/D	7.6	10.0
Projectile ogive radius to diameter ratio, CRH	2.0	5.0
Projectile mass (kg)	0.48	4.4
Impact velocity (m/s)	277	1024
Uni-axial compressive strength, f´c (MPa)	32.4	108
Penetration depth (mm)	173	1750
Penetration depth/projectile length, X/L	0.71	5.7

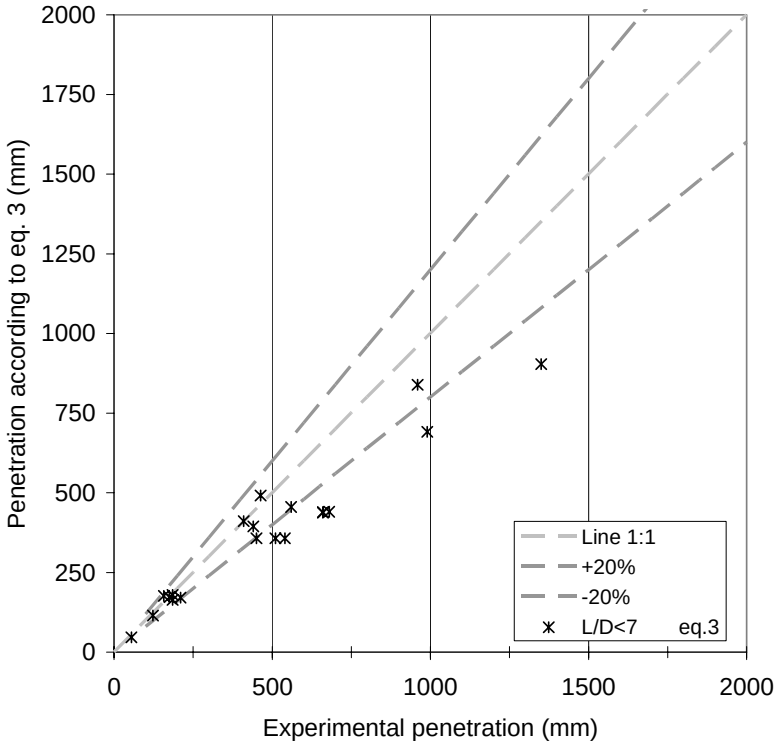

Figure 4.1. Comparison between predicted penetration depths according to eq. 3 and experimental results for projectiles with 3≤L/D≤7. Concrete with granite or gneiss aggregates is used for the tests.

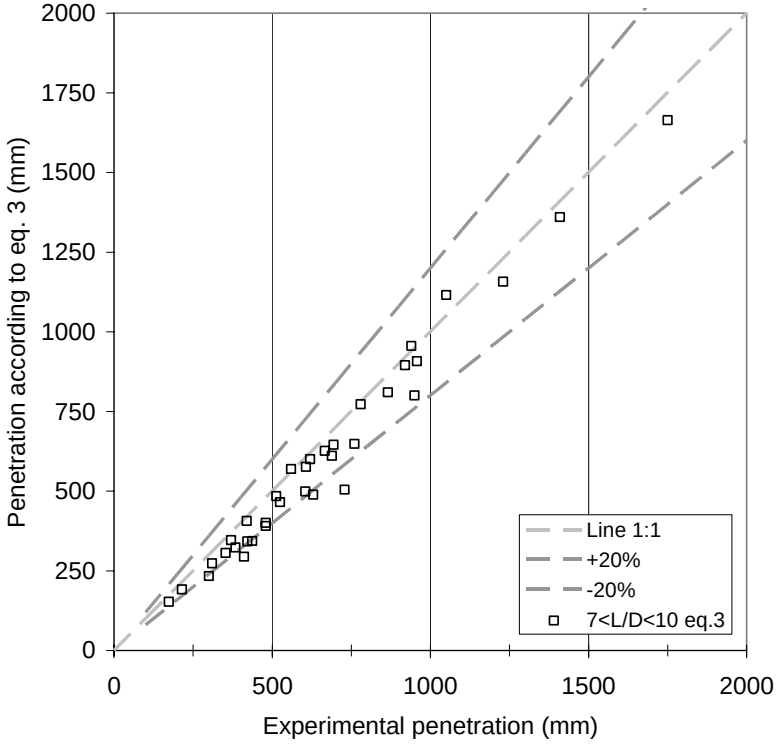

Figure 4.2. Comparison between predicted penetration depths according to eq. 3 and experimental results for projectiles with 7<L/D≤10. Concrete with granite or gneiss aggregates is used for the tests.

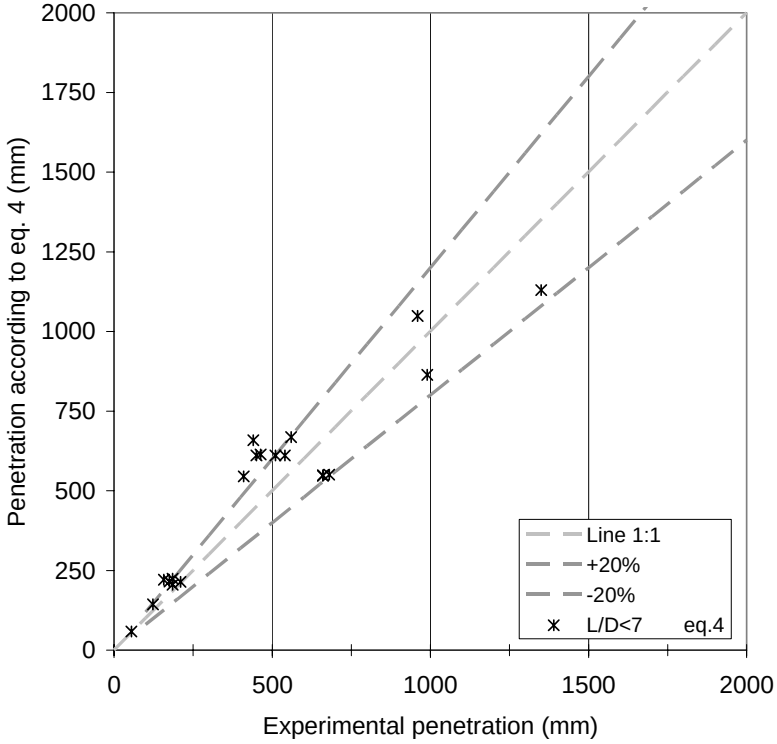

Figure 4.3. Comparison between predicted penetration depths according to the modified eq. 4 and experimental results for projectiles with 3≤L/D≤7. Concrete with granite or gneiss aggregates is used for the tests.

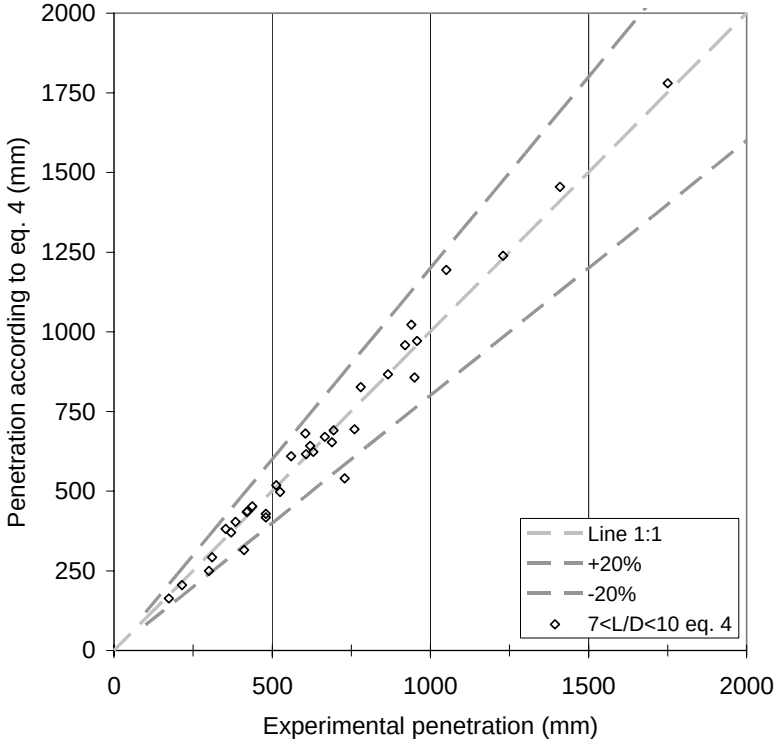

Figure 4.4. Comparison between predicted penetration depths according to the modified eq. 4 and experimental results for projectiles with 7<L/D≤10. Concrete with granite or gneiss aggregates is used for the tests.

As mentioned earlier the constant *k* should be chosen to 1.25 for concrete with limestone aggregates regardless of projectile type. Comparisons with the use of both eq. 3 and eq. 4 with *k* equal to 1.25 are shown in figure 4.5, with the used data range given below in table 4.3.

Table 4.3 Data ranges for test with targets constructed with the use of limestone aggregate, all the data are compiled in appendix 2.

Parameter	**Minimum value**	**Maximum value**
Projectile diameter (mm)	20.3	76.2
Projectile length (mm)	203	531
Projectile length to diameter ratio, L/D	6.9	10.0
Projectile ogive radius to diameter ratio, CRH	3.0	6.0
Projectile mass (kg)	0.48	13.0
Impact velocity (m/s)	238	1009
Uni-axial compressive strength, f´c (MPa)	39	58
Penetration depth (mm)	287	1960
Penetration depth/projectile length, X/L	0.57	6.4

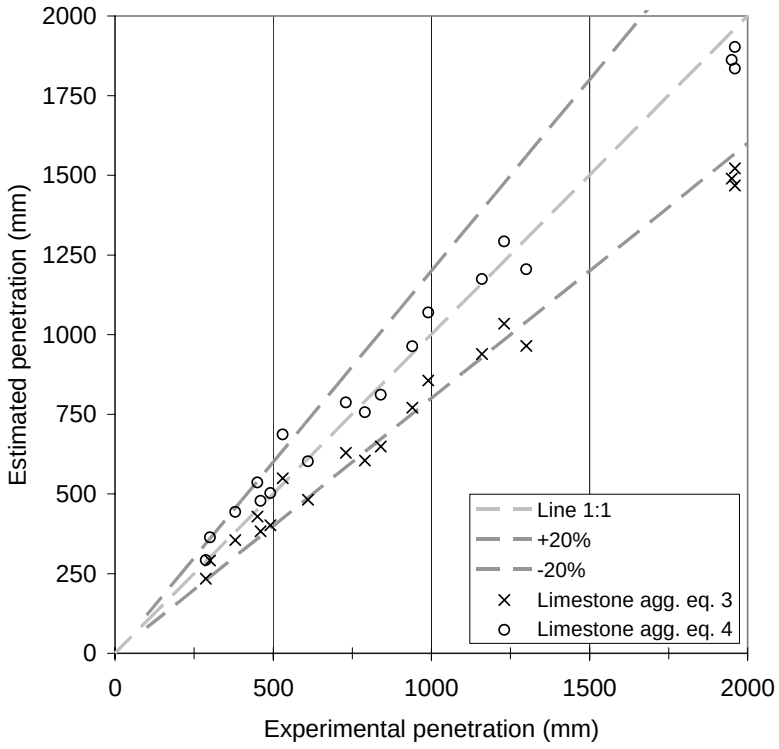

Figure 4.5. Comparison with predicted penetrations for tests using concrete with limestone aggregate for both eq. 3 and 4. The constant *k* in eq 4. is chosen as 1.25 for all L/D ratios.

The modified equation 4 was also used for an estimation of penetration for the tests performed at FOI, with data range according to table 4.4 below. This comparison is shown in figures 4.6 and 4.7.

Table 4.4 Data range for the test performed at FOI during 2002 and 2004.

Parameter	**Minimum value**	**Maximum value**
Projectile diameter (mm)	50.0	50.0
Projectile length (mm)	450	470
Projectile length to diameter ratio, L/D	9.0	9.4
Projectile ogive radius to diameter ratio, CRH	3.0	12.0
Projectile mass (kg)	3.65	4.50
Impact velocity (m/s)	407	463
Uni-axial compressive strength, f´c (MPa)	48	130
Penetration depth (mm)	380	690
Penetration depth/projectile length, X/L	0.84	1.53

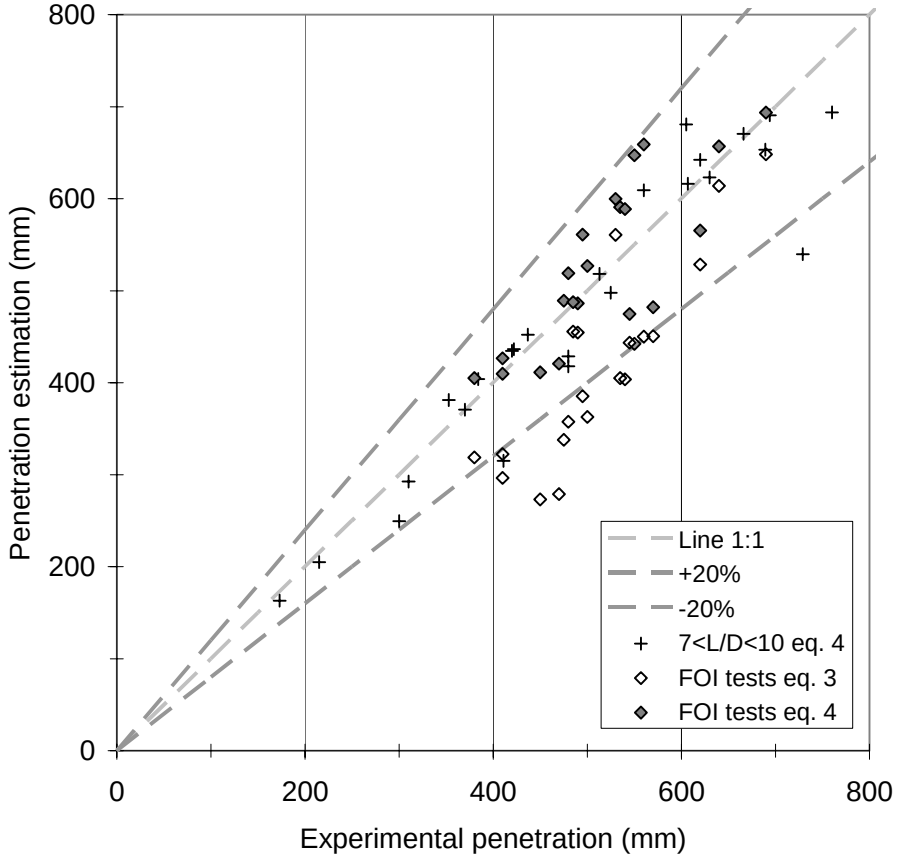

Figure 4.6. Comparison between predicted penetrations for the tests performed at FOI using both eq. 3 and 4, shown together with the data from the literature for projectiles with 7<L/D≤10 compared with eq. 4. Test no. 2002-3 is not plotted due to the fracturing of the projectile.

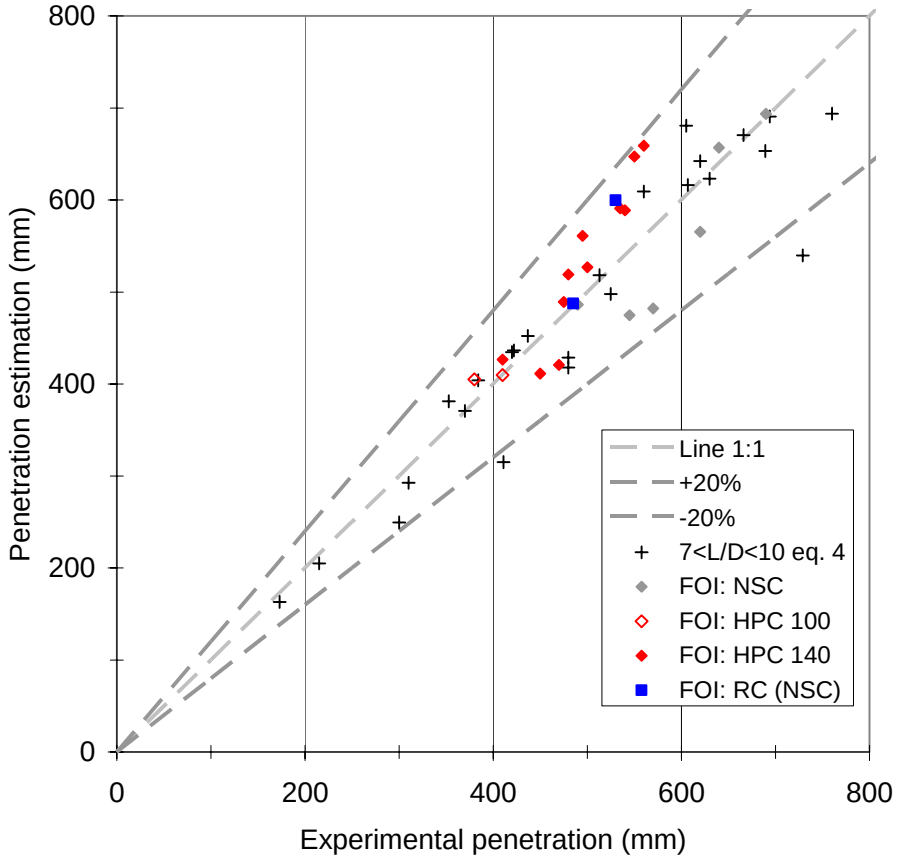

Figure 4.7. Comparisons between predicted penetrations according to eq. 4 and test results for the test performed at FOI, shown together with the data from the literature for projectiles with 7<L/D≤10. Test no. 2002-3 is not plotted due to the fracturing of the projectile.

In general eq. 4 shows a fair agreement with all data presented in figures 4.3 to 4.7, incl. the FOI tests. These tests used a 50 mm projectile with a length to diameter ratio of approximately 9, and CRH values between 3 and 12. However, there are several limitations to using this type of equations to determine penetration performance. This model results in conservative values for the predicted penetration depths for this HPC, and it is necessary to use more sophisticated models that consider the material behaviour at high pressures to take advantage of the full potential of the material. However, all the tests performed at FOI falls within the ±20% limits in figure 4.7. In average the penetration depths are underestimated for both the heavy reinforced normal strength concrete and the HPC with approximate 135 MPa compressive strength when compared to eq. 4 in figure 4.7. These specially designed targets have an enhanced protection level, and more sophisticated models are needed to take advantage of this increased protective performance in construction designs and to determine the penetration resistance.

The equation (eq. 4) can be used to give a first rough estimate of the penetration performance of a warhead (offensive performance), or an estimation of needed protective performance of a structure (defensive performance), for projectiles with L/D ratios between 3 and 10, and impact velocities below 1000 m/s. The different aims for the specifications for warheads and protective structures gives different levels of the penetration performance, see figure 4.8. The reason is that for the first case it is likely that the warhead penetrates to the desired depth, or deeper. For the later case it is unlikely that the warhead penetrates deeper than the given penetration depth. Further, cratering at the back side of the target, and thereby the risk of perforation of the target, also needs to be considered. The method can be used to predict penetration depths for different types of penetrating warheads or projectiles with a diameter greater than 20 mm, e.g. rocket propelled grenades, artillery shells and penetrating bombs. The use of shaped charges, explosively formed penetrators and other types of eroding projectiles are not considered with this method.

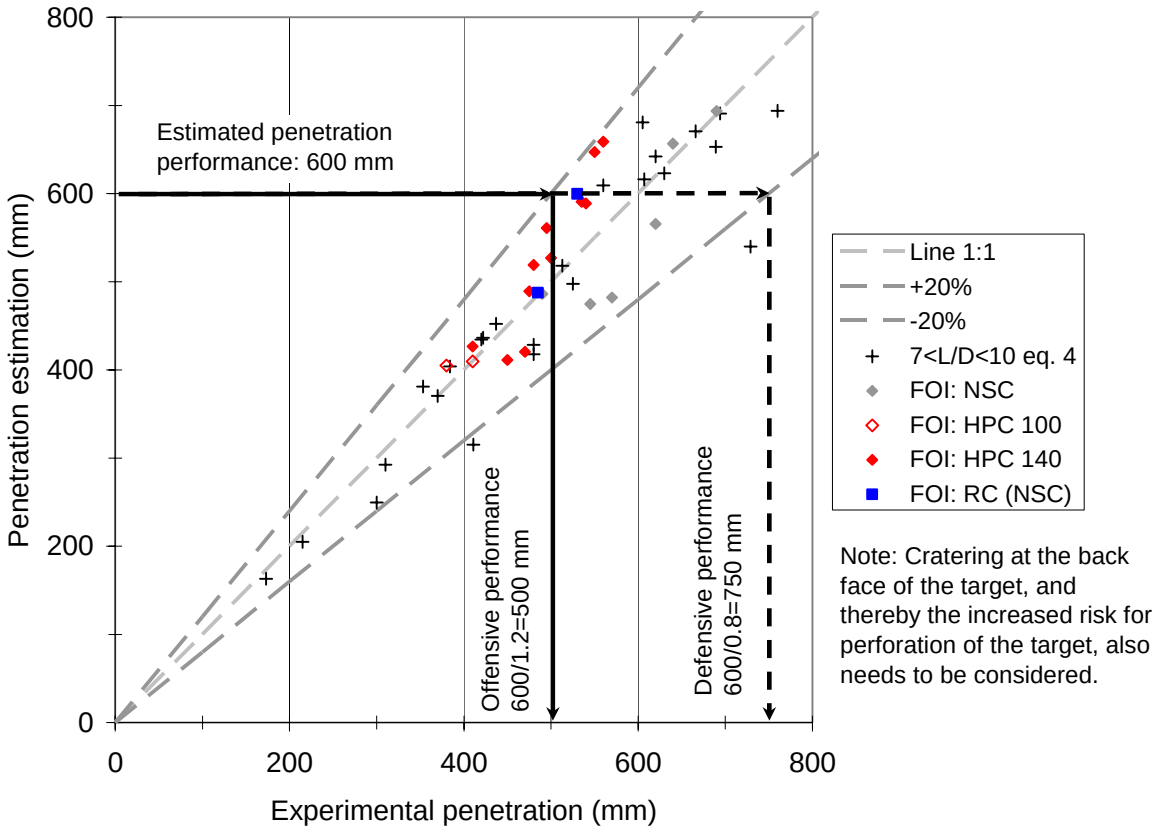

Figure 4.8. Example of estimations of warhead performances from offensive and defensive viewpoints.

5. Comparison with simulations

Simulations of penetration by projectiles with a length to diameter ratio of 9 in concrete are performed within another project financed by the Swedish Armed Forces. Some preliminary simulation results and comparisons with the experimental results are given here, and further information regarding the numerical simulations is given by Hansson (2005). The numerical method can be used for different types of projectiles within the verified velocity range, and for the used target materials. With further verified data and simulations for increased impact velocity, and other materials, it is possible to expand the range of weapon types and protective structures that can be considered.

The RHT concrete model was used for the simulations of projectiles, with a length to diameter ratio of 9, penetrating concrete targets. This advanced material model was developed at EMI (Riedel, 2000). The used version of the material model is implemented as a standard material model in Autodyn version 4.2, or higher. An earlier study of numerical simulation of concrete penetration with the use of the RHT model was performed by Hansson (2003a). This study showed that with the latest development in material and numerical modelling it is possible to use advanced material models together with alternative meshless formulations, e.g. SPH formulations. Another approach to avoid heavily distorted elements is to use an Eulerian formulation, i.e. with a fixed mesh for the target and with the material allowed to move through the mesh. However, both these methods are more time consuming than the normally used Lagrange formulation, and they also have other limitations (Hansson, 2003a). Therefore, these initial simulations were performed with the use of the Lagrange element formulation for the target.

A few simulations are compared with the test results given earlier. Further information regarding the numerical models is given by Hansson (2005). The simulations are performed with the value of 0.05 for the coefficient of friction, a uni-axial compressive strength of 48 MPa and approximately 5 mm elements in the central part of the concrete targets. The steel bars for the reinforced targets are simulated by using beam elements, and joining these to the solid elements representing the concrete.

It is likely that simulations of unreinforced concrete targets will only give fair results for both the penetration depths and exit velocities, this is due to the simple tensile failure description used in the RHT material model in combination with the large influence from surface effects, i.e. the formation of craters at the front and back face of the concrete target. The steel bars in the reinforced concrete targets prohibit the radial cracking and crater formation, and thereby the RHT model is likely to give more accurate predictions of penetration depths and exit velocities for these types of targets. This is shown in tables 5.1 and 5.2 where the simulations are compared with the test results. The deformations and damaged areas for the models are shown in figures 5.1 to 5.4.

Table 5.1. Comparison between test results and numerical simulations for un-reinforced concrete targets with Autodyn 3D.

Test/Model identity	**2004-3**	**PEN205**	**2004-6**	**PEN080-2**
Type, i.e. simulation or experiment	Experiment	Simulation	Experiment	Simulation
Target length	0.90 m	1.20 m	0.60 m	0.60 m
Boundary condition [1]	8 mm steel	5 mm steel	8 mm steel	5 mm steel
Projectile mass	≈4.50 kg	4.53 kg	≈4.50 kg	4.53 kg
Impact velocity	409 m/s	420 m/s	425 m/s	420 m/s
Yaw	0.49°	0°	0.21°	0°
Pitch	1.25°	0°	1.10°	0°
Impact angle	90°	90°	90°	90°
Model symmetry	---	¼	---	½
Element size	---	5 mm	---	5 mm
Number of elements	---	≈820 000	---	≈1090 000
Friction coefficient	---	μ=0.05	---	μ=0.05
Penetration depth	62.0 cm	51.2 cm	---	---
Exit velocity	---	---	139 m/s	98 m/s
Decrease of kinetic energy	---	---	89.3%	94.6%

Note: [1] Displacement of target in axial direction is free for all cases.

Table 5.2. Comparison between test results and numerical simulations for reinforced concrete targets with Autodyn 3D.

Test/Model identity	**2004-19**	**PEN242v5**	**2004-23-1**	**PEN257**
Type, i.e. simulation or experiment	Experiment	Simulation	Experiment	Simulation
Target length	0.60 m	0.60 m	0.54 m	0.54 m
Boundary condition [1]	Free surface	Free surface	Free surface	Free surface
Projectile mass	≈4.50 kg	4.53 kg	≈4.50 kg	4.53 kg
Impact velocity	422 m/s	420 m/s	421 m/s	420 m/s
Yaw	0.41°	0°	0.38°	0°
Pitch	0.55°	0°	1.59°	0°
Impact angle	90°	90°	59.5°	60°
Model symmetry	---	None	---	None
Element size	---	7.5×7.5×3.75 mm	---	7.5×7.5×3.75 mm
Number of elements	---	≈1810 000	---	≈1810 000
Friction coefficient	---	μ=0.05	---	μ=0.05
Penetration depth	48.5 cm	47.3 cm	39.0 cm	38.2 cm

Note: [1] Displacement of target in axial direction is free for all cases.

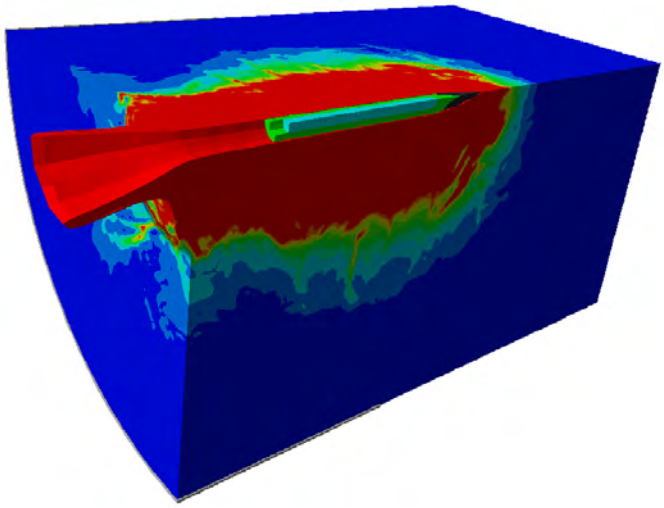

Figure 5.1. Calculated damage and deformations for model PEN205 with quarter symmetry.

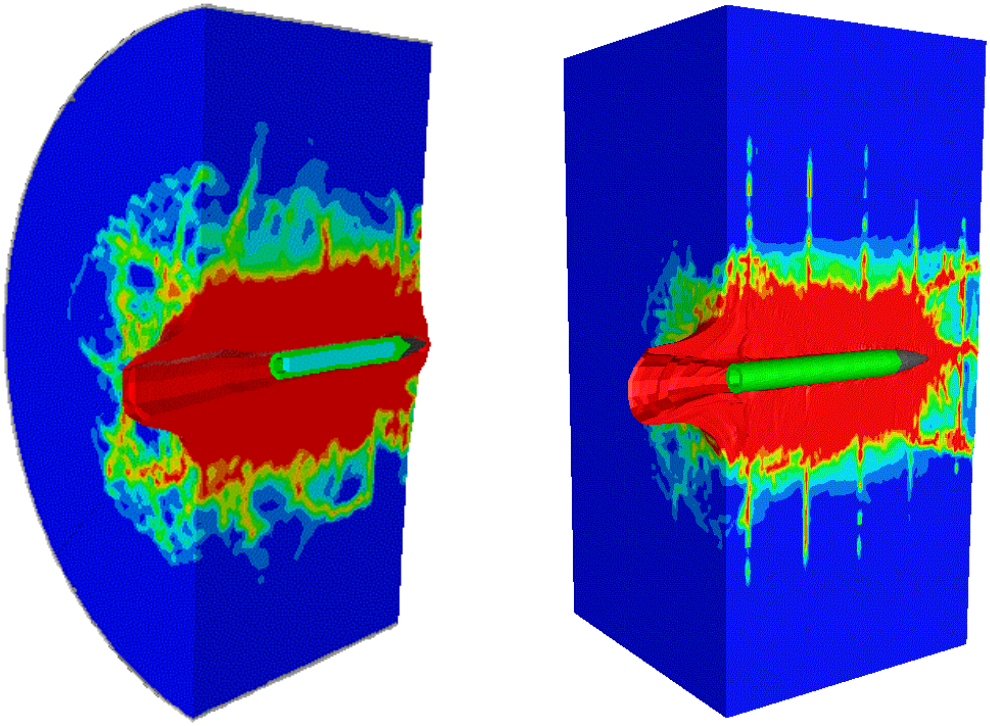

Figure 5.2. Calculated damage and deformations for 0.60 m thick targets without and with reinforcement. Model PEN080-2 without reinforcement shown to the left and model PEN242v5 with reinforcement shown to the right.

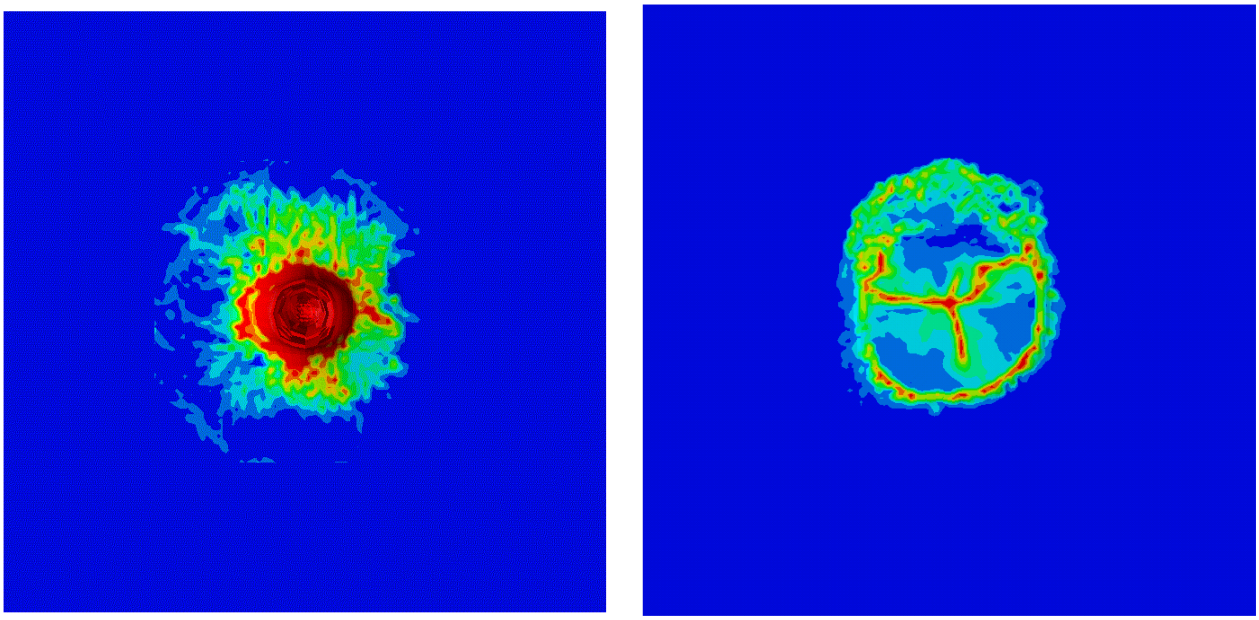

Figure 5.3. Front and back face of model PEN242v5 with reinforcement.

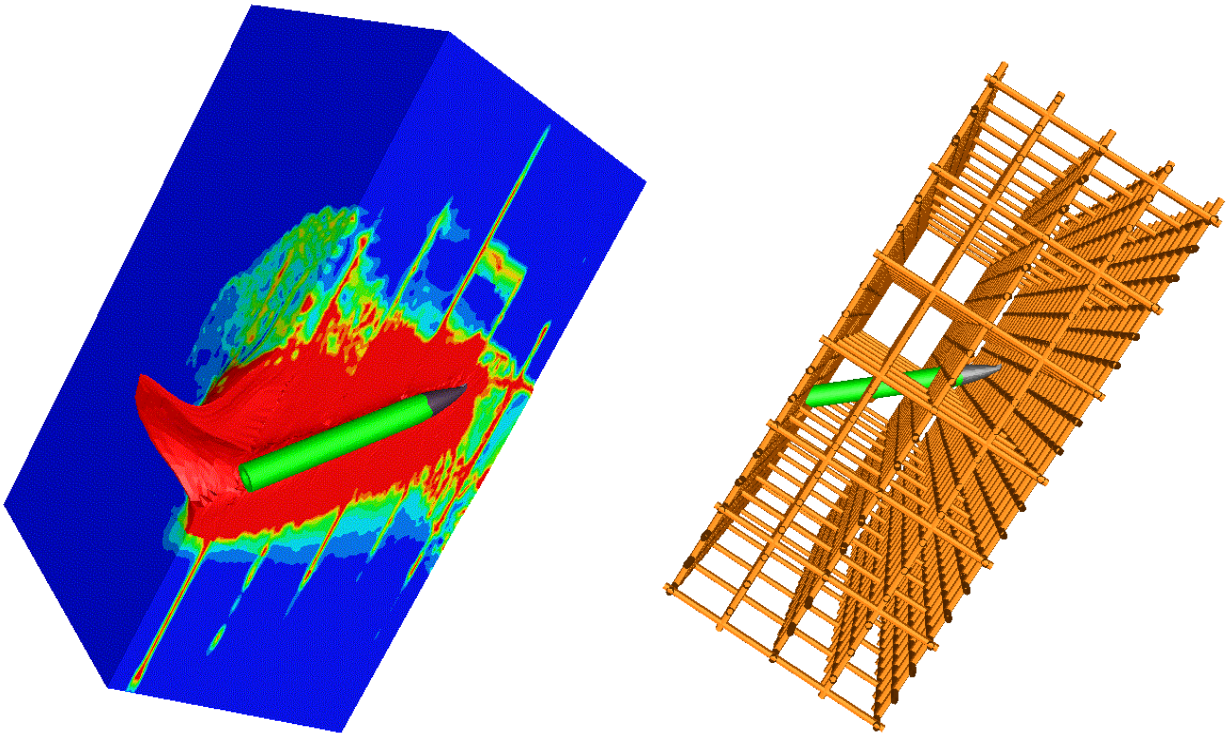

Figure 5.4. Calculated damage and deformations for model PEN257 with reinforced 0.54 m thick target.

Improved damage models for tensile cracking of concrete are developed by several research institutes, e.g. EMI (Shuler, 2004) and CTH (Leppänen, 2004). This type of models is likely to improve the possibility to simulate both penetration in concrete and structural response of reinforced concrete structures in the near future.

The advantages of numerical simulations are the ability to study a variety of different types of penetration cases, e.g. the influence of obliquity of projectiles, non-normal impact angles, reinforced targets and target thickness. It is also possible to combine different target types and weapon effects to study multiple impacts of projectiles and dual charge warheads. The interaction between the projectile and the target is also possible to study with the use of numerical simulations, this gives the opportunity to study damage and failure of the projectile. This was studied by Johnson et al. (1999) for non-normal impacts of projectiles with a L/D ratio of 8, and a fracture model for numerical simulations was also verified within the study. With a thorough description of the behaviour of the used materials it is possible to evaluate weapon effects from different types of both existing and future warheads, against different types of protective structures.

This page intentionally blank.

6. Discussion

Depending on the concrete type and impact velocity it was shown that this type of penetrators with a length to diameter ratio of 9 is likely to have a penetration performance into concrete of 1 to 1.6 times their length. The penetration depths depend on the mass of the penetrator, penetrator design, impact velocity, impact angle and also the properties of the target. A rough estimate of the penetration depth in concrete for projectiles with normal impact conditions can be obtained by using empirical equations. An empirical equation may give a good result for penetration cases that are similar to the penetration cases that were used to derive the equation. However, for evaluation of heavy reinforced concrete structures, special types of HPC targets, non-normal impact conditions for the projectile or to determine the risk for perforation of a target it seems that it is necessary to use experiments or advanced numerical simulation. Further, these two methods are suitable to be used in combination to increase the prediction possibility for this type of weapons. The use of numerical simulations is also necessary for studies of cratering of the target, and thereby also perforation of the target, and the interaction between projectile and target. Further, the use of numerical simulation gives the opportunity to study deformations of the penetrator.

The test results show that there is a decreased penetration depth for the used projectiles in the HPC in comparison with the normal strength concrete target. However, the craters in the targets are relatively deep when compared with the total penetration depth. It is therefore likely that the penetration depth in a HPC target is reduced, if the size of the crater can be reduced. The use of heavy reinforcement, i.e. approximately 5 vol-%, is therefore likely to decrease the penetration depth in a HPC target, by increasing the confinement of the HPC around the projectile path and thereby take advantage of the high compressive strength for this type of concrete. If the front crater of the target is reduced for a heavily reinforced HPC target in the same way as for the normal strength target, and the penetration channel in the HPC is constant, it is possible that the penetration depths for projectiles with an impact velocity of 420 m/s may be reduced by more than 40% for a reinforced HPC target compared with reinforced NSC or unreinforced HPC targets. Further, with the same considerations regarding the penetration depth for projectiles with an impact velocity of approximately 460 m/s, the decrease of the penetration depth in a reinforced HPC target may be more than 20% compared with reinforced NSC or unreinforced HPC targets. The penetration depths for this type of projectiles is then likely to be reduced to less than one projectile length in a reinforced HPC target for impact velocities up to 460 m/s. More important may be the ability of the reinforcement to confine the concrete at the back of the target, and thereby prohibit cratering and perforation of the target. Further, as the warhead detonates it is likely that the heavy reinforcement will contribute to reduced damage level of both the concrete slab and the surrounding structure. However, several types of HPC are developed for different purposes, and with quite different material properties. Therefore, different types of HPC with comparable uni-axial compressive strengths are likely to have quite different penetration resistance. This needs to be considered for designs that uses HPC for protective or hardened structures, and it is important to use a HPC with high penetration resistance for these types of structures if the main design criteria is protection against penetrating warheads. The variations between different types of normal strength concretes are much smaller, and the material behaviour is also better known.

The projectiles that impacted the inclined HPC targets with an impact angle of approximately 60° only created an impact crater, and were recovered in front of the target. This indicates that the high compressive strength of this HPC is a preferable material property for non-normal impact scenarios.

The earlier published empirical method for normal impact of concrete targets is modified and extended to consider projectiles with a maximum length to diameter ratio of approximately 10. The empirical method is now considered to give a fair prediction of penetration depths for projectiles with L/D ratios between 3 and 10, and impact velocities below 1000 m/s. The method can be used to predict penetration depths for different types of penetrating warheads or projectiles with a diameter greater than 20 mm, e.g. rocket propelled grenades, artillery shells and penetrating bombs. The use of shaped charges and explosively formed penetrators are not considered with this method. However, penetration of shaped charge jets into concrete and geological materials is studied within another project at FOI financed by the Swedish Armed Forces. An empirical equation that considers jet penetration in layered protective structures of geological material and concrete is presented by Elvfing et al. (2005).

The current development for penetrating weapons is to use dual-charge warheads, with a shaped charge jet first penetrating the target followed by a penetrator with an explosive charge. This type of weapon is in use, or under development, in several sizes from man portable rocket propelled versions to cruise missiles. When used during urban combat this type of bunker busters will be much more effective than an ordinary shaped charge rocket propelled grenades. Further, this type of dual charge warheads may also be equipped with thermobaric warheads instead of a high explosive charge in the future. A wall breaching tandem warhead with a diameter of 114 mm is developed at FOI, this warhead uses a single copper liner to form both a shaped charge jet and a ring shaped explosively formed penetrator (EFP) (Helte et al. 2005). The EFP with a velocity of approximately 2000 m/s is intended to cut a relatively large hole through walls, e.g. reinforced concrete or brick walls. The jet and EFP are shown in figure 6.1, and plots from a simulation of the effect from this charge on a concrete cylinder are shown in figure 6.2. Further, concrete penetration by eroding projectiles of copper and tantalum with impact velocities between 1500 and 1900 m/s was studied by Gold (1999). The penetration process in concrete within this velocity range is not studied to the same extent as for non-eroding penetrators and shaped charge jets, since warheads with impact velocities between 1500 and 2500 m/s normally are kinetic energy (KE) penetrators, or explosively formed penetrators, designed to be used against armoured vehicles.

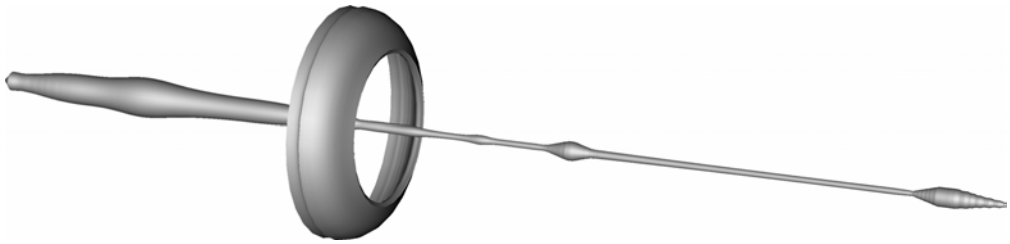

Figure 6.1. Shape of a tandem warhead with jet and ring shaped EFP calculated 80 µs after detonation (Helte et al., 2005).

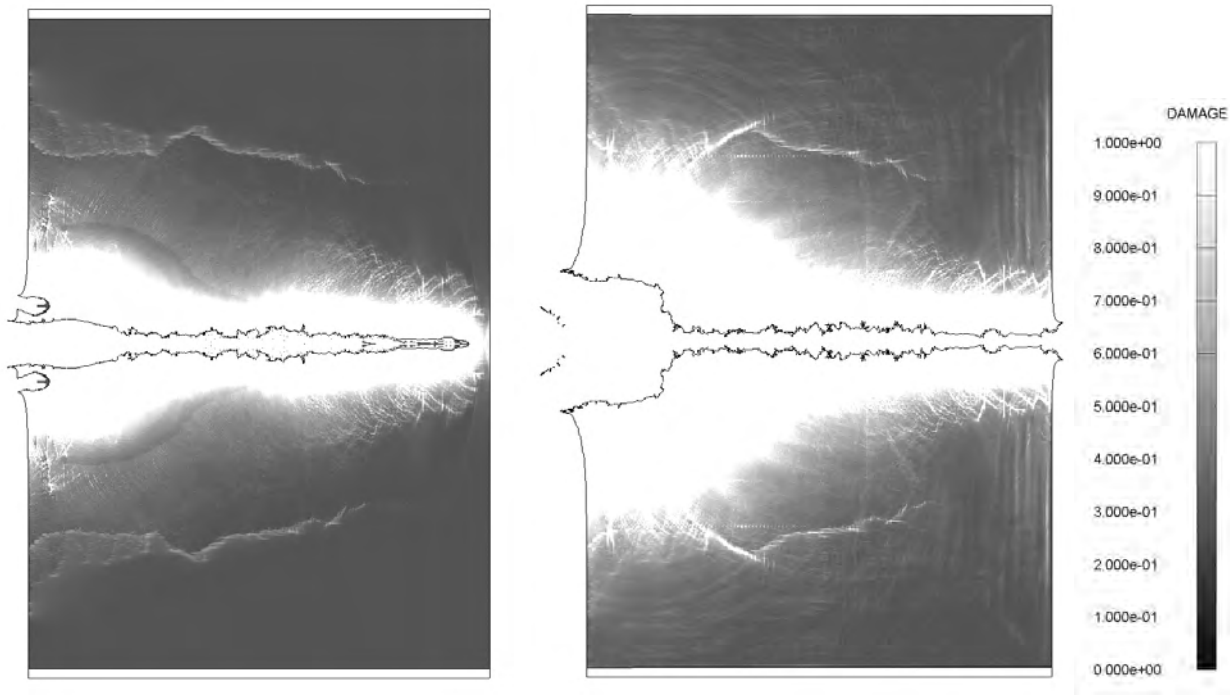

Figure 6.2. Cross section plots showing calculated damage levels in a 700 mm diameter concrete target for the case with both jet and EFP at times 275 µs (left) and 450 µs (right) (Helte et al., 2005). Times are given relative to the time of detonation of the charge.

A combination of traditional fortification constructions and modern type of armour steels increases the protection level of underground structures. This concept was studied within another project parallel to this experimental investigation (Hansson, 2004). The methodology can also be used to enhance the protection level of other type of structures, e.g. strengthening of buildings used for temporary protection or camps. Further, structures subjected to a combination of blast and fragment loads are likely to have an increased level of protection if penetration into the structural bearing parts of the construction is prohibited. The use of armour steel for protection against penetration may be one solution that can improve existing structures, e.g. of reinforced concrete.

For an underground hardened structure it is possible to further enhance the protection level by the use of several complementary techniques to obtain an acceptable protection level. A layered overburden could contain from top down: a layer of rubble, a burster slab of heavily reinforced concrete, backfilling, shock absorbing material and then a reinforced concrete structure. The use of yaw-inducing deflection grids constructed of reinforced concrete against penetrators with a L/D ratio of approximately 8 was studied by Underwood (1995). The deflection grid is intended to increase the yaw of an advanced penetrator, and thereby increase the bending forces during the penetration. One type of deflection grid is shown in figure 6.3.

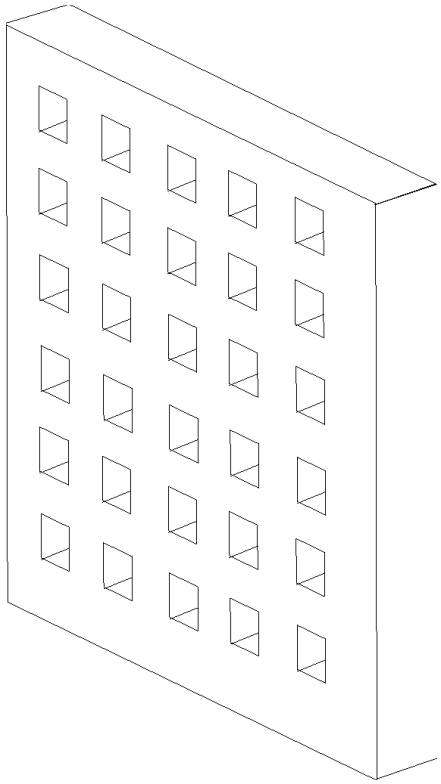

Figure 6.3. Example of a design for a yaw-inducing reinforced concrete deflector grid for the protection against advanced penetrating weapons.

7. Future research

The possibilities to predict penetration depths for projectiles with a length to diameter ratio of 9 to 10 is limited, especially when it comes to evaluate the penetration performance for non-normal impact conditions or in high performance concrete. The only available method, apart from well controlled experiments, that can be used for the moment is advanced numerical models, and these models are currently only suitable for research work. However, with the use of advanced material models and verified experimental work in both model and full scale it is possible to enhance the understanding of the penetration phenomena. Thereby, simplified penetration equations can be modified to consider these types of warheads and also HPC targets.

In the future it is likely that penetrating warheads with a diameter of 150 mm and a mass of 100 to 120 kg will penetrate 2.0 m normal strength concrete targets, and larger warheads with improved designs and materials is likely to penetrate up to 5.0 m concrete targets. With the introduction of dual charge penetrating warheads, e.g. KEPD 350, Mephisto or BROACH, it is possible to penetrate up to 6 m of concrete with a 500 kg warhead. This is equal to the performance of a unitary penetrating bomb with a mass of more than 2000 kg. To decrease the penetration depths in concrete and multi layered hardened structures it is necessary to improve the designs of protective structures. This is especially important if dual charge warheads and multiple impacts are considered. Therefore, future research should focus on the use of improved multi layered protective structures to reduce the penetration performance of warheads, and also to determine performance of the improved penetrating warheads that now are under development.

Dual charge warheads are also under development for man portable rocket propelled grenades for urban combat situations. Protection against these new types of small weapons with approximately 100 mm diameter shaped charges and a small follow through charge also needs to be considered. However, methods developed to estimate the performance of the heavier warheads mentioned above could also be used to study this type of man portable dual charge weapons.

It is recommended that a methodology for prediction of weapon effects on hardened structures, incl. field fortifications, should be established. This requires that several of the research topics mentioned above needs to be investigated, and the results should then be used to develop a methodology that can predict the overall behaviour of a protective structure. Complementary research regarding close in detonations, and also contact detonations, are needed to describe the performance of a penetrating warhead. The methodology could later be extended to consider an increased number of weapon types and effects, e.g. improvised explosive devices (IED).

Further experimental penetration studies are needed to obtain test results for comparison with numerical and analytical penetration models. It is therefore of interest to study several types of target configurations, e.g. layered structures and heavy reinforced HPC. Studies of different projectile designs, e.g. nose geometries, and the interaction of the projectile and target are also of interest in the future to predict the penetration performance and behaviour of a projectile in a target. The use of instrumented projectiles to obtain data for comparison with numerical simulations is recommended for future validating tests. This is especially important in the case of experiments and simulations of dual charge warheads.

Evaluation of simulation methods is performed in parallel with the experimental work at FOI, e.g Hansson (2003a and 2005). An initial study of the use of numerical simulations to evaluate the penetration experiments with L/D=9 projectiles is reported by Hansson (2005) with some preliminary results given in this report. The use of numerical simulations to study penetration phenomena in concrete seems promising. Therefore, further numerical simulations of the performed tests are recommended. It is recommended that the data from the tests, e.g. impact velocity, yaw and pitch, are used as input for these simulations. One parameter that is of great interest to study is the influence of different designs of the projectile nose, and to compare simulations with different nose shapes with experimental results. In general, the modelling of the interface between target and projectile for concrete targets, and especially reinforced concrete targets, is important to study to be able to improve both empirical equations for penetration and numerical simulations of penetration in concrete.

Simulations of the penetration tests performed in high performance concrete presented in this report, and also earlier by Hansson (2003b), are recommended. Material parameters for the P-α equation of state and the RHT material model were determined at EMI by Wicklein and Riedel (2002), and Riedel and Machens (2004). This makes it possible to combine material data determined for a specific high performance concrete, together with penetration results obtained for the same type of material. Thereby, a direct comparison of the experimental results and numerical simulations are possible.

Research regarding the damage evolution in concrete is also necessary to enhance the possibility to predict projectile penetration with the use of simulations. Especially, when perforation of a concrete target are considered. An improved damage model for concrete is developed at EMI (Schuler, 2004). Further, Chalmers University of Technology (CTH) also performs research regarding damage evolution in concrete subjected to air-blast loads and projectile impacts. A material description for concrete with a bi-linear crack softening tensile failure model is developed at CTH by Lepännen (2004). This tensile failure model uses a strain rate dependent tensile strength according to Malvar and Ross (1998), and a constant fracture energy. However, the dynamic fracture energy is approximately 2.5 to 3 times greater than the static value at strain rates of approximately 30 s^{-1} (Schuler, 2004), i.e. for spalling. Therefore, an increased value for the fracture energy might be necessary to use for this tensile failure model when spalling is considered to be the dominating failure mechanism. These improved failure models considers the influence of strain rate on the tensile strength, and the damage model from EMI also consider strain rate dependent fracture energy of concrete. The use of this type of failure models may enhance simulations of concrete penetration, especially for the case of shaped charge penetration and dual charge warheads, and also contact detonations against concrete structures.

It is recommended that the material model recently developed at EMI should be used for further studies of shaped charge jet penetration, and dual charge warhead performance, in reinforced concrete structures. Estimations of the performance of shaped charges and dual charge warheads should be possible to give for a reinforced normal strength concrete with the use of this material model and the available numerical tools. The use of a meshless formulation may further improve the numerical model. However, it is necessary to perform verifying experimental work regarding the performance of both shaped charges and dual charge warheads against hardened and protective structures. Combat situations in urban areas and international operations require that also normal building structures are considered. Further, it is necessary to determine the behaviour of HPC subjected to this type of combined weapons effect.

References

ConWep (Conventional weapons effects program), U.S. Army Engineer Waterways Experiment station, Vicksburg, 1992.

Elfving, C., Karlsson, S. and Hansson, H.: Model for penetration of shaped charges in protective coverings, FOI report, Tumba, 2005 (to be published). In Swedish.

Gold, V. M.: Concrete penetration by eroding projectiles: Experiments and analysis, ARAED-TR-96014, U.S. Army Armament Research, Development and Engineering center, December 1996.

Hansson, H.: 2D and 3D simulations of concrete penetration using the RHT Material Model, FOI-R--0922--SE, ISSN 1650-1942, Tumba, October 2003a.

Hansson, H.: Experimental study of concrete penetration for L/D=9 projectiles, FOI-RH--0226--SE, Tumba, October 2003b.

Hansson, H.: A note on empirical formulas for the prediction of concrete penetration, FOI-R--0968--SE, ISSN 1650-1942, Tumba, November 2003c.

Hansson, H.: Penetration in Armox 500 and concrete for a projectile with L/D=9, FOI-RH--0354--SE, Tumba, December 2004.

Hansson, H.: Simulation of penetration in NSC for a L/D=9 projectile, ISSN 1650-1942, FOI, Tumba, 2005 (to be published).

Helte, A., Calsson, T., Hansson, H., Karlsson, S., Lundgren, J., Westerling, L. and Örnhed, H.: Wall breaching tandem warhead, submitted to 22nd Int. Sym. on Ballistics, Vancouver 2005.

Johnson, G. R., Beissel, S. R., Anderson, Jr., C. E., Popelar, C. H. and Walker, J. D.: Penetrator case fracture predictive technology: Volume II-- Numerical algorithms and computations, AFRL-MN-EG-TR-1999-7054, Air Force Research Laboratory, June 1999.

Leppänen, J.: Concrete structures subjected to fragment impacts - Dynamic behaviour and material modelling, Chalmers University of Technology, ISBN 91-7291-511-0, Gothenburg, 2004.

Magnusson, J., Unosson, M. and Carlberg, A.: High performance concrete ”HPC”, Field experiments and production, FOI-R--0256--SE, ISSN 1650-1942, Tumba, November 2001.

Malvar, L.J. and Ross, C.A.: Review of static and dynamic properties of concrete in tension, ACI Materials Journal, vol. 95, no.6, November-December 1998.

Riedel, W.: Beton unter dynamishen lasten, Meso- und makromechanische modelle und ihre parameter. EMI-Bericht 6/00, Freiburg, July 2000.

Riedel, W. and Machens, M.: Mechanical properties of concrete and limestone, EMI Report E 07/04, Freiburg, 2004.

Schuler, H.: Experimentelle und numerische untersuchungen zur schädigung von stossbeanspruchten beton, Fraunhofer, Institut Kurzzeitdynamik Ernst-Mach-Institut, ISBN 3-8167-6463-0, Freiburg, 2004.

Underwood, J. M.: Effectiveness of yaw-inducing deflection grids for defeating advanced penetrating weapons, ESL-TR-92-61, Applied Research Associates, Tyndall Air Force Base, April 1995.

Wicklein, M. and Riedel, W.: Mesomechanical characterization of a high strength concrete - Experimental investigation and material modelling, EMI Report E 14/02, Freiburg 2002.

Appendix 1: High-speed films from tests performed in 2004.

The 70 mm high-speed films from the tests performed during 2004 are shown in this appendix.

Contents of appendix 1: High-speed films

Test no. 2004-1

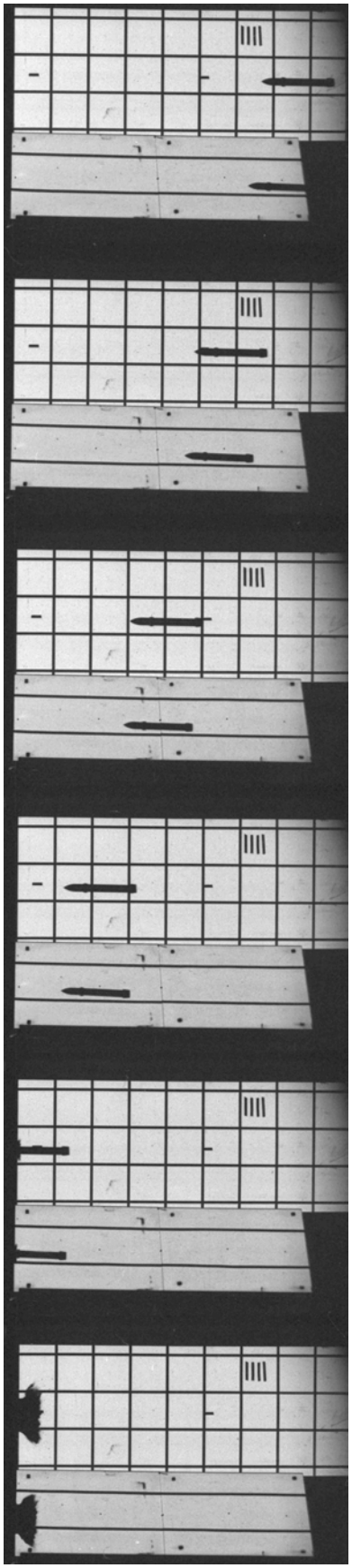

Test no. 2004-2

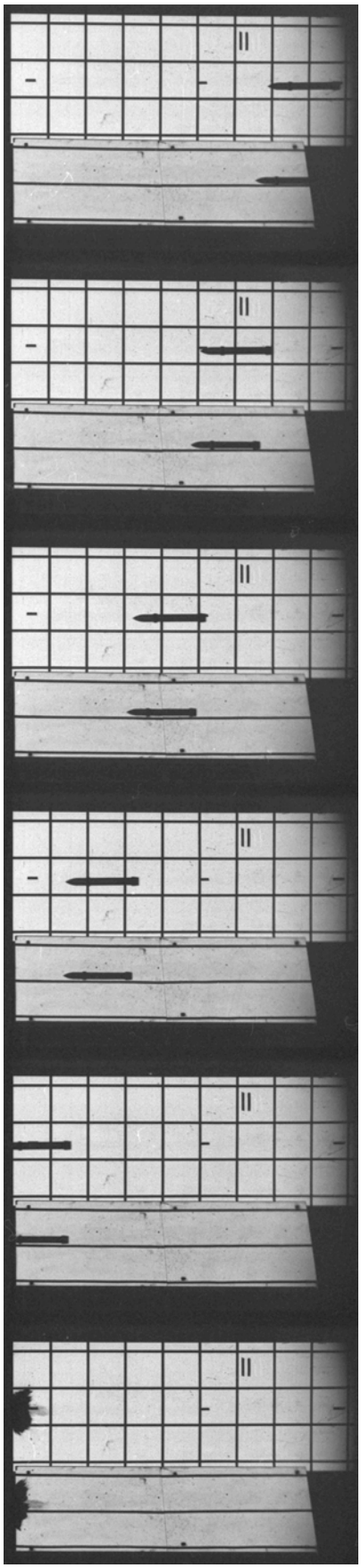

Test no. 2004-3

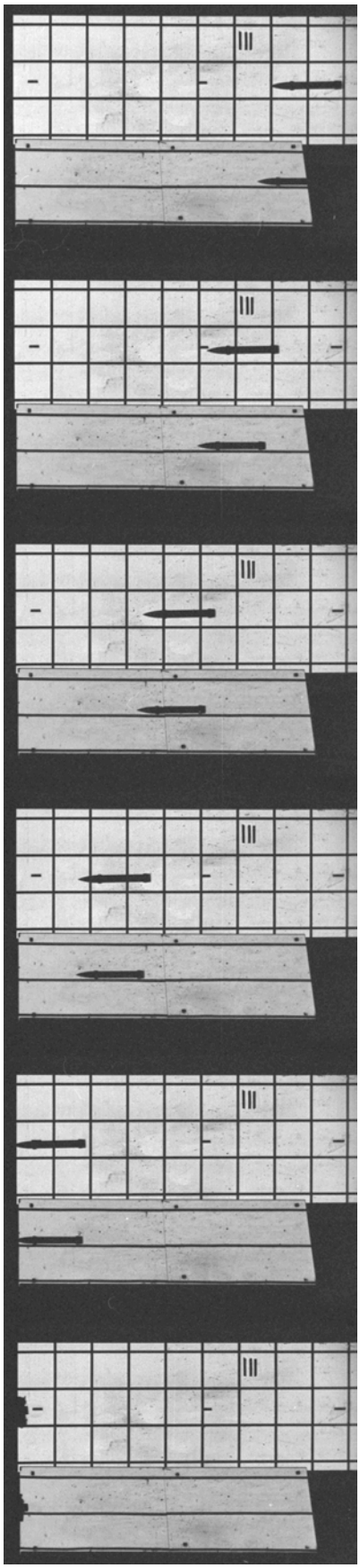

Test no. 2004-4

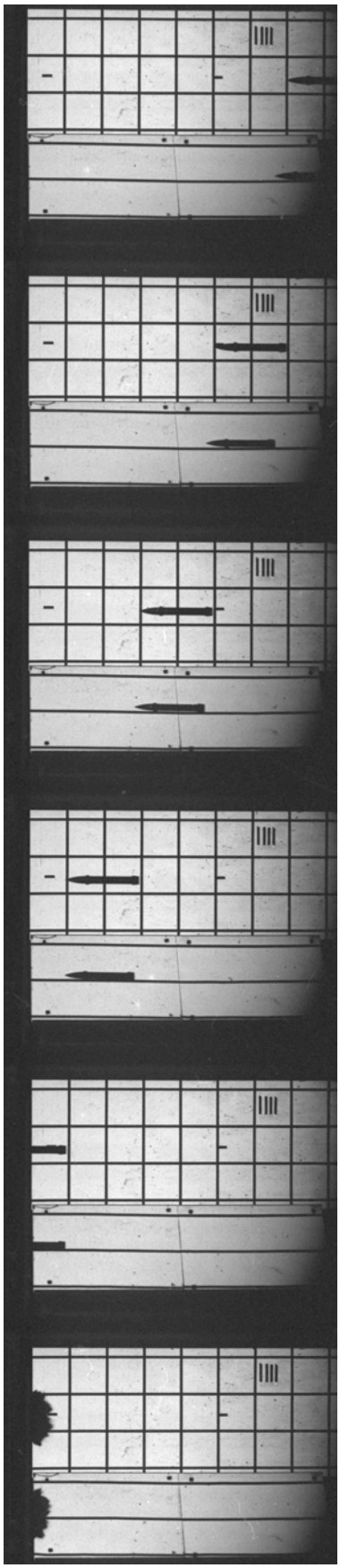

Test no. 2004-5

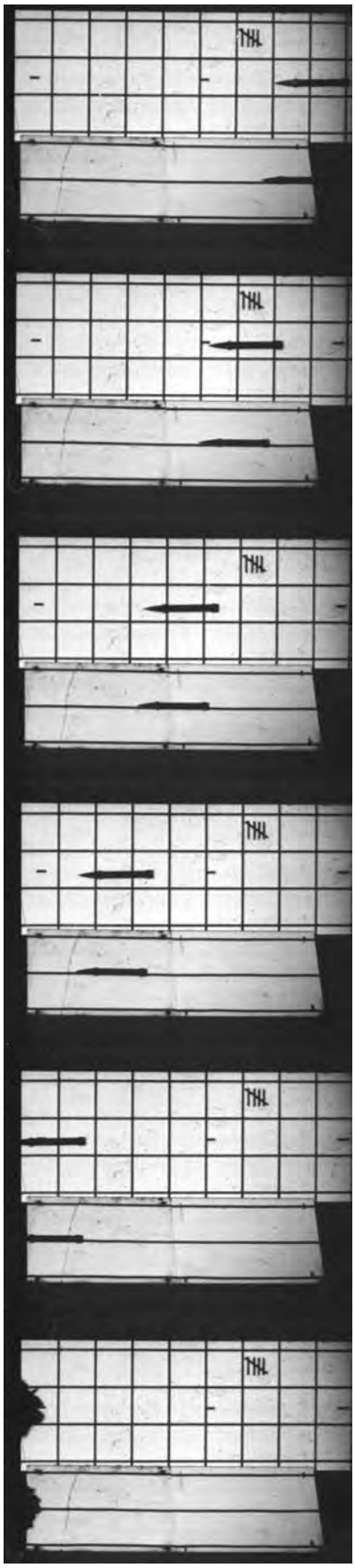

Test no. 2004-6

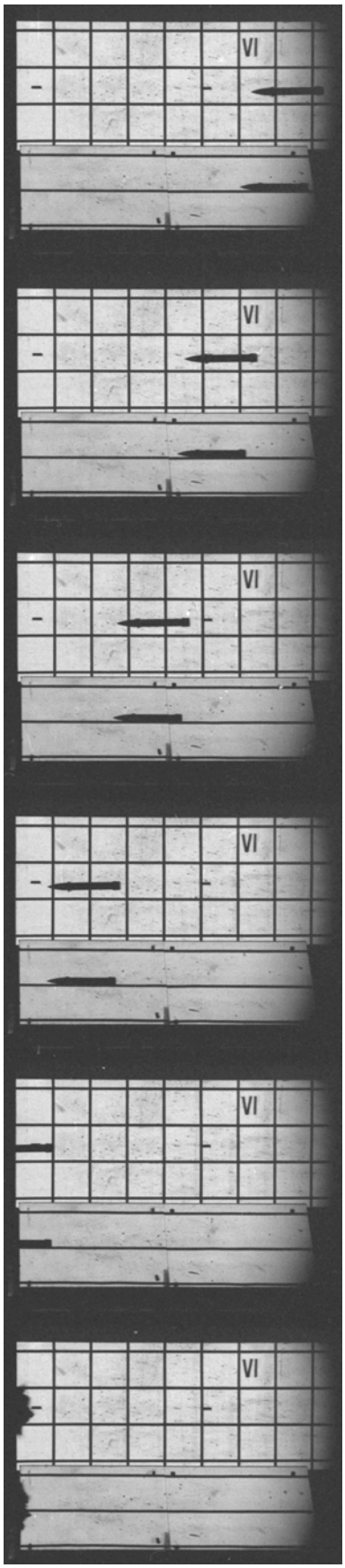

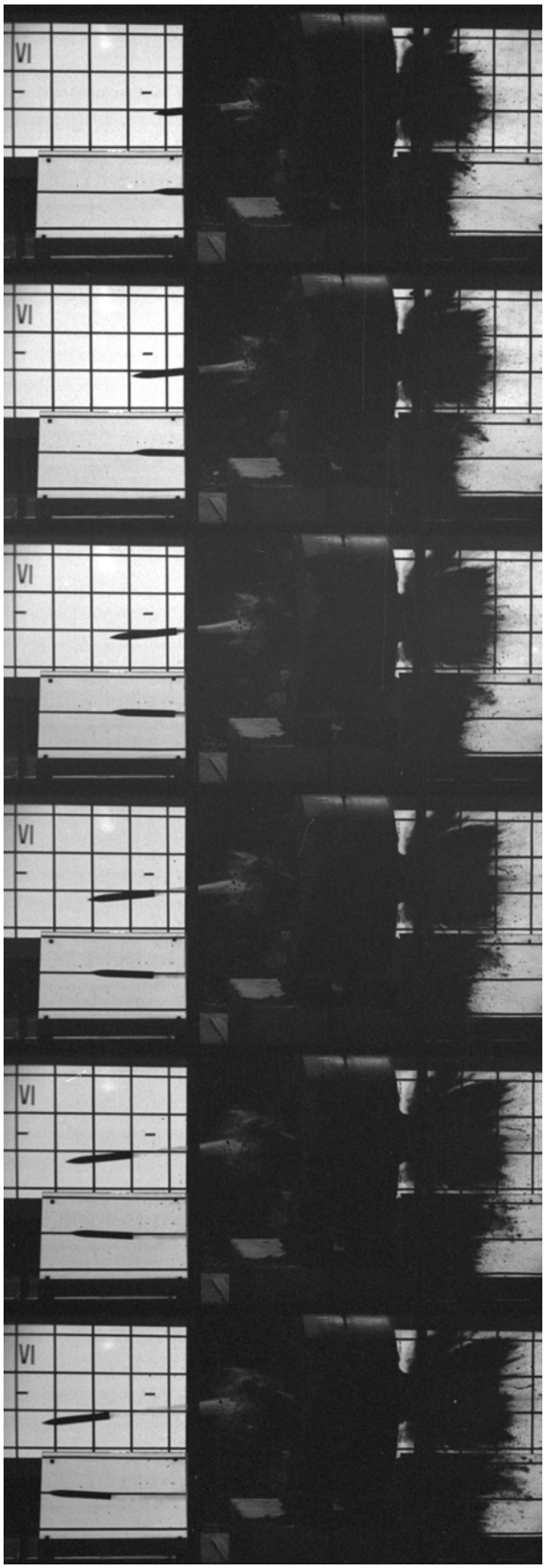

Test no. 2004-8

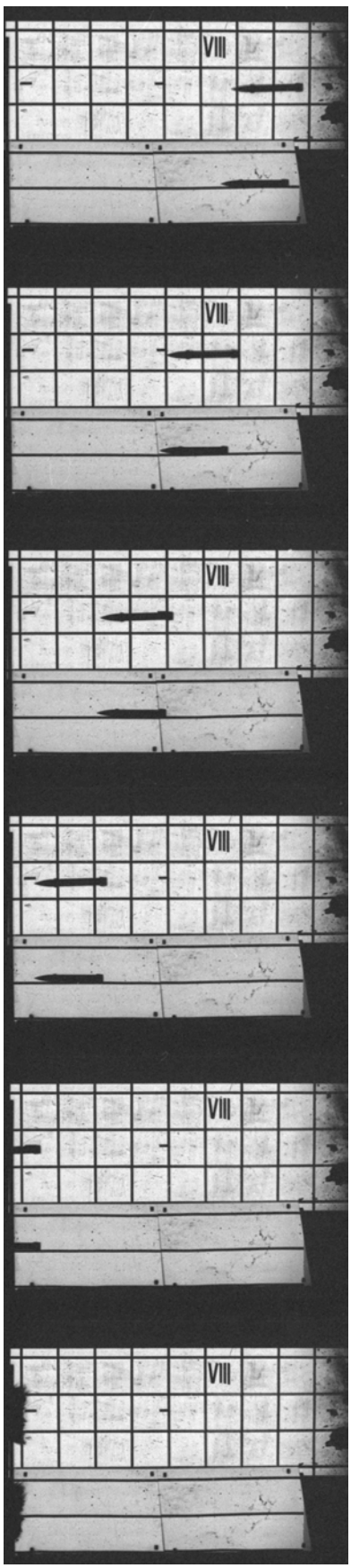

Test no. 2004-10

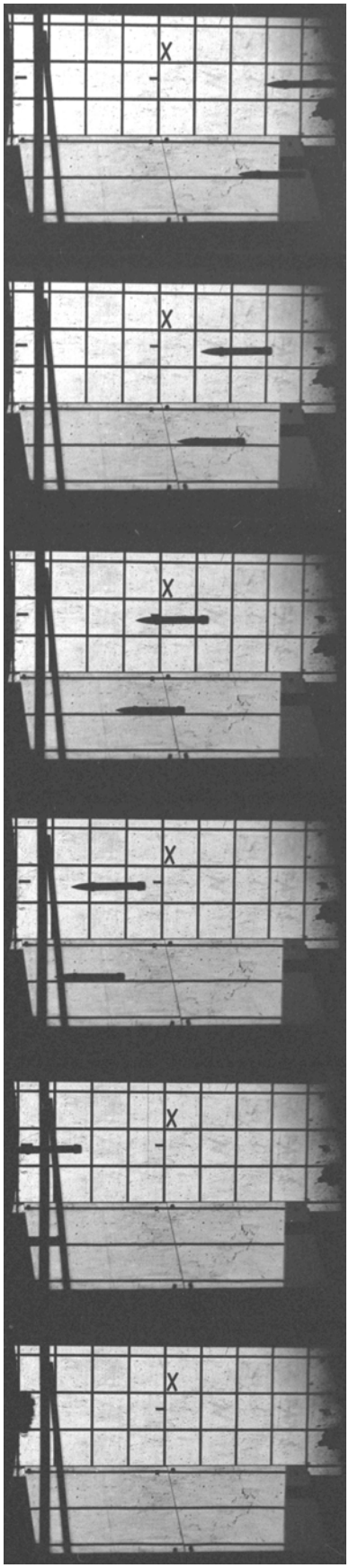

Test no. 2004-12

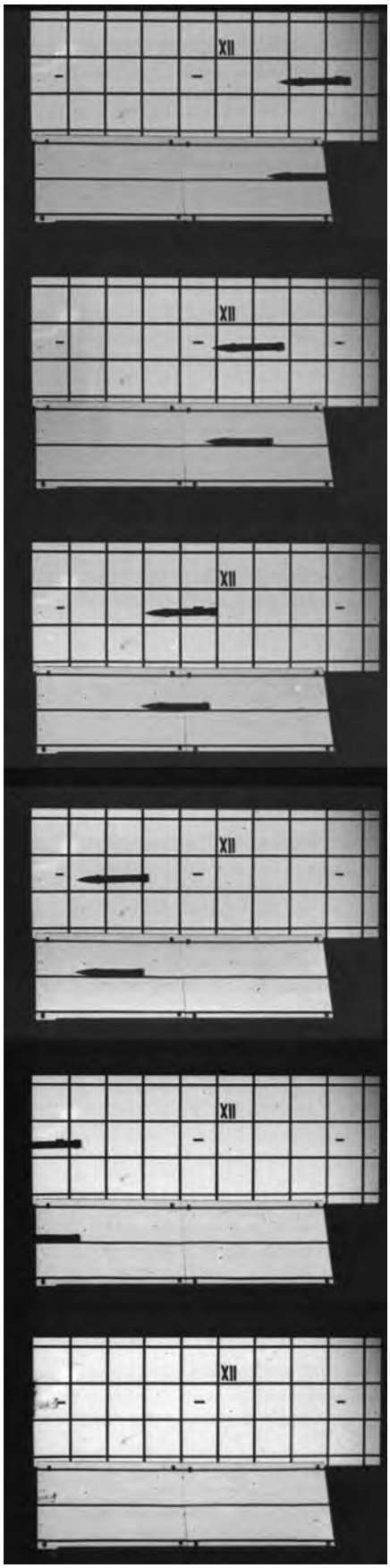

Test no. 2004-13

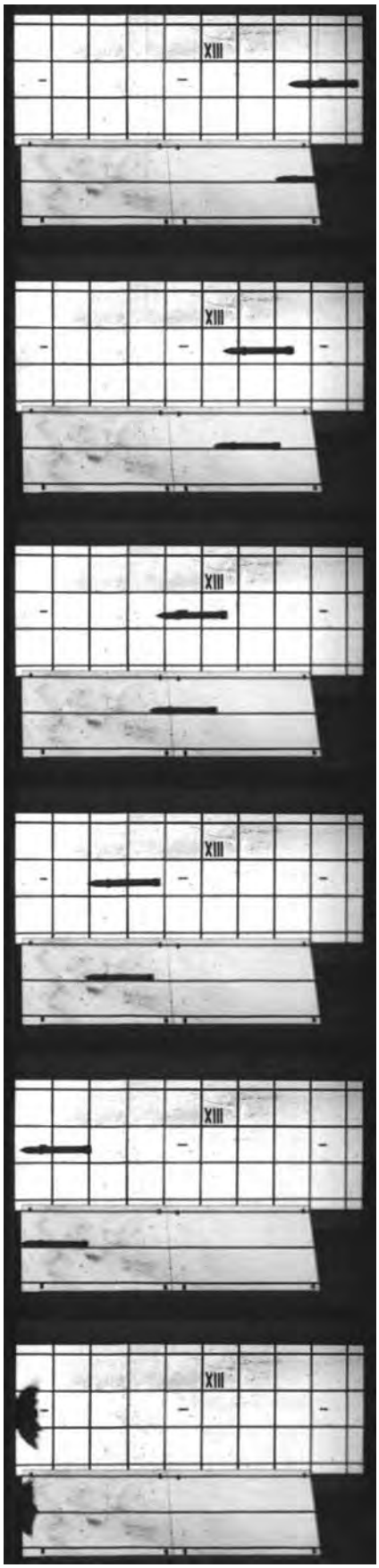

Test no. 2004-14

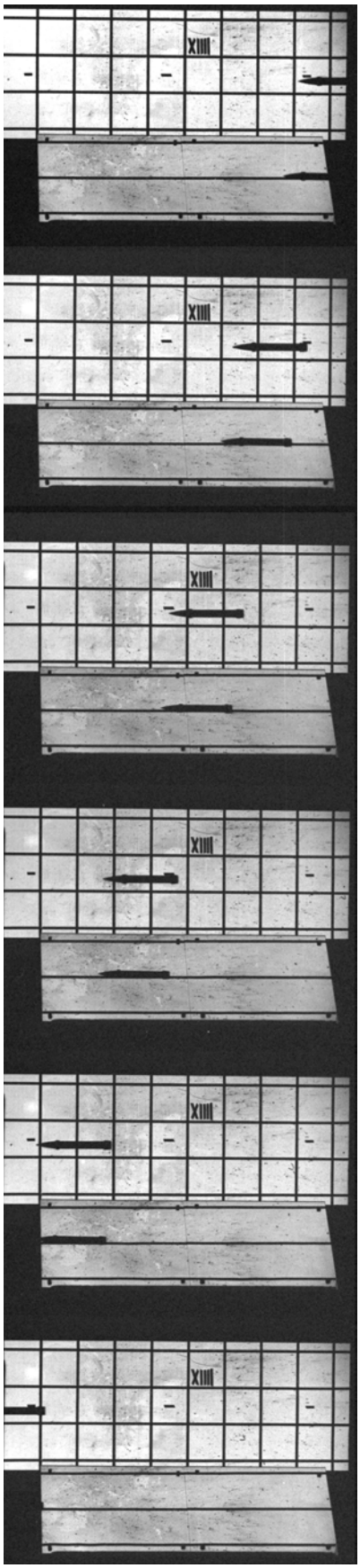

Test no. 2004-15

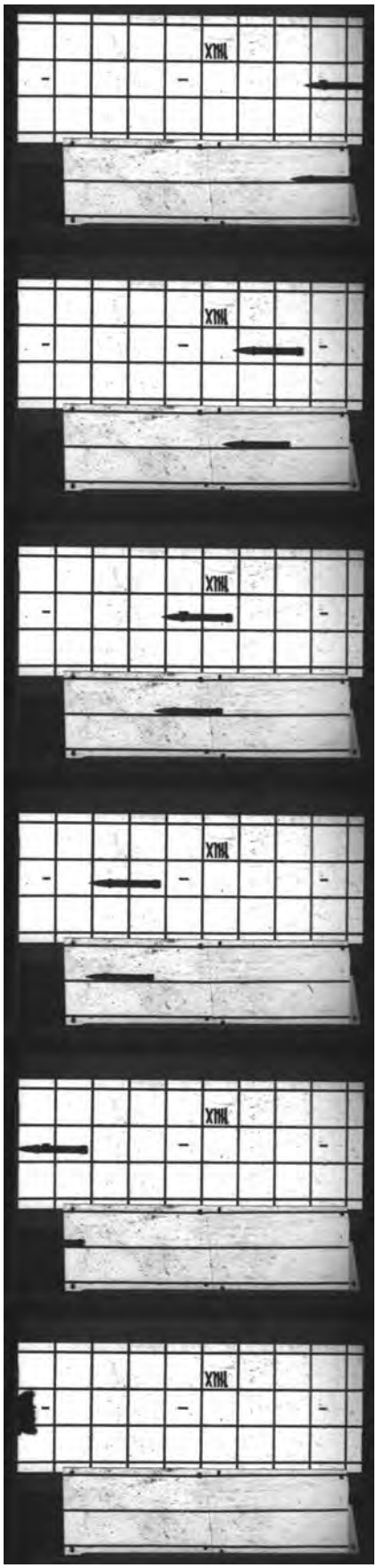

Test no. 2004-16

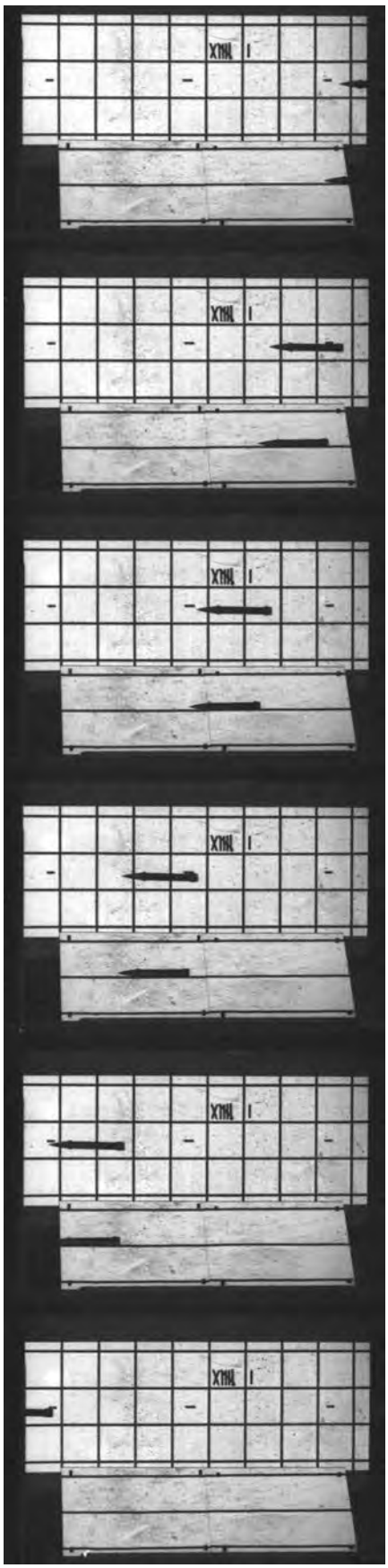

Test no. 2004-36

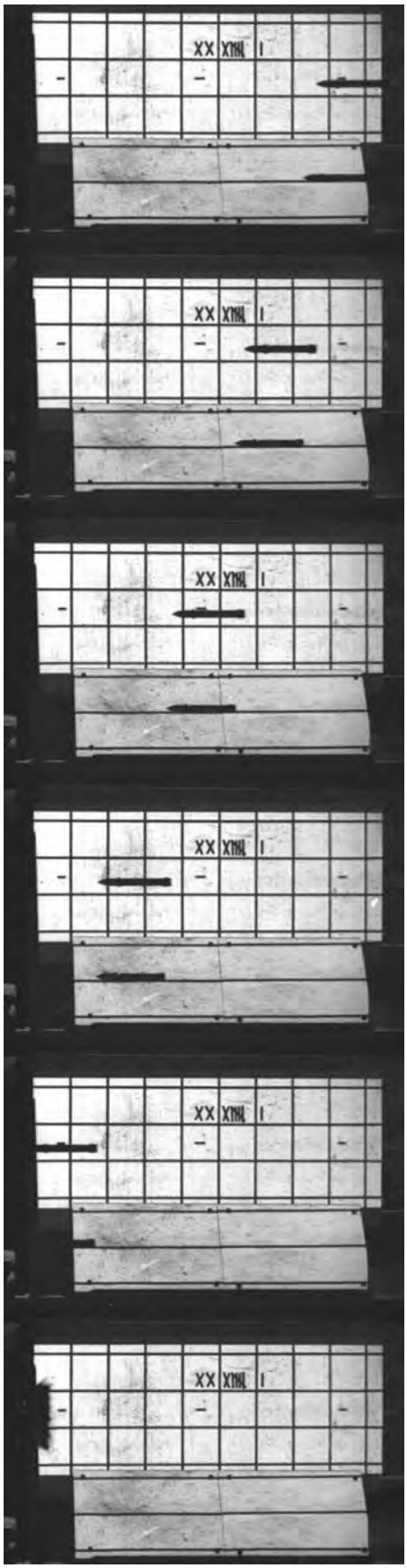

Test no. 2004-17

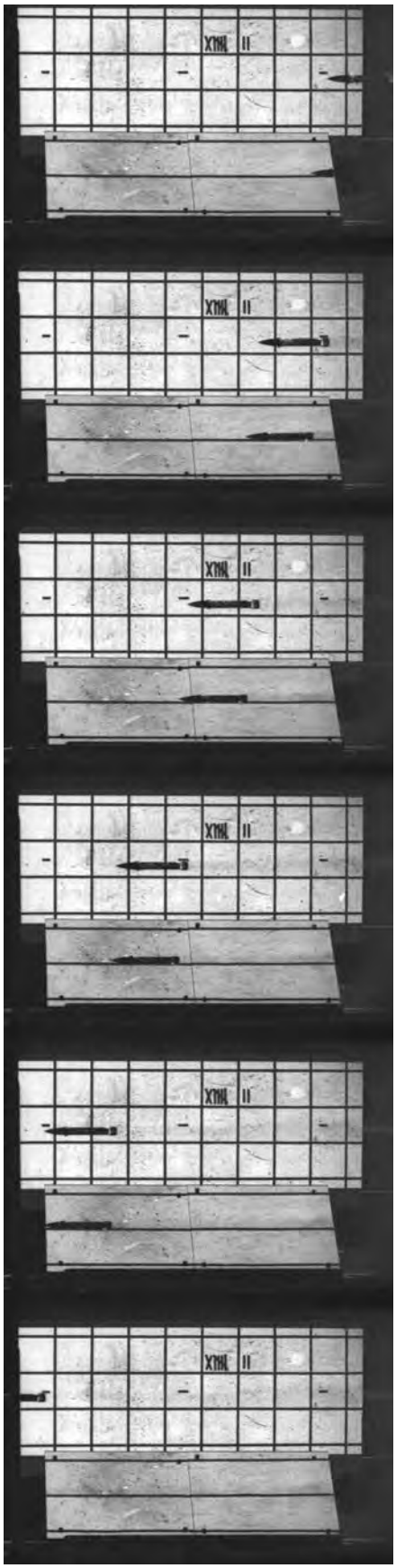

Test no. 2004-18

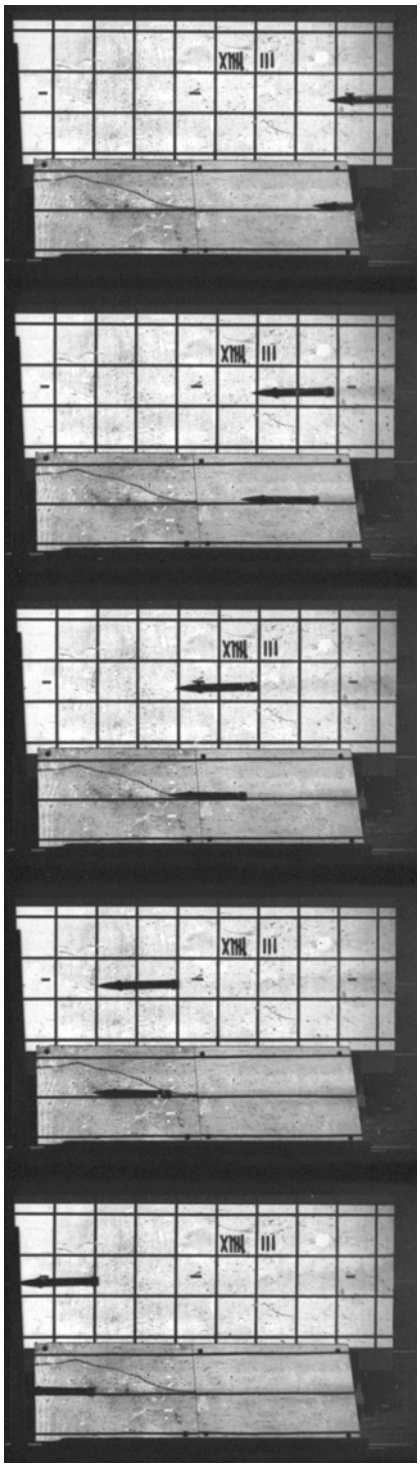

Test no. 2004-19

Test no. 2004-20

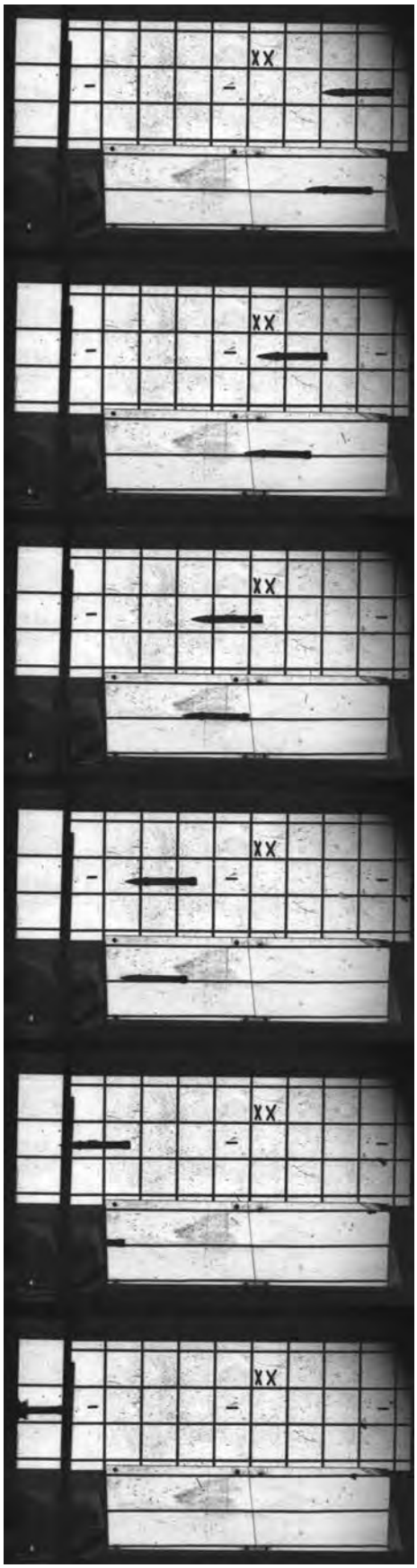

Test no. 2004-21

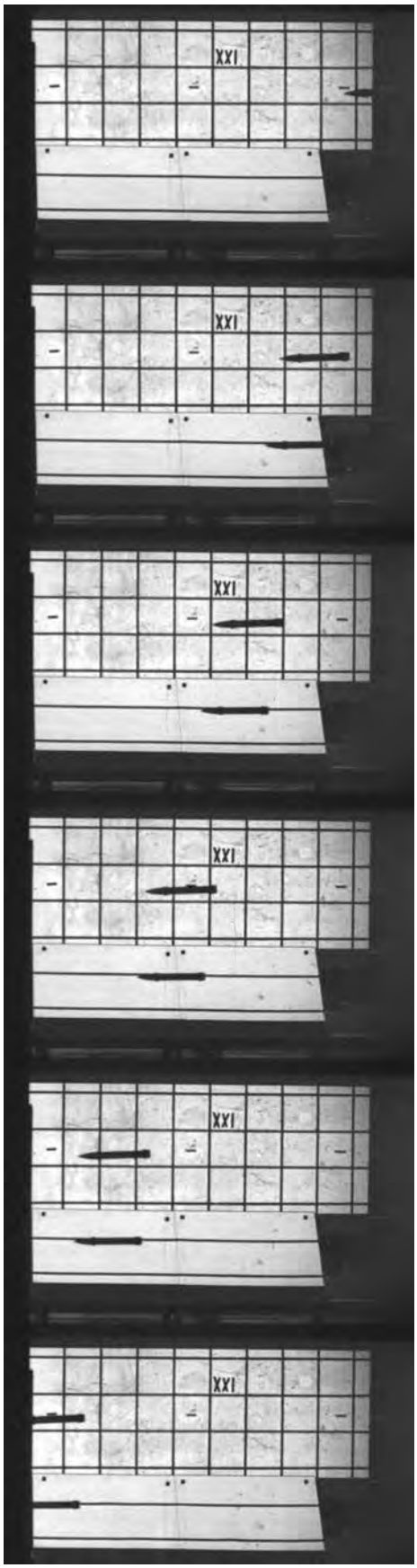

Test no. 2004-23-2

Test no. 2004-23-1

Test no. 2004-24-1

Test no. 2004-24-2

Test no. 2004-25

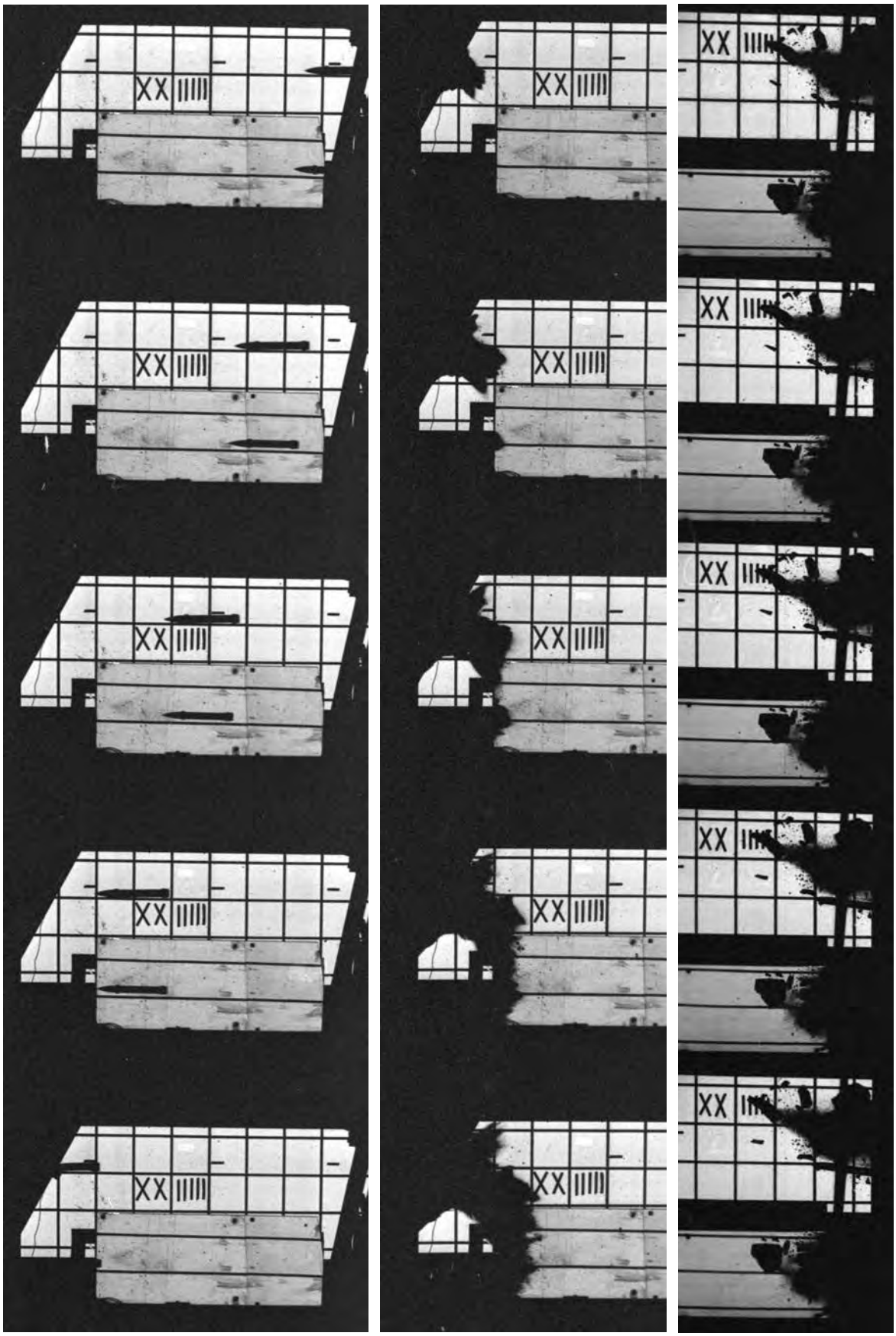

Test no. 2004-26

Test no. 2004-27

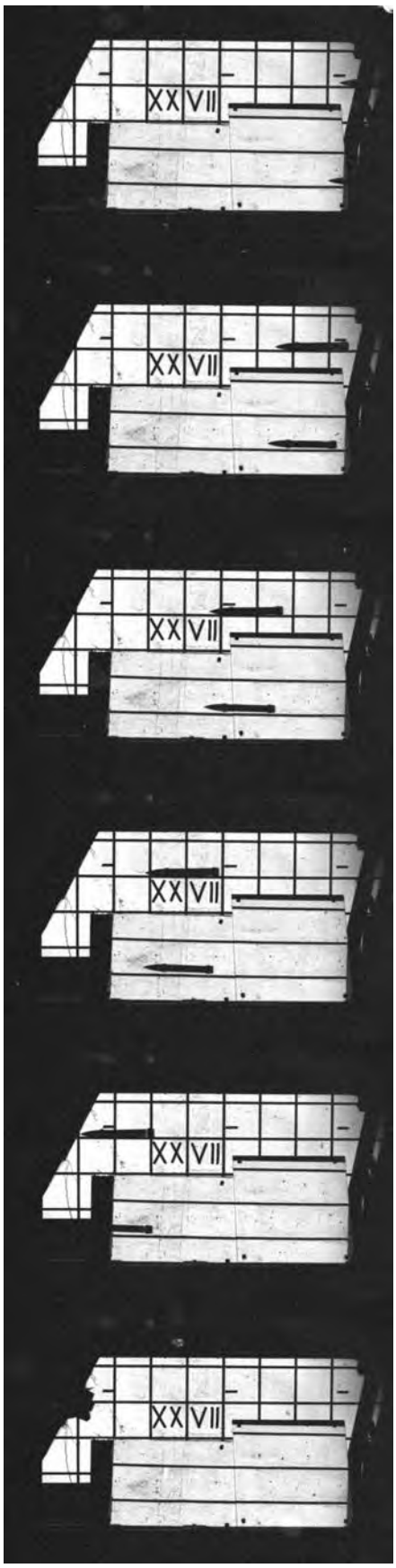

Test no. 2004-28

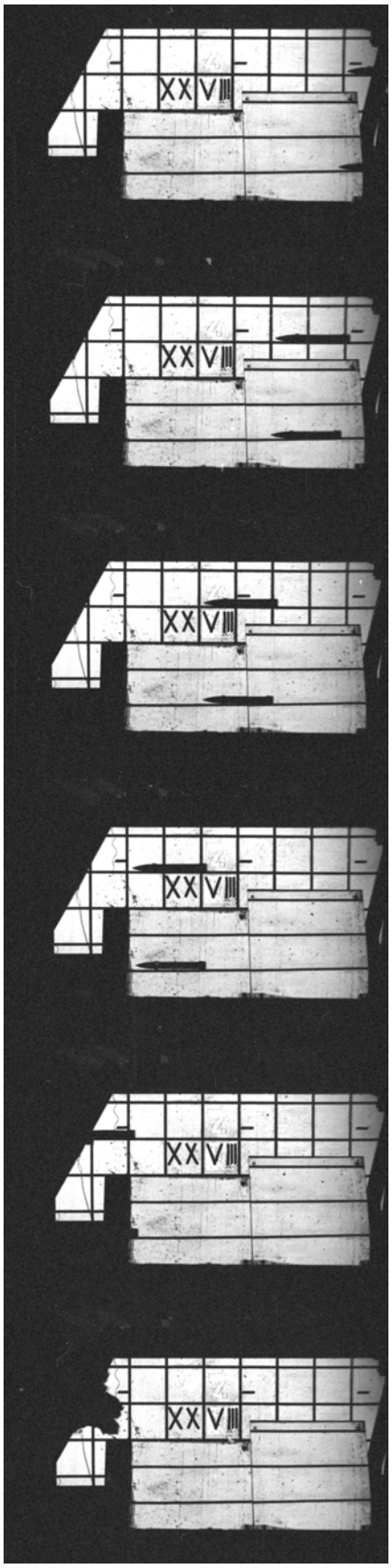

This page intentionally blank.

Concrete with granite or gneiss used for aggregates.

Test id	M (kg)	D (mm)	Ogive (mm)	f´c (MPa)	V (m/s)	L (mm)	L/D	CRH	N	Pen. (mm)	Reference
75 mm -97 Test no. 1	6.28	75.0	127	35 #	484	225	3.00	1.69	1.02	680	Magnusson et al. 2001
75 mm -97 Test no. 3	6.28	75.0	127	35 #	483	225	3.00	1.69	1.02	660	Magnusson et al. 2001
75 mm -97 Test no. 4	6.28	75.0	127	35 #	482	225	3.00	1.69	1.02	660	Magnusson et al. 2001
75 mm -98:2 Test no. 8	6.28	75.0	127	35 #	647	225	3.00	1.69	1.02	990	Magnusson et al. 2001
75 mm -98:2 Test no. 9	6.28	75.0	127	95 #	653	225	3.00	1.69	1.02	560	Magnusson et al. 2001
75 mm -98:2 Test no. 10	6.28	75.0	127	130 #	647	225	3.00	1.69	1.02	440	Magnusson et al. 2001
75 mm -98:2 Test no. 12	6.28	75.0	127	75 #	571	225	3.00	1.69	1.02	410	Magnusson et al. 2001
75 mm -99 Test 1	6.28	75	127	140 #	620	225	3.00	1.69	1.02	450	Magnusson et al. 2001
75 mm -99 Test 2	6.28	75	127	140 #	612	225	3.00	1.69	1.02	540	Magnusson et al. 2001
75 mm -99 Test 3	6.28	75	127	140 #	619	225	3.00	1.69	1.02	510	Magnusson et al. 2001
DA544	0.50	25.0	75	38.4	292	151	6.06	3.00	1.13	123	Buzaud et al., 1999
DA552	0.50	25.0	75	38.4	132	151	6.06	3.00	1.13	55	Buzaud et al., 1999
Test no. 1	2.30	50.8	152	43	320	356	7.00	3.00	1.13	185	Gran and Frew, 1997
Test no. 2	2.30	50.8	152	43	310	356	7.00	3.00	1.13	175	Gran and Frew, 1997
Test no. 3	2.30	50.8	152	43	316	356	7.00	3.00	1.13	157	Gran and Frew, 1997
WTD91 - 6	485	363	750	37	259	1200	3.31	2.07	1.06	1350	Riedel et al., 1999
WTD91 - 3	433	363	750	39	261	1200	3.31	2.07	1.06	960	Riedel et al., 1999
EMI - 1934	6.63	90.8	184	40.5	238	300	3.31	2.03	1.05	185	Riedel et al., 1999
EMI - 1935	6.64	90.8	184	42.4	254	300	3.31	2.03	1.05	210	Riedel et al., 1999
EMI	0.595	25.0	100	50	389			4.00	1.20	215	Hiermaier and Thoma, 1997
Test no. 4	4.37	50.8	152	40.5	516	387	7.62	3.00	1.13	694	Gran et al., 1999
Test no. 5	4.38	50.8	152	41.6	510	387	7.62	3.00	1.13	666	Gran et al., 1999
Test no. 6	4.38	50.8	152	42.4	505	387	7.62	3.00	1.13	689	Gran et al., 1999
Test #3	30.4	105	314	34.5	273	632	6.03	3.00	1.13	463	Baty et al, 2003
fc=35 Test no. 14	0.906	26.9	53.8	35.2	277	242	9.01	2.00	1.05	173	Forrestal et al., 1994
fc=35 Test no. 13	0.910	26.9	53.8	37.8	410	242	9.01	2.00	1.05	310	Forrestal et al., 1994
fc=35 Test no. 15	0.907	26.9	53.8	38.1	431	242	9.01	2.00	1.05	411	Forrestal et al., 1994
fc=35 Test no. 11	0.912	26.9	53.8	33.5	499	242	9.01	2.00	1.05	480	Forrestal et al., 1994
fc=35 Test no. 12	0.910	26.9	53.8	38.4	567	242	9.01	2.00	1.05	525	Forrestal et al., 1994
fc=35 Test no. 2	0.905	26.9	53.8	36.9	590	242	9.01	2.00	1.05	729	Forrestal et al., 1994
fc=35 Test no. 1	0.901	26.9	53.8	40.1	591	242	9.01	2.00	1.05	513	Forrestal et al., 1994

Note #: Estimated from measured cube strength.

Concrete with granite or gneiss used for aggregates.

Test id	M (kg)	D (mm)	Ogive (mm)	f´c (MPa)	V (m/s)	L (mm)	L/D	CRH	N	Pen. (mm)	Reference
fc=35 Test no. 3	0.903	26.9	53.8	35.4	631	242	9.01	2.00	1.05	607	Forrestal et al., 1994
fc=35 Test no. 4	0.905	26.9	53.8	34.7	642	242	9.01	2.00	1.05	620	Forrestal et al., 1994
fc=35 Test no. 5	0.901	26.9	53.8	36.0	773	242	9.01	2.00	1.05	866	Forrestal et al., 1994
fc=35 Test no. 6	0.904	26.9	53.8	32.4	800	242	9.01	2.00	1.05	958	Forrestal et al., 1994
fc=90 Test no. 2	0.907	26.9	53.8	90.5	561	242	9.01	2.00	1.05	353	Forrestal et al., 1994
fc=90 Test no. 1	0.898	26.9	53.8	91.0	584	242	9.01	2.00	1.05	384	Forrestal et al., 1994
fc=90 Test no. 3	0.908	26.9	53.8	95.0	608	242	9.01	2.00	1.05	422	Forrestal et al., 1994
fc=90 Test no. 4	0.905	26.9	53.8	101	622	242	9.01	2.00	1.05	437	Forrestal et al., 1994
fc=90 Test no. 6	0.907	26.9	53.8	94.0	750	242	9.01	2.00	1.05	630	Forrestal et al., 1994
fc=90 Test no. 5	0.900	26.9	53.8	108	793	242	9.01	2.00	1.05	605	Forrestal et al., 1994
1-0335	0.478	20.3	60.9	62.8	450	203	10.0	3.00	1.13	300	Forrestal et al., 1996
1-0336	0.478	20.3	60.9	62.8	612	203	10.0	3.00	1.13	480	Forrestal et al., 1996
1-0337	0.478	20.3	60.9	62.8	821	203	10.0	3.00	1.13	760	Forrestal et al., 1996
1-0341	0.478	20.3	60.9	62.8	926	203	10.0	3.00	1.13	950	Forrestal et al., 1996
1-0346	0.478	20.3	60.9	62.8	987	203	10.0	3.00	1.13	920	Forrestal et al., 1996
1-0338	0.478	20.3	60.9	62.8	1024	203	10.0	3.00	1.13	940	Forrestal et al., 1996
LROD-2	1.61	30.5	91.5	51	405	305	10.0	3.00	1.13	370	Forrestal et al., 1996
LROD-3	1.61	30.5	91.5	51	446	305	10.0	3.00	1.13	420	Forrestal et al., 1996
LROD-6	1.61	30.5	91.5	51	545	305	10.0	3.00	1.13	560	Forrestal et al., 1996
LROD-4	1.61	30.5	91.5	51	651	305	10.0	3.00	1.13	780	Forrestal et al., 1996
LROD-8	1.61	30.5	91.5	51	804	305	10.0	3.00	1.13	1050	Forrestal et al., 1996
LROD-5	1.61	30.5	91.5	51	821	305	10.0	3.00	1.13	1230	Forrestal et al., 1996
LROD-9	1.61	30.5	91.5	51	900	305	10.0	3.00	1.13	1410	Forrestal et al., 1996
LROD-10	1.61	30.5	91.5	51	1009	305	10.0	3.00	1.13	1750	Forrestal et al., 1996

Concrete with limestone aggregate.

Test id	M (kg)	D (mm)	Ogive (mm)	f´c (MPa)	V (m/s)	L (mm)	L/D	CRH	N	Pen. (mm)	Reference
SNL-00-11/3	12.9	76.2	229	39	238	531	6.96	3.00	1.13	300	Forrestal et al. 2003
SNL-00-12/4	12.9	76.2	229	39	276	531	6.96	3.00	1.13	380	Forrestal et al. 2003
SNL-00-09/1	12.9	76.2	229	39	314	531	6.96	3.00	1.13	450	Forrestal et al. 2003
SNL-00-10/2	12.9	76.2	229	39	370	531	6.96	3.00	1.13	530	Forrestal et al. 2003
SNL-00-14/5	13.0	76.2	229	39	456	531	6.96	3.00	1.13	940	Forrestal et al. 2003
SNL-00-15/2	12.9	76.2	457	39	313	528	6.94	6.00	1.32	610	Forrestal et al. 2003
SNL-00-16/3	12.9	76.2	457	39	449	528	6.94	6.00	1.32	990	Forrestal et al. 2003
1-0354	0.478	20.3	60.9	58.4	442	203	10.0	3.00	1.13	287	Frew et al., 1998
1-0355	0.478	20.3	60.9	58.4	610	203	10.0	3.00	1.13	491	Frew et al., 1998
1-0356	0.478	20.3	60.9	58.4	805	203	10.0	3.00	1.13	840	Frew et al., 1998
1-0357	0.478	20.3	60.9	58.4	1009	203	10.0	3.00	1.13	1300	Frew et al., 1998
1-0390	0.478	20.3	60.9	58.4	791	203	10.0	3.00	1.13	730	Frew et al., 1998
1-0391	0.478	20.3	60.9	58.4	994	203	10.0	3.00	1.13	1160	Frew et al., 1998
LROD95-1	1.62	30.5	91.5	58.4	445	305	10.0	3.00	1.13	460	Frew et al., 1998
LROD95-2	1.62	30.5	91.5	58.4	584	305	10.0	3.00	1.13	790	Frew et al., 1998
LROD95-3	1.62	30.5	91.5	58.4	796	305	10.0	3.00	1.13	1230	Frew et al., 1998
LROD96-0	1.62	30.5	91.5	58.4	980	305	10.0	3.00	1.13	1950	Frew et al., 1998
LROD95-4	1.62	30.5	91.5	58.4	992	305	10.0	3.00	1.13	1960	Frew et al., 1998
LROD96-1	1.62	30.5	91.5	58.4	972	305	10.0	3.00	1.13	1960	Frew et al., 1998

References for penetration tests

Baty, R. S., Lundgren R. G. and Patterson W. J., On Pilot-Hole Assisted Penetration, 11th Int. Symposium Interaction of the Effects of Munitions with Structures, 2003.

Buzaud, E., Don, D., Chapelle, S., Gary, G. and Bailly, P., Perforation Studies into Mb50 Concrete Slabs, 9th Int. Sym. Interaction of the Effects of Munitions with Structures, 1999.

Buzaud, E., Laurensou, R., Darrigade, A., Belouet, P. and Lissayou, C., Hard Target Defeat: An Analysis of Reinforced Concrete Perforation Process, 9th Int. Sym. Interaction of the Effects of Munitions with Structures, 1999.

Gran, J. K. and Frew, D. J., In-target radial stress measurements from penetration experiments into concrete by ogive-nose steel projectiles, Int. J. Imp. Engng. Vol 19, No. 8, pp 715-726, 1997.

Gran, J. K., Moxley, R. E. and Adley, M. D., Measurement of Triaxial Stresses during Deep Penetration into Concrete, 9th Int. Sym. Interaction of the Effects of Munitions with Structures, 1999.

Forrestal M. J., Altman B. S., Cargile J. D. and Hanchak S. J., An empirical equation for penetration depth of ogive-nose projectiles into concrete targets, Int. J. Imp. Engng 15:395–405, 1994.

Forrestal, M.J., Frew, D.J., Hickerson, J.P. and Rohwer, T.A., Penetration of concrete targets with deceleration-time measurements, Int. J. Imp. Engng 28:479–497, 2003.

Forrestal M.J., Frew D.J., Hanchak S.J. and Brar N.S., Penetration of grout and concrete targets with ogive-nose steel projectiles, Int. J. Imp. Engng 18:465–76, 1996.

Frew D.J., Hanchak S.J., Green M.L. and Forrestal M.J., Penetration of concrete targets with ogive-nose steel rods, Int. J. Imp. Engng 21:489–97, 1998.

Hiermaier, S. and Thoma, K., Numerical Simulation of Penetration in Concrete Using Different Types of Code, 8th Int. Symposium Interaction of the Effects of Munitions with Structures, 1997.

Magnusson, J., Unosson, M. and Carlberg, A., High performance concrete "HPC"-field experiments and production, FOI-R--0256--SE, ISSN 1650-1942, 2001.

Riedel, W., Thoma, K., Hiermaier, S. and Schmolinske,E., Penetration of Reinforced Concrete by BETA-B-500 Numerical Analysis using a New Macroscopic Concrete Model for Hydrocodes, 9th Int. Sym. Interaction of the Effects of Munitions with Structures, 1999.

FOI is an assignment-based authority under the Ministry of Defence. The core activities are research, method and technology development, as well as studies for the use of defence and security. The organization employs around 1350 people of whom around 950 are researchers. This makes FOI the largest research institute in Sweden. FOI provides its customers with leading expertise in a large number of fields such as security-policy studies and analyses in defence and security, assessment of different types of threats, systems for control and management of crises, protection against and management of hazardous substances, IT-security an the potential of new sensors.

FOI
Swedish Defence Research Agency
Weapons and Protection
SE-147 25 Tumba

Tel: +46 (0) 8 5550 3000
Fax: +46 (0) 8 5550 4143

www.foi.se